

EXPERIMENTAL ANALYSIS OF 3-D SWEEPING WINGS

A THESIS SUBMITTED TO  
THE GRADUATE SCHOOL OF NATURAL AND APPLIED SCIENCES  
OF  
MIDDLE EAST TECHNICAL UNIVERSITY

BY

HASAN ÇAKIR

IN PARTIAL FULFILLMENT OF THE REQUIREMENTS  
FOR  
THE DEGREE OF MASTER OF SCIENCE  
IN  
AEROSPACE ENGINEERING

AUGUST 2015



Approval of the thesis:

**EXPERIMENTAL ANALYSIS OF 3-D SWEEPING WINGS**

submitted by **HASAN ÇAKIR** in partial fulfillment of the requirements for the degree of **Master of Science in Aerospace Engineering Department, Middle East Technical University** by,

Prof. Dr. Gülbin Dural Ünver

\_\_\_\_\_

Dean, Graduate School of **Natural and Applied Sciences**

Prof. Dr. Ozan Tekinalp

\_\_\_\_\_

Head of Department, **Aerospace Engineering**

Assoc. Prof. Dr. Dilek Funda Kurtuluş

\_\_\_\_\_

Supervisor, **Aerospace Engineering Dept., METU**

**Examining Committee Members:**

Prof. Dr. Altan Kayran

\_\_\_\_\_

Aerospace Engineering Dept., METU

Assoc. Prof. Dr. Dilek Funda Kurtuluş

\_\_\_\_\_

Aerospace Engineering Dept., METU

Prof. Dr. Yusuf Özyörük

\_\_\_\_\_

Aerospace Engineering Dept., METU

Asst. Prof. Dr. A.Türker Kutay

\_\_\_\_\_

Aerospace Engineering Dept., METU

Asst. Prof. Dr. K. Bilge Arıkan

\_\_\_\_\_

Mechatronics Engineering Dept., ATU

**Date:** 26.08.2015

**I hereby declare that all information in this document has been obtained and presented in accordance with academic rules and ethical conduct. I also declare that, as required by these rules and conduct, I have fully cited and referenced all material and results that are not original to this work.**

Name, Last name : Hasan ÇAKIR

Signature :

## **ABSTRACT**

### **EXPERIMENTAL ANALYSIS OF 3-D SWEEPING WINGS**

Çakır, Hasan

M.S., Department of Aerospace Engineering

Supervisor: Assoc. Prof. Dr. Dilek Funda Kurtuluş

August 2015, 108 pages

The aim of this thesis is to modify the mechanism, which is capable of mimicking the insect flight and developed previously by the Aerospace Engineering Department, and to measure the forces and moments of three types of flapping wings fixed to this mechanism. The flapping wing design is a new research topic, comparably young area and can be the future for micro unmanned air vehicles. Time varying force and moment data obtained from the experiments conducted in water as part of this thesis can be used to determine which wing geometry can be chosen for different pitch and sweep angles. A sensor measuring even very small forces and moments simultaneously in 3 axis is employed in this mechanism. Before the experiments, various birds and mechanisms are investigated and a bird wing geometry has been chosen to compare its aerodynamic features with the other geometries. Furthermore, in order to improve the mechanism and to find out the best mechanism mimicking the hummingbird flight, various test setups was studied. A connector has been designed between the mechanism and the sensor in order to minimize errors. And also this connector let us measure the pitch angle precisely whereas the old mechanism was able to measure only an approximate pitch angle. Additionally a roller bearing has been located at the center of the gear in order to transfer the power efficiently. A program which is called as “Wing-Sim” is used to control motor drivers and wings. Totally, 21 cases has been

performed with three type of wings whose names are Flat Plate, Hummingbird and Zimmermann. The period of each case is 10 seconds and every cases have 50 periods. The wings have approximately the same size with each other which are 26 cm span, 7.9 cm chord and 3 mm thickness. Moreover, experimental uncertainties associated with low level fluid dynamic force measurements are addressed in this study. A drastic increase in drag force is observed after 30° pitch angle while lift force is not changed. The most efficient wing is the Zimmermann with its high L/D ratios.

Keywords: Flapping Wing Mechanism, Water Tank Experiments, Unsteady Aerodynamics, Force Measurement, Micro Air Vehicles

## ÖZ

### ÜÇ BOYUTLU SÜPÜRME HAREKETİ YAPAN KANATLARIN DENEYSEL ANALİZİ

Çakır, Hasan

Yüksek Lisans, Havacılık ve Uzay Mühendisliği Bölümü

Tez Yöneticisi: Doç. Dr. Dilek Funda Kurtuluş

Ağustos 2015, 108 sayfa

Bu tezin amacı, Havacılık ve Uzay Mühendisliği Bölümü tarafından daha önce üretilmiş olan ve böcek uçuşunu taklit edebilen mekanizmayı geliştirmek ve bu mekanizmaya sabitlenmiş olan 3 tip kanat üzerinde oluşan kuvvet ve momentlerin ölçümünü sağlamaktır. Çırpan kanat tasarımı gelişen bir araştırma konusu, diğer konulara nazaran yeni bir alan ve insansız hava araçlarının geleceği olabilecek bir çalışmadır. Bu tez kapsamında suda gerçekleştirilen deneylerden elde edilen ve zamana bağlı olarak değişen kuvvet ve moment dataları, değişik hücum ve sapma açılarında hangi profilin kullanılabileceği hakkında fikir sahibi olmak için kullanılabilir. Söz konusu mekanizmada, anlık olarak üç ekseninde çok küçük kuvvet ve momentleri bile ölçebilen bir sensor kullanılmıştır. Deneylere başlamadan önce çeşitli sinek kuşu türleri incelenmiş ve diğer iki kanatla aerodinamik özelliklerini karşılaştırmak üzere bir adet sinek kuşu kanat seçilmiştir. Ayrıca mekanizmayı daha da geliştirmek ve sinek kuşunun uçuşunu en iyi taklit edebilecek mekanizmayı bulmak amacıyla çeşitli deney düzenekleri incelenmiştir. Mekanizma ve sensor arasındaki yerleşimden kaynaklanabilecek sorunları en aza indirmek amacıyla bir bağlantı parçası tasarlanıp üretilmiştir. Ayrıca yunuslama açısı daha önceki deneylerde yaklaşık olarak ölçülebiliyorken üretilen bu bağlantı parçası sayesinde daha net bir şekilde ölçülebilmektedir. Bunlara ek olarak, bir dişlinin ortasına rulman eklenerek güç

transferinin daha rahat yapılması sağlanmıştır. “Wing-Sim” adındaki programla motor sürücüleri ve kanatların kontrolü sağlanmıştır. Düz Plaka, Sinek Kuşu ve Zimmermann isimli kanatlar ile toplamda 21 deney yapılmıştır. Her bir deneyin periyodu 10 saniye olup ve her deneyde toplam 50 periyot vardır. Söz konusu kanatlar yaklaşık olarak aynı ölçülere sahiptir ve ölçüleri 26 cm açıklık, 7.9 cm veter ve 3 mm kalınlık şeklindedir. İlave olarak, akışkan dinamik kuvvetlerinin düşük seviyede olmasından kaynaklanan, deneysel belirsizliklerin analizleri yapılmıştır. 30° yunuslama açısından sonra sürüklenme kuvvetinde açıkça bir artış görülürken, taşıma kuvvetinde bir artış gözlenmemiştir. En verimli kanat, yüksek L/D oranları sebebiyle Zimmermann isimli kanattır.

Anahtar Kelimeler: Çırpan Kanat Mekanizması, Su Tankı Deneyleri, Zamana Bağlı Aerodinamik, Kuvvet Ölçümü, Mikro Hava Aracı

*to my parents...*

## ACKNOWLEDGMENTS

I would like to express my deep and sincere gratitude to my supervisor Assoc. Prof. Dr. Dilek Funda Kurtuluş for her invaluable kindness, patience, academic experience and knowledge at all steps of this study. I could not be able to complete this study without her support, energy and enthusiasm.

I would also like to thank my jury members Prof. Dr. Altan Kayran, Prof. Dr. Yusuf Özyörük, Asst. Prof. Dr. Ali Türker Kutay, Asst. Prof. Dr. Kutluk Bilge Arıkan and my older sister Assoc. Prof. Dr. Sevgi Demirel for reviewing my thesis.

I would especially like to thank Capt. Ebubekir Teke, Lt.Col. Altay Duman, 1<sup>st</sup> Lt. Buğra Büyükyavuz, Lt.Col. Ünal Ünver and Col. Ersin Göse for their deep tolerance during my Master Education. Moreover, I would like to thank my friends F. Yudum Çömez and M. Gülay Şenol for helping me to make my experiments.

Lastly, but most importantly, I would like to express my eternal gratitude to my family for their love, support and encouragement throughout my life.

This study was supported by 213M327 TUBITAK project and TUBA GEBIP Award 2012-18.

## TABLE OF CONTENTS

ABSTRACT .....	v
ÖZ.....	vii
ACKNOWLEDGMENTS .....	x
TABLE OF CONTENTS .....	xi
LIST OF TABLES.....	xiv
LIST OF FIGURES .....	xv
NOMENCLATURE .....	xx
CHAPTERS	
1 INTRODUCTION.....	1
1.1 Background Information .....	1
1.2 Outline of the Thesis .....	2
1.3 Major Goals .....	2
2 LITERATURE SURVEY.....	3
2.1 Unsteady Mechanisms for Extra Lift Generating.....	3
2.1.1 Dynamic Stall or Leading Edge Vortex (LEV).....	3
2.1.2 Clap and Fling .....	5
2.1.3 Wake Capturing Phenomenon.....	5
2.1.4 Rotational Lift (Kramer Effect) .....	6
2.2 Wagner Effect.....	6
2.3 Remarkable Non-dimensional Parameters and Dynamic Scaling.....	7

2.4	Flapping Aerodynamics in Nature.....	9
2.5	Flapping Wing Mechanisms in Literature .....	11
3	FLAPPING MECHANISM.....	19
3.1	System Definition .....	19
3.2	Mechanical Specifications .....	20
3.2.1	Mechanical Wrist, Gearbox and Transmission Shafts .....	21
3.2.2	Motor Compartments .....	22
3.2.3	Control Box .....	23
3.2.4	The Mechanism on Which the Sensor is Located .....	23
3.3	Motion Kinematics .....	24
3.4	Hardware .....	26
3.5	Software.....	27
3.6	User Interface .....	28
4	EXPERIMENTAL METHOD.....	31
4.1	Experimental Setup.....	31
4.1.1	Wing Models .....	31
4.1.2	Water Tank.....	33
4.1.3	Positioning System.....	33
4.1.4	Force and Moment Measurement.....	34
4.2	Flow Characteristic.....	34
4.3	Transducer .....	35

4.4	Labview Measurement Block.....	35
4.5	Coordinate Transformation .....	37
4.6	Motion Kinematics and Wing Trajectory.....	38
4.7	Results of Previous Experimental Setup and Verification Study.....	39
4.8	Experimental Procedure .....	41
5	RESULTS AND DISCUSSION .....	43
5.1	Cases.....	44
5.2	Mean and Peak Values of the Lift Forces Drag Forces and $C_L$ Values.....	70
5.3	Lift Forces, Drag Forces and $C_L$ Values for All Cases of Flat Plate.....	74
5.4	Lift Forces, Drag Forces and $C_L$ Values for All Cases of Hummingbird ...	76
5.5	Lift Forces, Drag Forces and $C_L$ Values for All Cases of Zimmermann ....	77
5.6	Experimental Uncertainties and Added Mass Effect .....	79
6	CONCLUSION.....	83
6.1	Recommendations for the Further Studies .....	84
	REFERENCES.....	85
	APPENDICES	
A	DATA ANALYSIS.....	93

## LIST OF TABLES

### TABLES

Table 2. 1 Dimensions and parameters calculated by actuator disk theory for some birds and insects performing normal hovering (Adapted from Ref. [2]). .....	9
Table 2. 2 Several flapping wing mechanism characteristics .....	17
Table 3. 1 Motion limits of Robot-Wings (Adopted from Ref. 3).....	20
Table 4. 1 Transducer Sensing ranges and resolution (Adopted from Ref. 3).....	35
Table 5. 1 Experimental conditions for all cases .....	44
Table 5. 2 Mean and peak values of lift forces for all cases .....	71
Table 5. 3 Mean and peak values of drag forces for all cases.....	72
Table 5. 4 Mean and peak values of $C_L$ coefficients for all cases.....	73

## LIST OF FIGURES

### FIGURES

Figure 2.1 Leading edge vortex lift contribution (from Ref. [4]) .....	4
Figure 2.2 Leading edge and tip vortex formation (from Ref. [5]).....	4
Figure 2.3 Leading edge vortex development in 2-D and 3-D during linear translation (from Ref. [4]).....	4
Figure 2. 4 Clap and Fling mechanism (from Ref. [4]) .....	5
Figure 2. 5 Wake capture formation (from Ref. [7]).....	6
Figure 2. 6 Wagner effect on circulation (from Ref. [4]).....	7
Figure 2. 7 General wing trajectory of the Fruit fly (from Ref. [14]).....	10
Figure 2. 8 Hummingbird in hovering flight (from Ref. [15]).....	10
Figure 2. 9 The wing trajectory of Hummingbird (from Ref. [16]).....	11
Figure 2. 10 Han's experimental setup for flow visualization and force measurement (from Ref. [17]).....	11
Figure 2. 11 Flow structure for different $t/T$ times (from Ref. [17]) .....	12
Figure 2. 12 George's flapping wing mechanism (from Ref. [18]) .....	12
Figure 2. 13 George's flapping wing mechanism (from Ref. [18]) .....	13
Figure 2. 14 Load cell configuration of Isaac's flapping mechanism (from Ref. [19]) .....	13
Figure 2. 15 Isaac's flapping and pitching mechanism (from Ref. [19]).....	14
Figure 2. 16 Hu and Deng's schematic diagram for test setup (from Ref. [20]) .....	14
Figure 2. 17 Hu and Deng's test setup (from Ref. [20]) .....	14
Figure 2. 18 Maybury's flapping wing mechanism (from Ref. [21]) .....	15
Figure 2. 19 Zhang's 3D flapping mechanism (from Ref. [22]).....	15
Figure 2. 20 Morrison's flapping wing mechanism (from Ref. [23]) .....	16
Figure 2.21 Zimmermann wing geometry which is used by Morrison (from Ref. [23]) .....	16
Figure 2. 22 Nagai's schematic mechanical model and wing geometry (from Ref. [24]) .....	17

Figure 3. 1 Hummingbird and Robot-wing principle axis placement (Adopted from Ref. [3]).....	20
Figure 3. 2 Transmission shafts.....	21
Figure 3. 3 Bevel gears with and without roller bearing .....	22
Figure 3. 4 The motor box of the Robot-Wings (Adopted from Ref. [3]) .....	22
Figure 3. 5 Control-Box of the robotic wings .....	23
Figure 3. 6 The Part on which the sensor is located.....	23
Figure 3. 7 The old (left) and new (right) mechanism .....	24
Figure 3. 8 Hardware of the control box (Adopted from Ref. [3]) .....	26
Figure 3. 9 Hardware block diagram (Adopted from Ref. [3]) .....	26
Figure 3. 10 Flow chart of the software (Adopted from Ref. [3]).....	27
Figure 3. 11 PWM signal versus position error (from Ref. [3]).....	28
Figure 3. 12 Trajectory setting menu .....	29
Figure 3. 13 Position settings menu .....	30
Figure 3. 14 Advanced settings menu .....	30
Figure 4. 1 Flat plate wing geometry .....	32
Figure 4. 2 Hummingbird wing geometry.....	32
Figure 4. 3 Zimmermann wing geometry.....	32
Figure 4. 4 Water tank with its dimensions (Adopted from Ref. [3]) .....	33
Figure 4. 5 Wings position in water .....	34
Figure 4. 6 Labview program block-1 .....	36
Figure 4. 7 Labview program block-2.....	36
Figure 4. 8 Labview program block-3.....	37
Figure 4. 9 Earth-fixed and wing-fixed coordinate systems .....	37
Figure 4. 10 Wing trajectory and stroke plane illustration.....	39
Figure 5. 1 Wing trajectory in one stroke for Case 1 .....	44
Figure 5. 2 Normal force harmonic content of the Case 1 .....	45
Figure 5. 3 Time history of normal force components in both impulsive and periodic region for 5 stroke cycles with sweep angle and angular velocity variations for Case 1 .....	45
Figure 5. 4 Phase averaged and filtered normal force components in both impulsive and periodic region with sweep angle and angular velocity variations for Case 1 ....	46
Figure 5. 5 Phase averaged total forces of three wings for Case 1 .....	46

Figure 5. 6 Phase averaged lift and drag forces of three wings with sweep angle and angular velocity variations for Case 1.....	47
Figure 5. 7 $C_L$ coefficient variations for each three wings for Case 1 .....	47
Figure 5. 8 L/D ratios of 3 wings during one cycle for Case 1 .....	48
Figure 5. 9 Wing trajectory in one cycle for Case 2 .....	48
Figure 5. 10 Normal force harmonic contents of each three wings for Case 2.....	49
Figure 5. 11 Time history of normal force component in both impulsive and periodic regions for 5 stroke cycle with sweep angle and angular velocity variations for Case 2 .....	49
Figure 5. 12 Phase averaged and filtered normal force components in both impulsive and periodic region with sweep angle and angular velocity variations for Case 2 ....	50
Figure 5. 13 Phase averaged total forces of three wings for Case 2 .....	50
Figure 5. 14 Phase averaged lift and drag forces of three wings with sweep angle and angular velocity variations for Case 2.....	51
Figure 5. 15 $C_L$ coefficient variations for each three wings for Case 2 .....	51
Figure 5. 16 Figure 5.8 L/D ratios of 3 wings during one cycle for Case 2.....	52
Figure 5. 17 Wing trajectory in one cycle for Case 3 .....	52
Figure 5. 18 Normal force harmonic contents of each three wings for Case 3.....	53
Figure 5. 19 Time history of normal force component in both impulsive and periodic regions for 5 stroke cycle with sweep angle and angular velocity variations for Case 3 .....	53
Figure 5. 20 Phase averaged and filtered normal force components in both impulsive and periodic region with sweep angle and angular velocity variations for Case 3 ....	54
Figure 5. 21 Phase averaged total forces of three wings for Case 3 .....	54
Figure 5. 22 Phase averaged lift and drag forces of three wings with sweep angle and angular velocity variations for Case 3.....	55
Figure 5. 23 $C_L$ coefficient variations for each three wings for Case 3 .....	55
Figure 5. 24 L/D ratios of 3 wings during one cycle for Case 3 .....	56
Figure 5. 25 Wing trajectory in one cycle for Case 4 .....	56
Figure 5. 26 Normal force harmonic contents of each three wings for Case 4.....	56
Figure 5. 27 Time history of normal force component in both impulsive and periodic regions for 5 stroke cycle with angle and angular velocity variations for Case 4 ....	57

Figure 5. 28 Phase averaged and filtered normal force components in both impulsive and periodic region with sweep angle and angular velocity variations for Case 4 ....	57
Figure 5. 29 Phase averaged total forces of three wings for Case 4 .....	58
Figure 5. 30 Phase averaged lift and drag forces of three wings with sweep angle and angular velocity variations for Case 4.....	58
Figure 5. 31 $C_L$ coefficient variations for each three wings for Case 4 .....	59
Figure 5. 32 L/D ratios of 3 wings during one cycle for Case 4 .....	59
Figure 5. 33 Wing trajectory in one cycle for Case 5 .....	60
Figure 5. 34 Normal force harmonic contents of each three wings for Case 5.....	60
Figure 5. 35 Time history of normal force component in both impulsive and periodic regions for 5 stroke cycles with angle and angular velocity variations for Case 5 ....	61
Figure 5. 36 Phase averaged and filtered normal force components in both impulsive and periodic regions with sweep angle and angular velocity variations for Case 5...	61
Figure 5. 37 Phase averaged total forces of three wings for Case 5 .....	62
Figure 5. 38 Phase averaged lift and drag forces of three wings with sweep angle and angular velocity variations for Case 5.....	62
Figure 5. 39 $C_L$ coefficient variations for each three wings for Case 5 .....	63
Figure 5. 40 L/D ratios of 3 wings during one cycle for Case 5 .....	63
Figure 5. 41 Wing trajectory in one cycle for Case 6 .....	64
Figure 5. 42 Normal force harmonic contents of each three wings for Case 6.....	64
Figure 5. 43 Time history of normal force component in both impulsive and periodic regions for 5 stroke cycles with angle and angular velocity variations for Case 6 ....	64
Figure 5. 44 Phase averaged and filtered normal force components in both impulsive and periodic region with sweep angle and angular velocity variations for Case 6 ....	65
Figure 5. 45 Phase averaged total forces of three wings for Case 6 .....	65
Figure 5. 46 Phase averaged lift and drag forces of three wings with sweep angle and angular velocity variations for Case 6.....	66
Figure 5. 47 $C_L$ coefficient variations for each three wings for Case 6 .....	66
Figure 5. 48 L/D ratios of 3 wings during one cycle for Case 6 .....	67
Figure 5. 49 Wing trajectory in one cycle for Case 7 .....	67
Figure 5. 50 Normal force harmonic contents of each three wings for Case 7.....	67

Figure 5. 51 Time history of normal force component in both impulsive and periodic regions for 5 stroke cycle with sweep angle and angular velocity variations for Case 7 .....	68
Figure 5. 52 Phase averaged and filtered normal force components in both impulsive and periodic region with sweep angle and angular velocity variations for Case 7 ....	68
Figure 5. 53 Phase averaged total forces of three wings for Case 7 .....	69
Figure 5. 54 Phase averaged lift and drag forces of three wings for Case 7 .....	69
Figure 5. 55 $C_L$ coefficient variations for each three wings for Case 7 .....	70
Figure 5. 56 L/D ratios of 3 wings during one cycle for Case 7 .....	70
Figure 5. 57 Mean lift values of 3 geometries for all cases .....	71
Figure 5. 58 Mean drag values of 3 geometries for all cases .....	72
Figure 5. 59 Mean $C_L$ values of 3 geometries for all cases.....	73
Figure 5. 60 Lift force curves of Flat plate for 7 cases .....	74
Figure 5. 61 Drag force curves of Flat plate for 7 cases .....	75
Figure 5. 62 $C_L$ curves of Flat plate for 7 cases .....	75
Figure 5. 63 Lift force curves of Hummingbird for 7 cases.....	76
Figure 5. 64 Drag force curves of Hummingbird for 7 cases.....	76
Figure 5. 65 $C_L$ curves of Hummingbird for 7 cases.....	77
Figure 5. 66 Lift force curves of Zimmermann for 7 cases .....	77
Figure 5. 67 Drag force curves of Zimmermann for 7 cases .....	78
Figure 5. 68 $C_L$ curves of Zimmermann for 7 cases .....	78

## NOMENCLATURE

<b>Latin Symbol</b>	<b>Description</b>	<b>Units</b>
$A$	Motion function amplitude	deg
$C$	Chord length	m
$C$	Conversion matrix	-
$F$	Frequency	Hz
$l_t$	Reference length	m
$K$	Reduced frequency	-
$Re_1$	MAC based Reynolds number	-
$Re_2$	Root chord based Reynolds number	-
$St$	Strouhal number	-
$T$	Time variable	s
$T$	Period of the motion	s
$t/T$	Non-dimensional time variable	-
$\bar{U}$	Reference velocity	m/s
$X$	Pitch axis	-
$Y$	Plunge axis	-
$Z$	Sweep axis	-

<b>Greek Symbol</b>	<b>Description</b>	<b>Units</b>
$\sigma$	Standard deviation (in force, velocity)	N, m/s
$\alpha$	Pitch angle	deg
$\beta$	Plunge angle	deg
$\theta$	Sweep angle	deg
$\dot{\alpha}$	Pitch rate	deg/s
$\dot{\beta}$	Plunge rate	deg/s
$\dot{\theta}$	Sweep rate	deg/s
$\varepsilon$	Position error	deg
$\varphi$	PWM signal	-
$\mu$	Dynamic viscosity of the fluid	kg/m.s
$\nu$	Kinematic viscosity of the fluid	m <sup>2</sup> /s
$\omega$	Angular velocity	rad/s

## **Abbreviations**

2-D	Two-Dimensional
3-D	Three-Dimensional
FFT	Fast Fourier Transformation
LEV	Leading Edge Vortex
MAC	Mean Aerodynamic Chord
MAV	Micro Air Vehicle
PIV	Particle Image Velocimetry
PIC	Peripheral Interface Controller
PWM	Pulse Width Modulation
TEV	Trailing Edge Vortex



# CHAPTER 1

## INTRODUCTION

### 1.1 Background Information

Human beings have imitated nature to make their life easier from the beginning of the history. Likewise, when humans first dreamed of flight, many people naturally thought to imitate birds and create flappable wings [1]. However, a vehicle carrying the weight of a human must flap its wing too fast, and the structure of this vehicle must be sound enough to endure. Therefore, people were not able to fly until they tried using stable wings which are much less complicated. But, an airplane having fixed wing have to have an engine too whereas birds don't need it with their flapping wings.

Animals have their nervous systems capable of sensing the environment around them and alter their flight path instantaneously. However, machines are not as good as animals so we have still got a long way to figure out their capabilities and apply them to our machines [1].

For the last two decades, several studies have been conducted about Low Reynolds number regime which has become very important because of the advances in micro-technologies enabling the development of Micro Air Vehicles (MAV's). One of the main concerns of the studies about Micro Air Vehicles (MAV's) is the flapping motion concept [2]. Since one of the main objective of MAV applications is constant position surveillance, hover mode needs to be more researched [2].

Additionally, flapping wing shows superior flight characteristics comparing to most of the advanced aircrafts. While an advanced fighter aircraft can cover roughly 30 body length per second, a European starling can cover 120 body length per second [3]. Moreover, a Barn Swallow has a roll rate of  $5000^\circ/\text{s}$  while a typical aerobatic aircraft can perform only  $720^\circ/\text{s}$  [3]. Finally, Reynolds number of flapping wing and typical aircrafts are very different from each other. Reynolds number of aircraft is approximately  $10^4$  times bigger than Reynolds number of the insects which means air

must be much more viscous for a typical aircraft to fly at the same Reynolds number with the insects and still generates enough lift in order to stay up [3].

## **1.2 Outline of the Thesis**

The aim of the present study is to understand the aerodynamics phenomena and vortex topology [2]. It is very hard to imitate a real bird wing to make these experiments so a simplified model is used to investigate the aerodynamics and vortex formation of the sweeping motion in 21 cases.

This study is comprised of 6 chapters to fulfill the objectives stated in Section 1.3. First chapter provides the aim of this study and background of the flapping flight. In Chapter 2, what have been done in literature about unsteady lift generating mechanism of the flapping wing has been explained. Additionally, the important non-dimensional parameters and the dynamic scaling have been cited and related wing mechanisms in literature are presented. In Chapter 3, the modifying process of the robotic wing mechanism is explained and a brief explanation about the mechanism is given. The experimental setup, force measurement, data acquisition and experimental procedure are explained in Chapter 4. Chapter 5 gives the results for the present study and experimental analysis of the present study. Chapter 6 presents the conclusion and the recommendation parts.

## **1.3 Major Goals**

The major objectives of the present study are:

- To modify the mechanism, which is capable of mimicking the insect flight and developed previously by the Aerospace Engineering Department;
- To measure the forces and moments occurring around three types of flapping airfoils fixed to this mechanism,
- To determine uncertainties in the experiment.

## CHAPTER 2

### LITERATURE SURVEY

In this chapter, which has five sections, we focus on a detailed literature search about studies which are carried out previously. First section covers brief information about the studies about how lift is generated by unsteady mechanisms which have flapping wing. In second part, Wagner effect which is the impulsive starting effect on lift generation will be sorted out. Third part includes information about three non-dimensional parameters. Fourth part is about natural flapping wing mechanisms. The last part investigates the experiments which are carried out before by several researchers.

#### **2.1 Unsteady Mechanisms for Extra Lift Generating**

There are four main unsteady mechanisms for extra lift generation during flapping flight [3]. These are Dynamic Stall or Leading Edge Vortex (LEV), Clap and Fling, Wake Capturing Phenomenon and Rotational Lift (Kramer Effect).

##### **2.1.1 Dynamic Stall or Leading Edge Vortex (LEV)**

Steady and unsteady flows show difference in many ways. In steady flow, there is a flow separation after exceeding a certain angle of attack. In time depending flow, a vortex is formed at high angles of attack at the leading edge and this vortex attaches the flow to the wing before it reaches the trailing edge. Since the flow reattaches to the wing, the fluid can able to flow smoothly again and the Kutta condition is maintained [4]. This phenomenon is called as Leading Edge Vortex (LEV) and it is one of the most important mechanisms of the flapping wing. This vortex causes an extra lift on the wing since it induces a downward velocity [3].

As it is seen on Figure 2.1 that there is a suction because of the vortex and this suction acts like additional velocity for the wing.

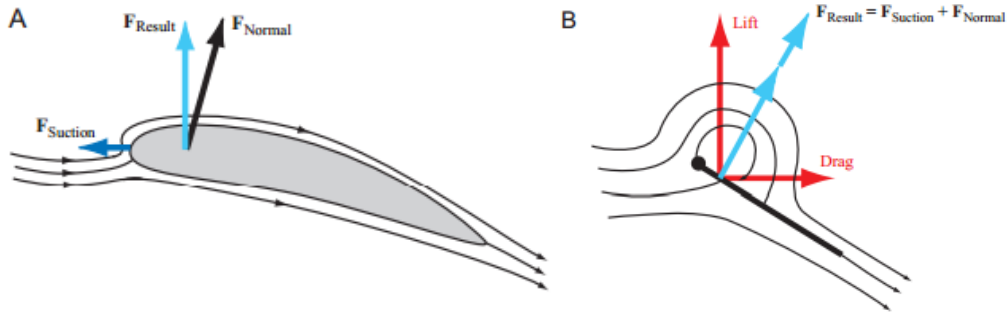


Figure 2.1 Leading edge vortex lift contribution (from Ref. [4])

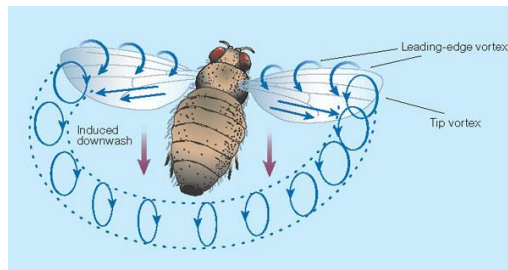


Figure 2.2 Leading edge and tip vortex formation (from Ref. [5])

Figure 2.2 shows leading-edge vortex formation and tip vortex at the same time and Figure 2.3 shows that in 2-D flow there is a trailing edge vortex since the flow cannot attach to the wing. However in 3-D flow, it is attached to the wing. It shows the stability of the leading edge vortex is only valid for 3-D case.

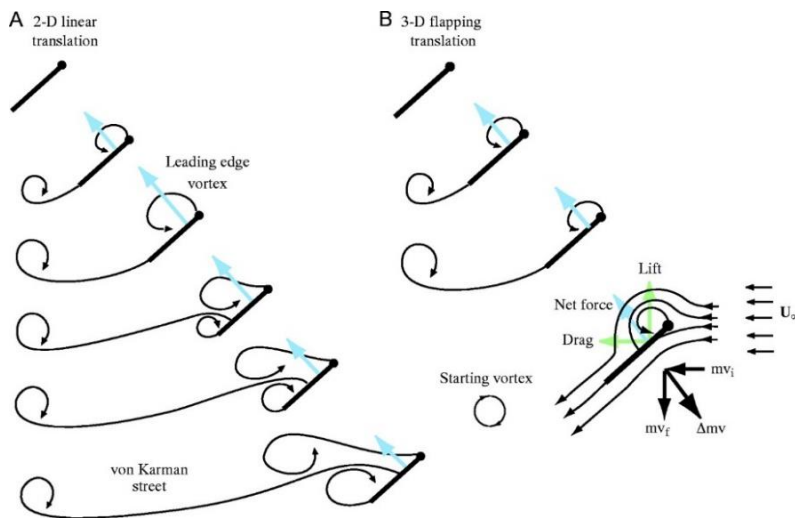


Figure 2.3 Leading edge vortex development in 2-D and 3-D during linear translation (from Ref. [4])

### 2.1.2 Clap and Fling

Figure 2.4 shows a Clap and Fling mechanism schematically. Leading edges of the flapping wings touch each other initially when a cycle starts (A). Wings start to rotate around leading edges until they meet each other (B). As rotating continues, vorticity shed from the trailing edge rolls up in the form of stopping vortices (C). The leading edge vortices lose strength too. After a while, wings start to rotate around trailing edge (D). Fluid fills the gap between two wing sections expeditiously, giving an initial boost in circulation around the wing system (E). Finally a leading edge vortex forms however trailing edges vortices start to vanish (F) [4].

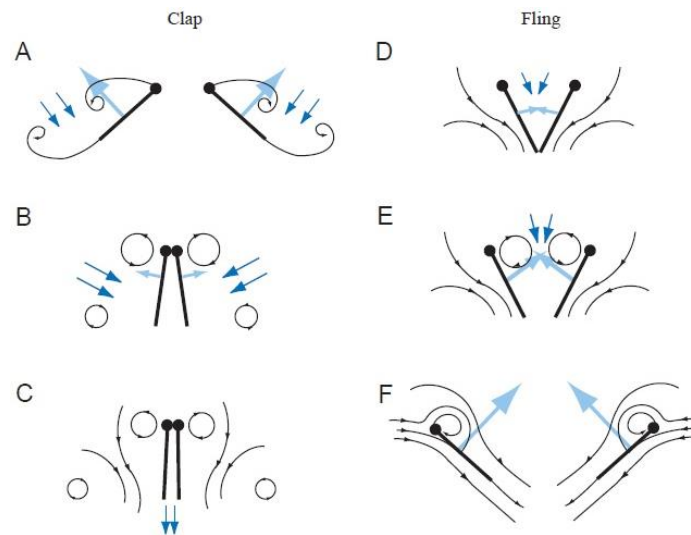


Figure 2. 4 Clap and Fling mechanism (from Ref. [4])

### 2.1.3 Wake Capturing Phenomenon

Especially during hover or low-speed flight, while wings are flapping, the flow around the wing is no longer steady and the flapping wing repeatedly moves into its own wake [6]. The upstroke and downstroke motion of the wings causes wing interaction with shed vorticity of prior strokes. This motion causes extra lift generation [3]. The fluid surrounding the wings makes a wake flow behind the wing which contains energy of that flow in the form of momentum and heat [6]. When the wing acts to the reverse side it is effected by the wake flow which ends up with increased lift generation. Wing passage through the wake could, therefore, be a method to recover some of this lost

energy and utilize it usefully for flight. The insects and birds have special mechanisms whereby they extract energy back from their near vortex wake [6].

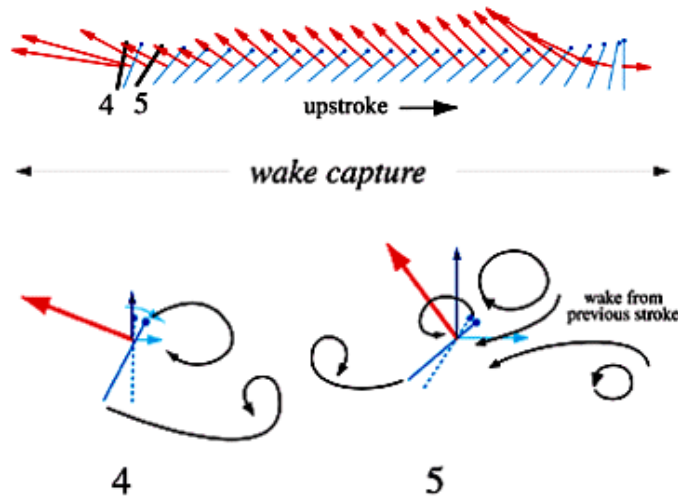


Figure 2. 5 Wake capture formation (from Ref. [7])

#### 2.1.4 Rotational Lift (Kramer Effect)

Lift-generating surfaces of the animals are not same as wings of planes and helicopters. Helicopters and planes don't need to change the direction of the wing since they always have a positive angle of attack. Because lift-generating mechanisms of animals have upstrokes and downstrokes in a cycle, they will have a negative angle of attack if they don't change the direction of their wings. During stroke reversals, the rotational velocity of the wing can be high while the translational velocity is low. So classical aerodynamic rules are not very effective during stroke reversals. However, according to Ellington (1984c), wing rotation is itself a source of circulation that will be especially large during supinations [8]. Kramer proved this idea by using experimental methods in 1932 [3].

#### 2.2 Wagner Effect

Wagner effect which means inertness in the development of circulation was first put forward by Wagner in 1925 and studied experimentally by Walker in 1931. The circulation around a wing rises slowly to steady-state value, when an inclined wing

starts impulsively from rest. Two phenomena, which are inherent latency in the viscous action on the stagnation point and the generated vorticity at the trailing edge, are thought to be provoking this delay [4]. As it is seen in the Figure 2.6 the wing has maximum steady circulation, after the starting vortex has moved sufficiently far from the trailing edge.

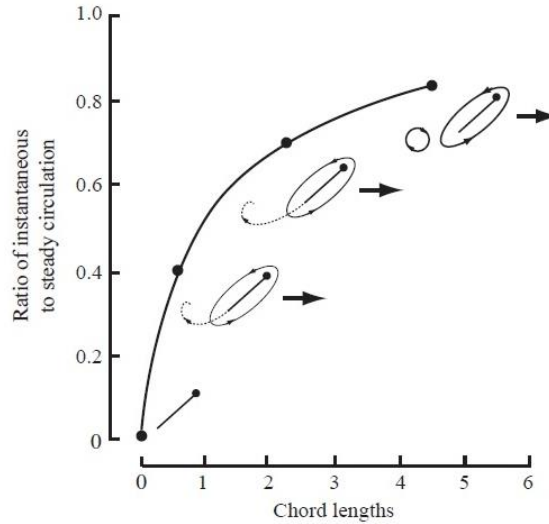


Figure 2. 6 Wagner effect on circulation (from Ref. [4])

### 2.3 Remarkable Non-dimensional Parameters and Dynamic Scaling

There are two important non-dimensional parameters in flapping wing aerodynamics which can be used to study the performance of a flapping wing. These parameters are Reynolds number ( $Re$ ) and reduced frequency ( $k$ ) [9]. However with regard to Dynamic Scaling, the two fundamentals parameters are Reynolds number ( $Re$ ) and Strouhal number ( $St$ ) [3]. The reduced frequency ( $k$ ) is the ratio of vertical velocity to the axial velocity. For plunging airfoils the term relates the flapping velocity to the free stream velocity and signifies the flapping frequency [10]. The  $k$  value characterizes the unsteady aerodynamics of the flapping wing. Reynolds number means the ratio of the inertial forces to the viscous forces for a flow. The ratio of flapping speed to the forward speed represents the Strouhal number [3]. These numbers can be calculated by using several parameters which are defined below.

$$\bar{U} = 2l_t\psi f = \omega l_t \quad (1)$$

Where  $\bar{U}$  is the translational velocity,  $l_t$  is the length between the center of the rotation and the tip of the wing,  $\psi$  is the total sweep angle covered in one period and  $f$  is the frequency of the system. Reynolds number, Strouhal number and reduced frequency can be defined as follows [9] [3].

$$Re = \frac{\bar{U}c}{\nu} = \frac{2l_t\psi fc}{\nu} \quad (2)$$

$$St = \frac{f\psi}{\bar{U}} = \frac{k\psi}{\pi c} \quad (3)$$

$$k = \frac{\omega c}{2\bar{U}} = \frac{\pi fc}{\bar{U}} = \frac{\pi c}{2l_t\psi} \quad (4)$$

In this study, two types of Reynolds number are used, one of them is the mean aerodynamic chord based in which  $\bar{U}$  is accepted as the directional velocity at mean aerodynamic chord and the other one is root chord based in which  $\bar{U}$  is accepted as the directional velocity at the tip of the wing.

Since the experiments are carried out in water, Dynamic Scaling calculations must be done for all cases in determination of the flapping frequency for which the experiments are valid. We can compare a case in real life with our experimental conditions as follows;

$$Re_r = \frac{\bar{U}_r c_r}{\nu_r} \quad \text{and} \quad Re_e = \frac{\bar{U}_e c_e}{\nu_e} \quad (5)$$

The Strouhal numbers for both cases are as follows;

$$St_r = \frac{f_r \psi_r}{\bar{U}_r} \quad \text{and} \quad St_e = \frac{f_e \psi_e}{\bar{U}_e} \quad (6)$$

If we take the ratio of the velocities for both numbers;

$$\frac{\bar{U}_r}{\bar{U}_e} = \frac{\nu_r c_e}{\nu_e c_r} \quad \text{and} \quad \frac{\bar{U}_r}{\bar{U}_e} = \frac{f_r \psi_r}{f_e \psi_e} \quad (7)$$

Then, equating the velocity ratios gives us required frequency as follows;

$$f_e = \left(\frac{\nu_e}{\nu_r}\right) \left(\frac{c_r}{c_e}\right) \left(\frac{\psi_r}{\psi_e}\right) (f_r) \quad (8)$$

Note that, our experiment frequency depends on viscosity ratios, chord length ratios, and Stroke amplitude ratios. If we determine all these parameters for the experiment,

we can choose the frequency of the case or vice versa. These parameters are named as scaling parameters.

## 2.4 Flapping Aerodynamics in Nature

This section focuses on the wing trajectories of several animals to learn about flapping animals since it is vital to investigate these animals to design a wing mechanism about our experiment. Searching hovering insects and birds provides sufficient information about the flapping mechanisms.

These animals make a figure-of-eight motion with symmetrical half-strokes by moving through a large angle in an approximately horizontal plane to have hovering motion [2]. Birds, the most successful practitioners employing flapping wings, combine unsteady aerodynamics, variable geometry, flexible surfaces of non-uniform porosity, and rapid, adaptive biological systems to achieve their outstanding flight performance [11]. Table 2 shows different parameters about hummingbirds and some species of insects.

Table 2. 1 Dimensions and parameters calculated by actuator disk theory for some birds and insects performing normal hovering (Adapted from Ref. [2]).

	Body mass [kg]	Wing semi-span [m]	Disk loading [Nm <sup>-2</sup> ]	Stroke Period [s]	Feathering Parameter, f	L/D Ratios at 30° Pitch Angle
Fruit Fly, <i>Drosophila virilis</i>	$2 \times 10^{-6}$	0.003	0.69	0.004	0.0137	1.87 [58]
Crane fly, <i>Tipula paludosa</i>	$2.8 \times 10^{-5}$	0.0173	0.29	0.018	0.0036	3.03 [59]
Hover fly, <i>Eristalis tenax</i>	$1.5 \times 10^{-4}$	0.0127	2.90	0.0055	0.0056	3.79* [59]
Bumble bee, <i>Bombus terrestris</i>	$8.8 \times 10^{-4}$	0.0173	9.18	0.0064	0.0130	1.55 [60]
Hummingbird, <i>Amazilia fimbriata</i>	$5.1 \times 10^{-3}$	0.059	4.57	0.0285	0.0111	2 [61]

\* The pitch angle is 13° for that L/D ratio for this insect.

*Drosophila* is a fruit fly, a little insect about 3 mm long, of the kind that accumulates around spoiled fruit [2]. This insect has a wing beat frequency of 212 Hertz in hovering mode [12]. The Reynolds number for a slowly flying *Drosophila* is approximately 100, which is several orders of magnitude below the turbulent transition for a flat plate [13]. Figure 2.7 shows the general flapping trajectory of fruit fly at hover.

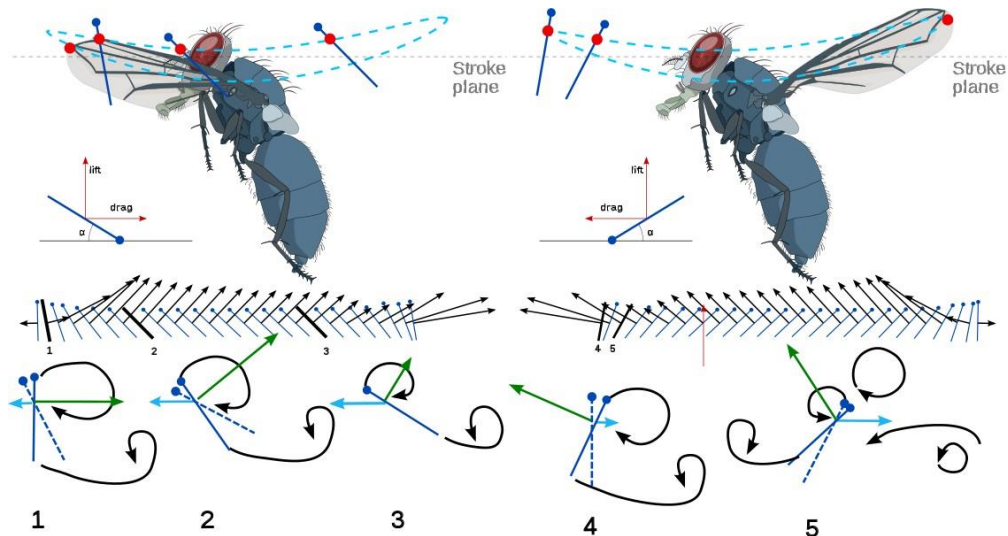


Figure 2. 7 General wing trajectory of the fruit fly (from Ref. [14])



Figure 2. 8 Hummingbird in hovering flight (from Ref. [15])

Although birds usually flap their wings in vertical direction only, they can create both lift and thrust at the same time. A normal force vector which contains lift and thrust is created by means of flapping a wing in a free stream flow. An effective angle of attack is formed by this flapping. This phenomenon is named as Knoller-Betz effect [3]. Figure 2.9 shows the trajectory of the hummingbird wing in both hovering and forward flight.

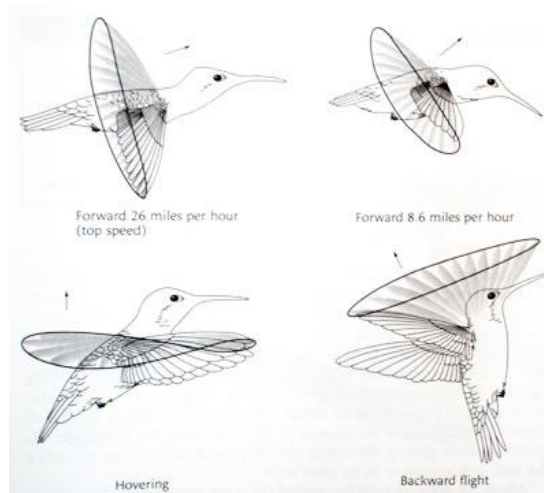


Figure 2. 9 The wing trajectory of Hummingbird (from Ref. [16])

## 2.5 Flapping Wing Mechanisms in Literature

Several wing mechanisms are investigated in this section to understand how wing flapping systems are designed. Studies like ours are chosen to understand the mechanisms and compare the results.

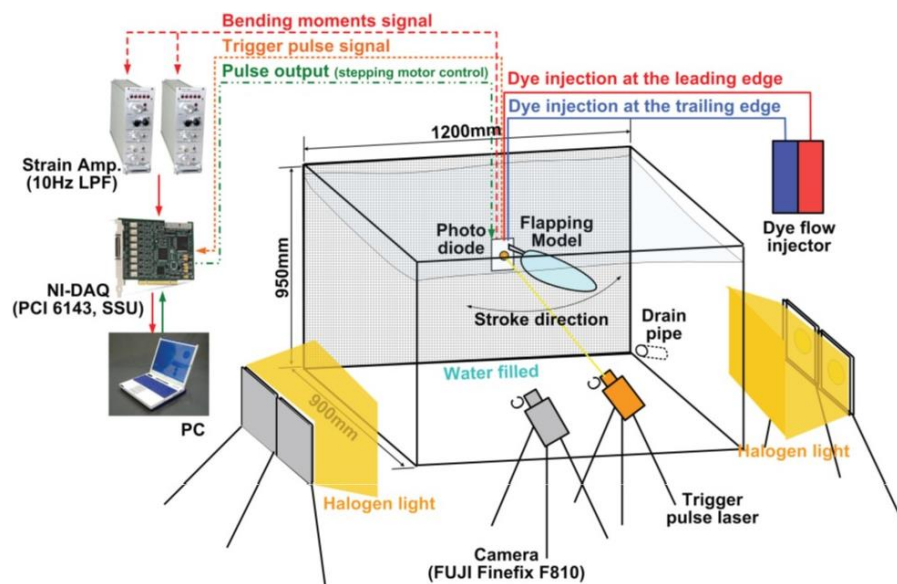


Figure 2. 10 Han's experimental setup for flow visualization and force measurement (from Ref. [17])

Han's experimental setup for flow visualization and force measurement uses bending moments signal to measure forces occurring around the wing geometry [17].

The mechanism can only control the pitch and sweep angles and is used in water tank. Particle Image Velocimetry (PIV) and force measurement can be done with this system. Figure 2.10 shows the experimental setup and Figure 2.11 presents the flow structure of the wing at different  $t/T$  times.

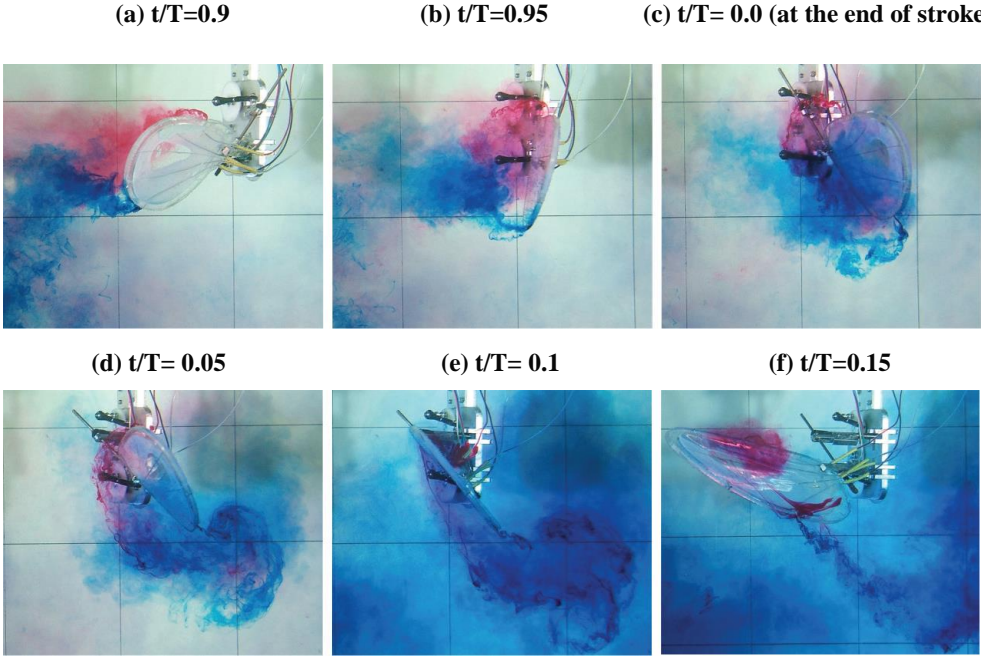


Figure 2. 11 Flow structure for different  $t/T$  times in Han’s study (from Ref. [17])

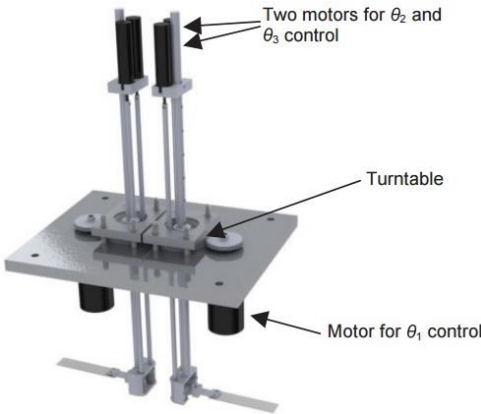


Figure 2. 12 George’s flapping wing mechanism (from Ref. [18])

George’s flapping wing mechanism which is capable of executing arbitrary flapping trajectories in 3 axis was developed to explore the relationship between flapping trajectory, forces and patterns (Figure 2.13). Maximum frequency of the system is

0.667 Hz [18]. There is a differential assembly housed inside a frame in this mechanism. Spur gears are mounted on the two input-differential gears. Spur gears are driven by the worm gears which are behind the spur gear. The worm gears are mounted to long shafts that extend upwards out of the working fluid. Motors are directly mounted to the worm gear shaft to drive the two differential inputs [18].

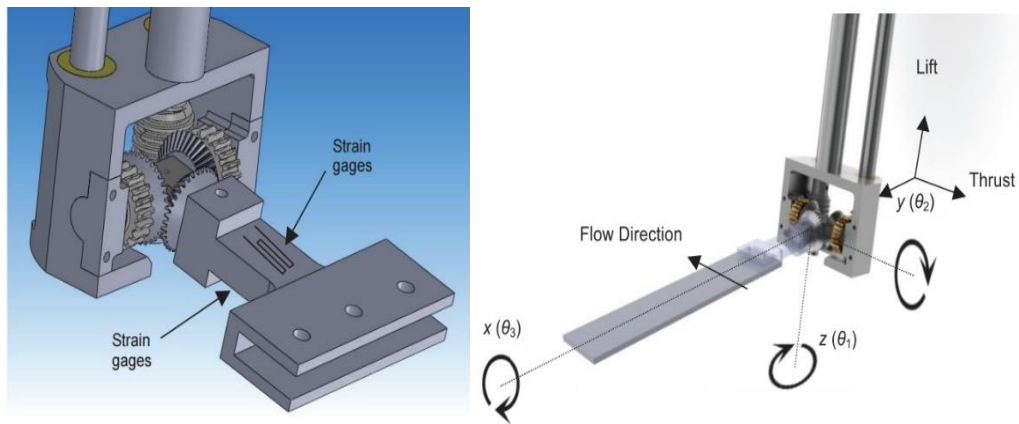


Figure 2. 13 George's flapping wing mechanism (from Ref. [18])

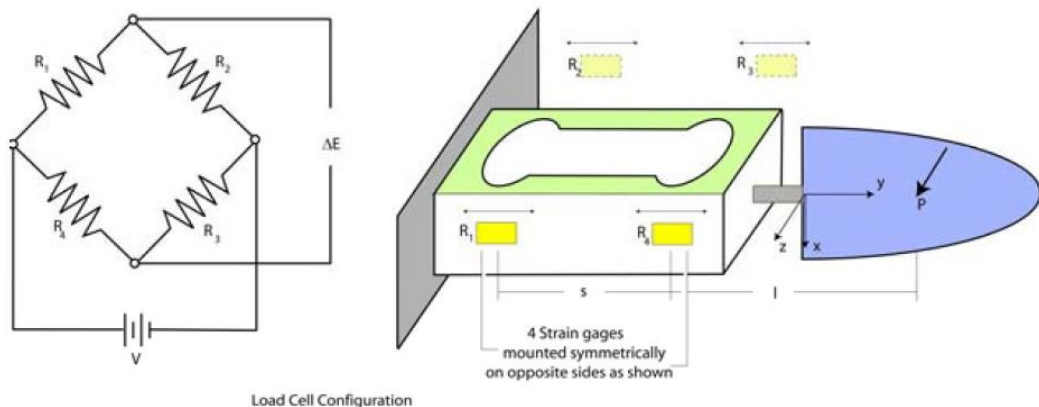


Figure 2. 14 Load cell configuration of Isaac's flapping mechanism (from Ref. [19])

Isaac's flapping-and-pitching thin flat plate wing mechanism whose load cell is seen above is used to measure forces (Figure 2.14). The mechanism has a force transducer to obtain time varying force data. There is a wheel driven by a DC motor. This rotation is transferred to the wing by using one rod and one pivot which makes the mechanism capable of flapping. Pitching is done via using a mounted servo motor below the fixed pivot. Four strain gages mounted symmetrically on opposite sides are used to measure aerodynamic forces occurring around the wing [19] (Figure 2.15).

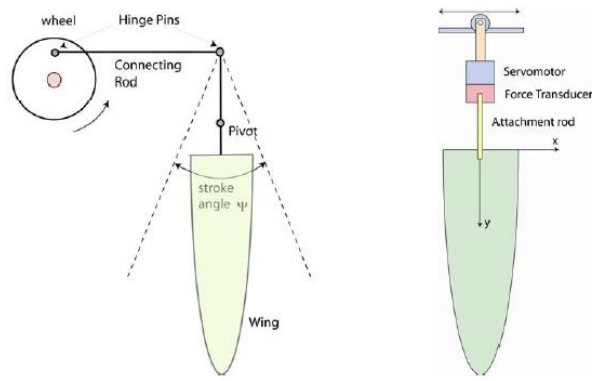


Figure 2. 15 Isaac's flapping and pitching mechanism (from Ref. [19])

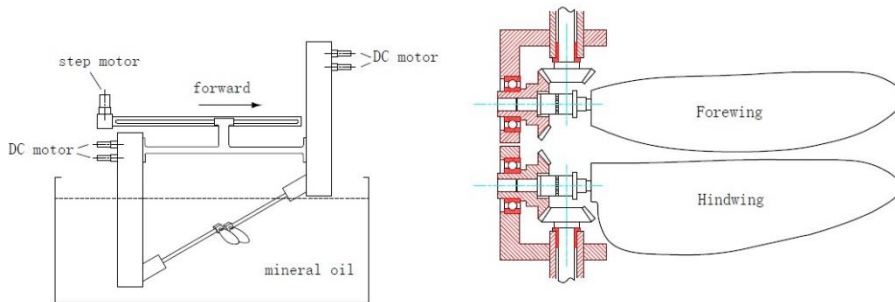


Figure 2. 16 Hu and Deng's schematic diagram for test setup (from Ref. [20])

Hu and Deng's Forewing-Hindwing Interactions test setup, which has a  $60^\circ$  inclined stroke plane, investigates the aerodynamic effect of phase difference during hovering and forward flight (Figure 2.16). This setup is constructed to replicate dragonfly wing motion and measure the instantaneous aerodynamic forces and torques by using a six component force sensor ATI NANO-17 [20] (Figure 2.17).

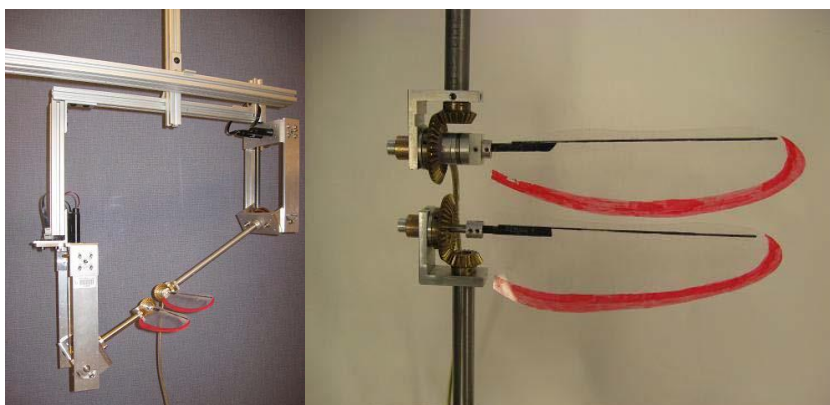


Figure 2. 17 Hu and Deng's test setup (from Ref. [20])

Maybury's flapping wing mechanism, which is able to perform force measurements, is used for investigating the effect of changing the fore and hind wing stroke-phase relationship during hovering flight conditions [21].

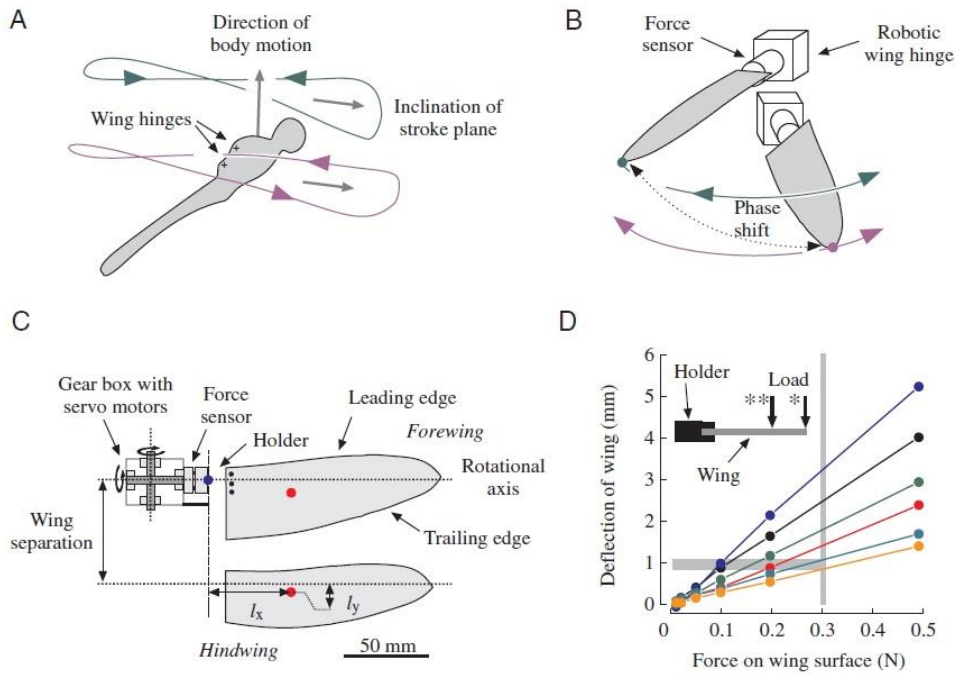


Figure 2. 18 Maybury's flapping wing mechanism (from Ref. [21])

Zhang's 3D flapping mechanism, which is used in a large water tank, is capable of executing various insect flapping motions and measuring forces around the wing. This study presents ground effects on three-dimensional insect-like flapping motion [22] (Figure 2.19).

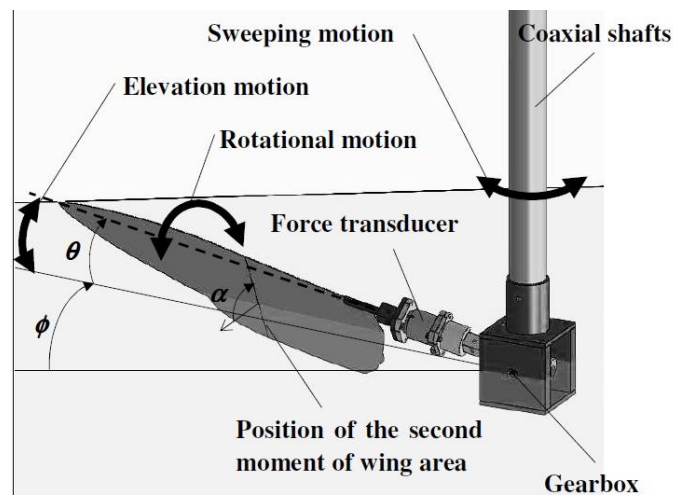


Figure 2. 19 Zhang's 3D flapping mechanism (from Ref. [22])

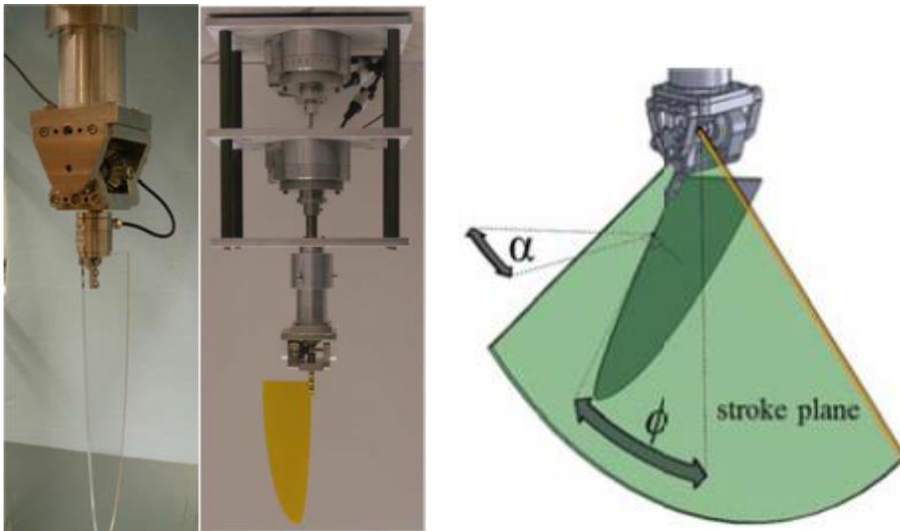


Figure 2.20 Morrison's flapping wing mechanism (from Ref. [23])

Morrison's flapping wing mechanism is capable of performing 2 DoF pitch and plunge flapping motion. Bevel gears are used to transfer the power to the wing to perform pitch and plunge motion. Experiments are conducted in water tank by using a force and torque sensor [23] [3].

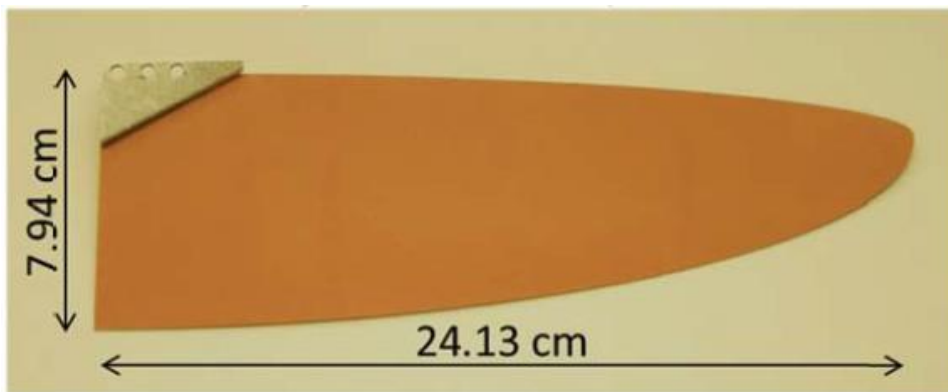


Figure 2.21 Zimmermann wing geometry which is used by Morrison (from Ref. [23])

Nagai's dynamically scaled mechanical model in water tunnel investigates the effects of motion kinematics of a flapping wing in hovering and forward flight on the aerodynamic characteristics. He used two types of motion kinematics, which are trapezoidal and sinusoidal type, to see their effect on the performance. His reference of the test win mimicked that of bumblebee, *Bombus terrestris* [24].

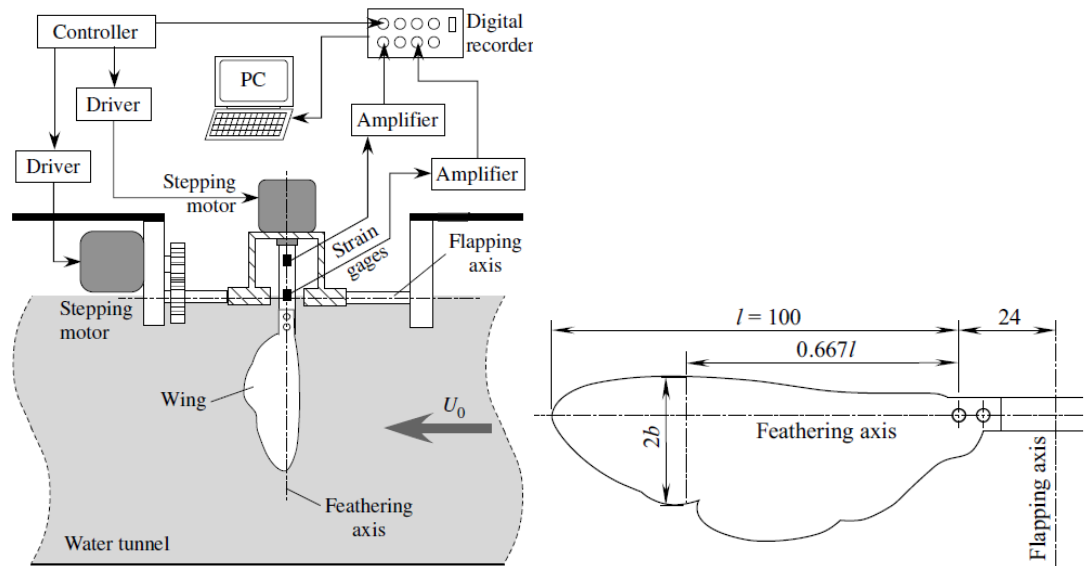


Figure 2. 22 Nagai's schematic mechanical model and wing geometry  
(from Ref. [24])

Several mechanism used to mimicking flapping flight are investigated in this section. General characteristics of these mechanisms are given Table 2.2 below. They provide a basis for a new flapping mechanism design and modification [3].

Table 2. 2 Several flapping wing mechanism characteristics

Flapping Mechanism	DoF	Flapping Frequency	Re	Operating Medium	Measurement System
Han et al. [17]	2	0.0868-0.278	5000-16000	Water	PIV-Force
George et al. [18]	3	0.667	31250	Water	Force
Isaac et al. [19]	2	0.22-0.29	5402-7054	Water	Force
Hu et al. [20]	4	0.5	1160	Oil	Force-Moment
Maybury et al. [3][21]	6	0.6	137	Oil	Force-PIV
Zhang et al. [22]	3	0.1	10000	Water	Force
Morrison et al. [23][3]	2	0.14	7100	Water	Force-Moment
Nagai et al. [24]	2	0.2-0.5	1000-5000	Water	Force



## CHAPTER 3

### FLAPPING MECHANISM

In this chapter, the technical features of the flapping mechanism which was developed previously by the Aerospace Engineering Department and the modifications which are made on this mechanism are presented. Reynolds number and Strouhal number are used to scale the mechanism [3]. The maximum angular velocity for each wing is 290deg/s. The mechanism has 3 DoF which makes it capable of mimicking different flapping trajectories. There are three computer controlled brushless motors for each wing. Each motor, which is controlled by computer, rotates only one shaft and each shaft is responsible for one rotational axis. The robotic wings are controlled by the software which is written by the department and the software has graphic user interference (GUI). The coupled kinematic equations of the three rotation axes are solved by the software to acquire the desired motion trajectories [3].

#### 3.1 System Definition

The mechanism was designed to imitate the flapping wing motion [3]. So the principle axis of the system was placed like the principle axis of the hummingbird (Figure 3.1). Wings are capable to rotate around x-axis which we called as pitch angle and it is shown with  $\alpha$ , y-axis which we called as plunge angle and it is shown with  $\beta$ , z-axis which we called as sweep angle and it is shown with  $\theta$  [3]. The flow distribution near the wing tried to be minimized by modifying the compact gear-box of the old system. The experiments done with this mechanism can be conducted in water, oil and even in air. The dimensions of the system was determined with equalization of the Reynolds and Strouhal numbers for both real cases and experimental cases [3]. An ATI Nano-17 force and moment transducer is used between wing and gear-box to measure force and moments occurring around the wing geometry. An additional part was designed to measure the pitch angle of the system.

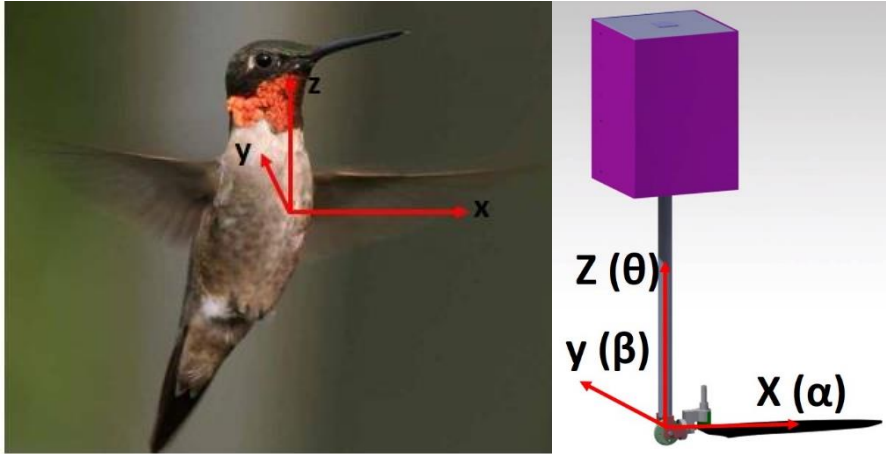


Figure 3. 1 Hummingbird and Robot-wing principle axis placement  
(Adopted from Ref. [3])

Angular position and velocity limits of the system at each axis are presented in Table 3.1. Motor specifications determine the maximum angular rates for the system [3]. Software of the system is restraining the limits of the maximum angular rates.

Table 3. 1 Motion limits of Robot-Wings (Adopted from Ref. 3)

	with Load Cell	without Load Cell
$\alpha$	$\pm 90^\circ$	$\pm 180^\circ$
$\beta$	$+45^\circ/-90^\circ$	$+45^\circ/-225^\circ$
$\theta$	$\pm 180^\circ$	$\pm 180^\circ$
$\dot{\alpha}$		160°/s
$\dot{\beta}$		290°/s
$\dot{\theta}$		290°/s

### 3.2 Mechanical Specifications

Flapping wing mechanism has mainly three sub parts which are the mechanical wrist, the transmission shaft, and the motor box. Since the transmission part and the mechanical wrist are working in the water, they were manufactured either stainless steel or aluminum [3]. Between the mechanical wrist and the wings, an ATI Nano-17 force and moment sensor is placed on. In motor box, timing belts are used to transfer the rotational power. The transmission shaft has three coaxial shafts, each of them is

used for one rotational axis. The mechanical wrist has bevel gears inside of it. Furthermore, data acquisition, system control and wing modules powering are provided by the control box [3].

### 3.2.1 Mechanical Wrist, Gearbox and Transmission Shafts

Mechanic arm is connected to the motor box via transmission shafts. As it is seen in the Figure 3.2 there are three coaxial shafts transmitting the power to the bevel gears. The yellow shaft is transmitting the power to the brown gears and brown gears is responsible for controlling the plunge motion. Blue shaft is rotating the green gears and green gears are responsible for controlling the pitch motion. The grey shaft is responsible for controlling the sweep motion and it is not directly connected to any gears, however it is directly connected to aluminum “U” part of the wrist. On the motor box side, all shafts are attached to the pulleys. Radio controlled model car differential gears are used to create the bevel gears [3]. All shafts have ball bearings between each other.

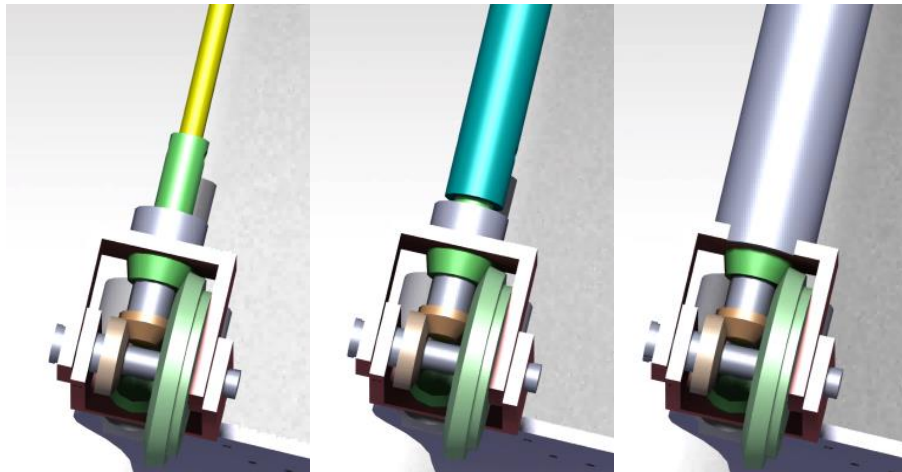


Figure 3. 2 Transmission shafts

Some modifications has been done on the mechanical wrist since there was a problem with the plunging and pitching motion. Every motion are coupled in this mechanism however by using software these coupled motions are being separated from each other. The inertia of the green gear which is responsible for controlling the pitch motion is much bigger than other gears since it is the biggest gear of the system. So if you want

to move the system on the pitch axis, system wants to move on the plunge axis too. It causes extra load and deformation on the motors and bearings. By using a roller bearing at the center of the biggest gear, the inertia of the gear is tried to be decreased (Figure 3.3).

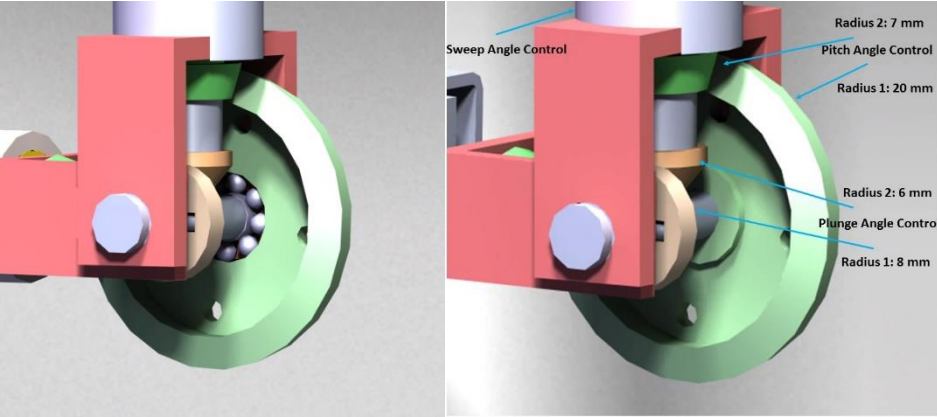


Figure 3. 3 Bevel gears with and without roller bearing

### 3.2.2 Motor Compartments

Three brushless MAXON DC motors with integrated encoders are used to transmit the power to the coaxial arm [3]. Power generated from the motors is transferred to the transmission shafts by using timing belts (Figure 3.4). Motor box has three compartments for each motors. Motors are connected to the transmission shafts in these compartments via using timing belts. The motor box is connected to heavy steel profiles via M8 bolts so mechanical vibrations are absorbed [3].

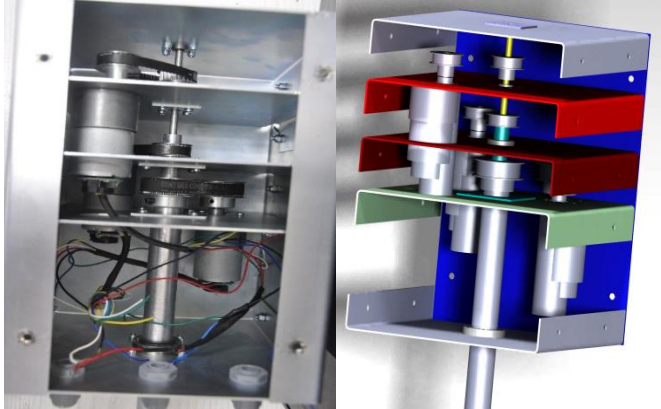


Figure 3. 4 The motor box of the Robot-Wings (Adopted from Ref. [3])

### 3.2.3 Control Box

Control-box has a 12V power supply, six motor drivers, two PIC based micro controller circuit for data acquisition, an embedded 2 GB memory for necessary drivers and an emergency power cut switch on the front panel [3]. Flapping wing mechanisms are connected to the Control-box. Control-box is connected to the PC via two USB as seen on the Figure 3.5.



Figure 3. 5 Control-Box of the robotic wings

### 3.2.4 The Mechanism on Which the Sensor is Located



Figure 3. 6 The Part on which the sensor is located

Between mechanical wrist and the sensor, an additional part must be inserted, since sensor should not be directly located on the mechanical wrist. Figure 3.6 presents the

old mechanism on which the sensor is located. Figure 3.7 shows the old and the new mechanism on which the sensor is located. The old mechanism as you see on the left side was made of carbon fiber plate. There were several problems about that part. Firstly the cable of sensor was being deformed when we gave act to the motors since the cable was not fixed anywhere. Once, we had to send the mechanism to the company for repairing since it was damaged. Secondly the old mechanism did not fit properly and there were spaces on the connection parts so the power was not being able to translate accurately. So a new mechanism was designed and manufactured by using 3D printer. Acrylonitrile Butadiene Styrene (ABS) which is a kind of plastic and used mostly in manufacturing the mechanical parts is used as the core material. The new material covers the sensor cable and preserve it to the potential damages. Also since it is monolithic, potential errors due to spaces between parts are avoided.

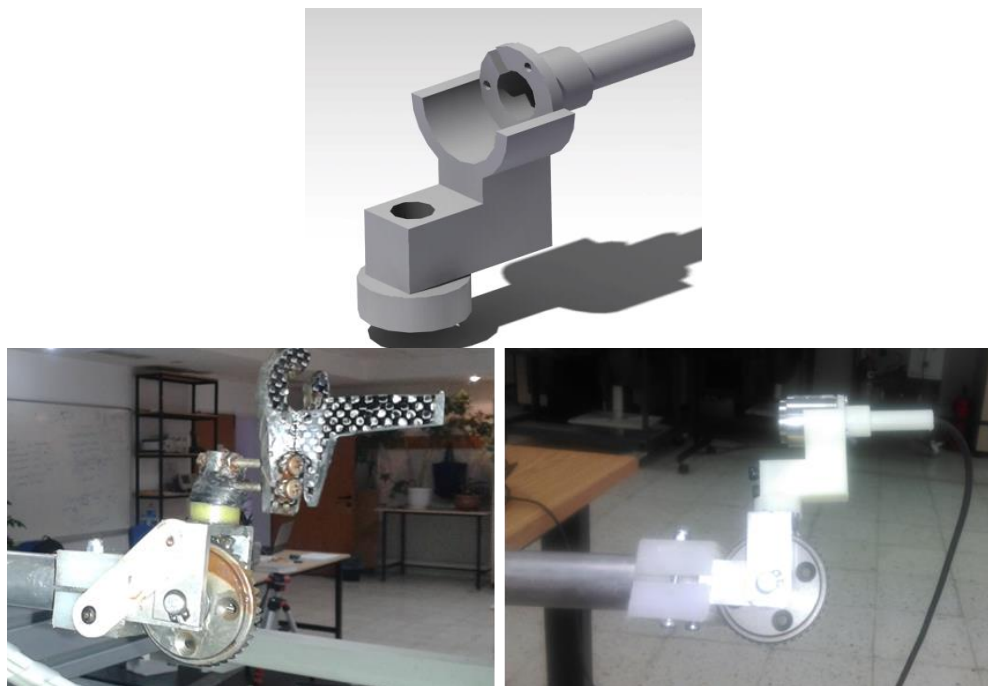


Figure 3. 7 The old (left), the new (right) mechanism and CAD drawing (above) of the new mechanism

### 3.3 Motion Kinematics

Since our robotic mechanism is new and it is in an experimental stage, the trajectories of the cases are chosen in clean configurations. Wing motion for this study is only in sweep axis since the pitch angle of the wing is set before the experiment was started.

However it is being planned to have complicated trajectories in future works. The trajectories of the future works will be as the trajectories in nature. In present study, only the outer shaft is moving during the experiment. Therefore the sinusoidal function which defines the wing motion is only time and frequency dependent. It can be easily shown as given in the Equation 9.

$$\theta(t) = A_0 * \sin(2\pi ft) \quad (9)$$

Where  $\theta$  is the sweep angle,  $f$  is frequency of the system and  $t$  is time after the experiment is started.

Our study is about only sweeping motion, however the mechanism is capable of performing three motions by using three electric motors. Since all motions are coupled a conversion matrix between motor motion and wing motion is needed in order to solve the complex coupling of the rotation axis [3]. The coefficients in the matrix, which are obtained by using the gears radius ratios, are valid for ideal gear system. Although we had some modifications on the mechanism, the coefficients are valid for new gear system too. Since we are trying to get the ideal gear system by doing these modifications, it could be assumed that these coefficients can be used in our matrix.

$$\begin{bmatrix} -1 & -3.308 & 1 \\ 0 & -1.8 & -1 \\ 0 & 0 & 1 \end{bmatrix} \begin{bmatrix} \alpha_w \\ \beta_w \\ \theta_w \end{bmatrix} = \begin{bmatrix} \alpha_m \\ \beta_m \\ \theta_m \end{bmatrix} \quad (10)$$

$$[C] \begin{bmatrix} \alpha_w \\ \beta_w \\ \theta_w \end{bmatrix} = \begin{bmatrix} \alpha_m \\ \beta_m \\ \theta_m \end{bmatrix} \quad (11)$$

Since the gears are coupled each other, the inner and mid-shafts must rotate reverse side while the outer shaft is rotating to prevent deformation on the motors and bearings and/or the unintentional pitch and plunge motion. Their relative angular velocity between shafts must be zero [3].

### 3.4 Hardware

The hardware is consisted of two wing modules and one control box. Each wing modules has three MAXON motors, three wings, one mechanical wrist and three coaxial shafts. The control box has two micro-controller circuits, which are used to control the wings, motor drivers, position reader and one power supply inside of it (Figure 3. 8).



Figure 3. 8 Hardware of the control box (Adopted from Ref. [3])

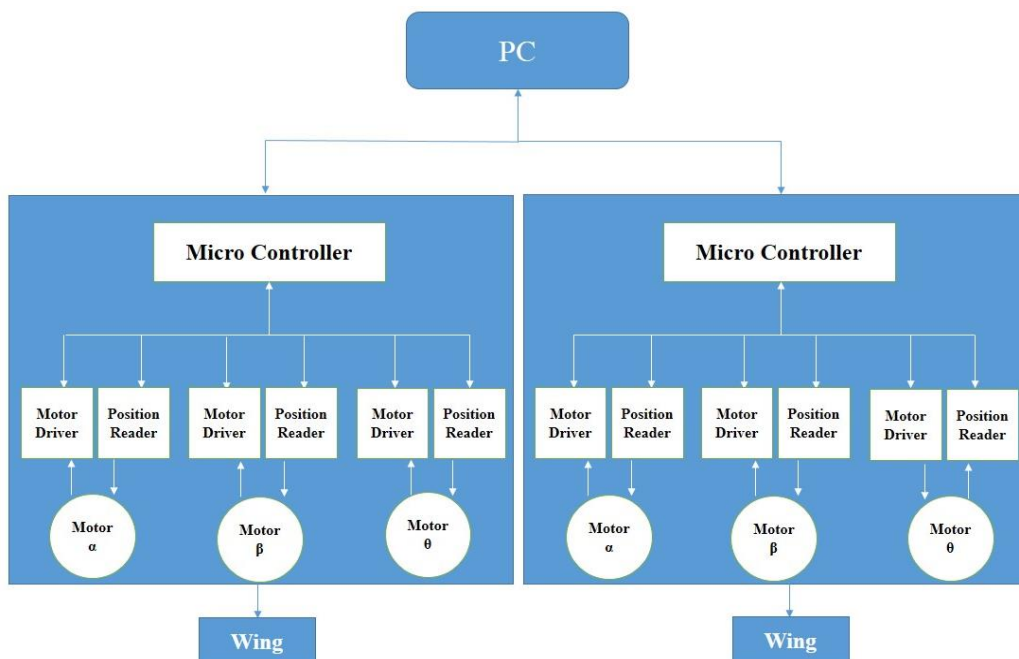


Figure 3. 9 Hardware block diagram (Adopted from Ref. [3])

As it is seen on the schematic diagram of the hardware, commands which comes from PC are going to the Micro Controllers. The Micro Controllers control the motors via using data coming from position readers. Each of the motors is responsible from only one axis rotation.

### 3.5 Software

The necessary motor motions for user defined wing positions are calculated by Wing-Sim, which is in-house software written for Robot-Wings. By multiplying the motor coupling matrix with the position vector  $(\alpha, \beta, \theta)$  of the wing axis, which is given in Equation 10, the position of three motors are calculated. The values are sent to micro-controllers constantly throughout the system runtime. Micro-controllers give the feedback (Motor positions) to the computer and the computer converts it to axis positions [3].

The flow chart for the control algorithm is given in Figure 3. 10. There are two data buffers for each motor. If the position data is lost, data from old buffer can be used for input position calculation. The computer sends the data to a new buffer, each time the motor use data of one buffer [3].

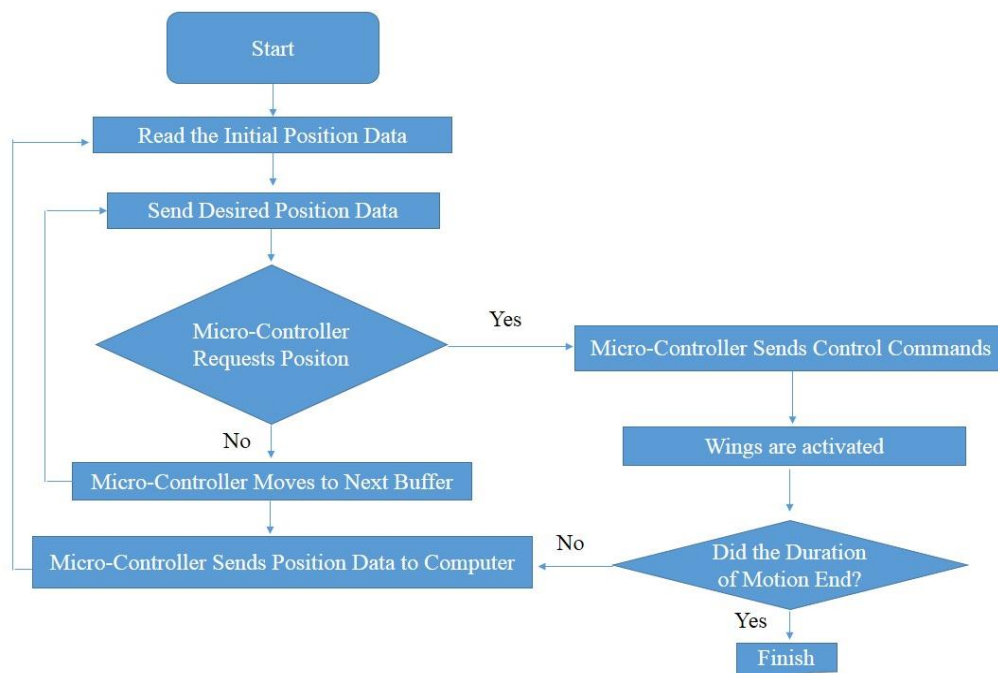


Figure 3. 10 Flow chart of the software (Adopted from Ref. [3])

The controller uses P-Controller to control the motions. P-constants for each motor were determined experimentally. P-constant must be recalculated, if operational mediums or wing geometries are changed. Since proportional controller could not compensate the small values of the Pulse-Width Modulation (PWM), a piecewise function is needed to be used which means when the error is big the K value will be used, when the error is small the PWM value will be constant and finally when it is too small then PWM value will be zero.

$$\psi(\varepsilon) = \begin{cases} 0 & , \quad \varepsilon \leq \varepsilon_0 \\ \psi_1 & , \quad \varepsilon_0 < \varepsilon \leq \varepsilon_1 \\ K_p \varepsilon & , \quad \varepsilon > \varepsilon_1 \end{cases}$$

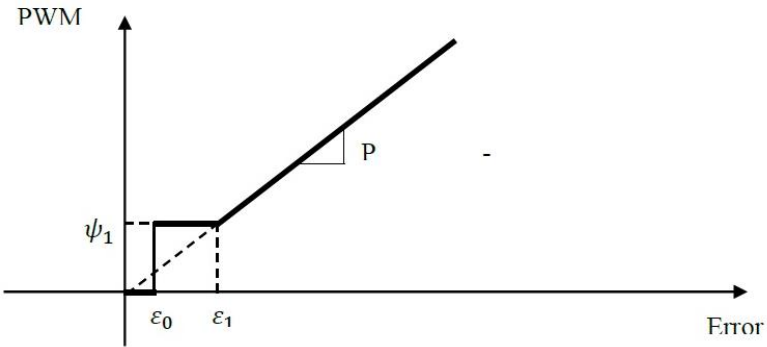


Figure 3. 11 PWM signal versus position error (from Ref. [3])

### 3.6 User Interface

Wing simulator, which is a software developed by the Department, is written to operate the Robot wings. Initial position of the wings is adjusted before the experiment is started via using this program. The program saves this initial data and wings return their initial position after the experiment is completed. As it is shown on Figure 3.10, there are sine, ramp or step function which defines the path of the wings during the experiment. Amplitude, period, offset, phase difference, delay and the motion duration can be defined for each wing independently [3].

<input type="checkbox"/> Wing 1 Pitch Active	<input type="checkbox"/> Wing 1 Plunge Active	<input type="checkbox"/> Wing 1 Sweep Active
Select Waveform: <input checked="" type="radio"/> Sine Function <input type="radio"/> Ramp Function <input type="radio"/> Step Function	Select Waveform: <input checked="" type="radio"/> Sine Function <input type="radio"/> Ramp Function <input type="radio"/> Step Function	Select Waveform: <input checked="" type="radio"/> Sine Function <input type="radio"/> Ramp Function <input type="radio"/> Step Function
Select Amplitude: <input type="text" value="360"/> deg	Select Amplitude: <input type="text" value="360"/> deg	Select Amplitude: <input type="text" value="360"/> deg
Select Period: <input type="text" value="2"/> Sec	Select Period: <input type="text" value="2"/> Sec	Select Period: <input type="text" value="2"/> Sec
Select Offset: <input type="text" value="0"/> deg	Select Offset: <input type="text" value="0"/> deg	Select Offset: <input type="text" value="0"/> deg
Phase Difference <input type="text" value="0"/> deg	Phase Difference <input type="text" value="0"/> deg	Phase Difference <input type="text" value="0"/> deg
Delay <input type="text" value="0"/> Sec	Delay <input type="text" value="0"/> Sec	Delay <input type="text" value="0"/> Sec
Duration <input type="text" value="0"/> Sec	Duration <input type="text" value="0"/> Sec	Duration <input type="text" value="0"/> Sec
<input type="checkbox"/> Wing 2 Pitch Active	<input type="checkbox"/> Wing 2 Plunge Active	<input type="checkbox"/> Wing 2 Sweep Active
Select Waveform: <input checked="" type="radio"/> Sine Function <input type="radio"/> Ramp Function <input type="radio"/> Step Function	Select Waveform: <input checked="" type="radio"/> Sine Function <input type="radio"/> Ramp Function <input type="radio"/> Step Function	Select Waveform: <input checked="" type="radio"/> Sine Function <input type="radio"/> Ramp Function <input type="radio"/> Step Function
Select Amplitude: <input type="text" value="360"/> deg	Select Amplitude: <input type="text" value="360"/> deg	Select Amplitude: <input type="text" value="360"/> deg
Select Period: <input type="text" value="2"/> Sec	Select Period: <input type="text" value="2"/> Sec	Select Period: <input type="text" value="2"/> Sec
Select Offset: <input type="text" value="0"/> deg	Select Offset: <input type="text" value="0"/> deg	Select Offset: <input type="text" value="0"/> deg
Phase Difference <input type="text" value="0"/> deg	Phase Difference <input type="text" value="0"/> deg	Phase Difference <input type="text" value="0"/> deg
Delay <input type="text" value="0"/> Sec	Delay <input type="text" value="0"/> Sec	Delay <input type="text" value="0"/> Sec
Duration <input type="text" value="0"/> Sec	Duration <input type="text" value="0"/> Sec	Duration <input type="text" value="0"/> Sec

Figure 3. 12 Trajectory setting menu

Figure 3.12 shows another menu of Wing-Sim program, on which we can adjust the initial position of the wings and save them. Left side of the menu shows the angular positions of the wings. Middle side is the cursor block, which provides control over the wing axes by sliding the cursers. Right side of the menu shows the angular position of the motors and PWM signal for each motor [3].

### No Connection

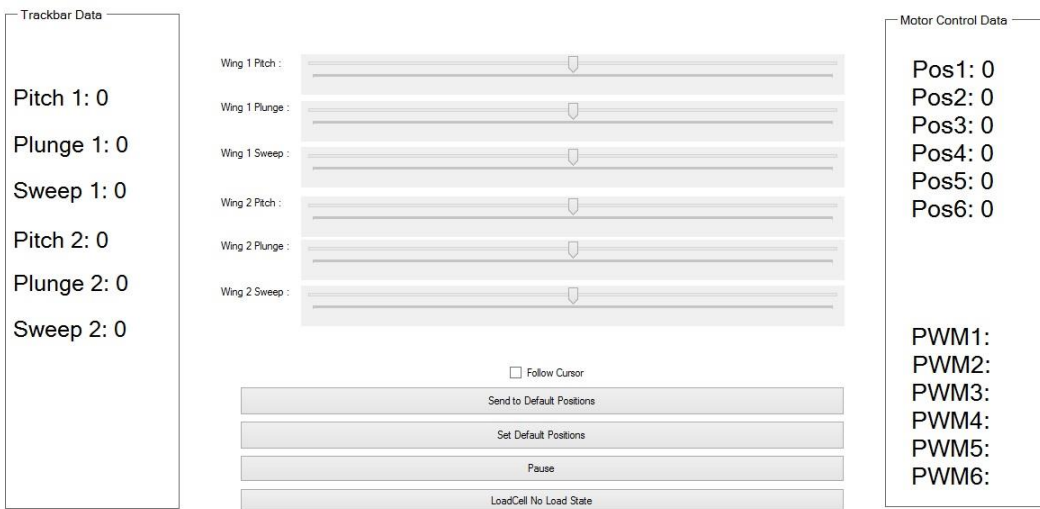


Figure 3. 13 Position settings menu

Proportional constants of the system and sampling time of the system can be changed by using the Advanced Settings menu. Moreover, a minimum PWM value can be defined for the axis [3].

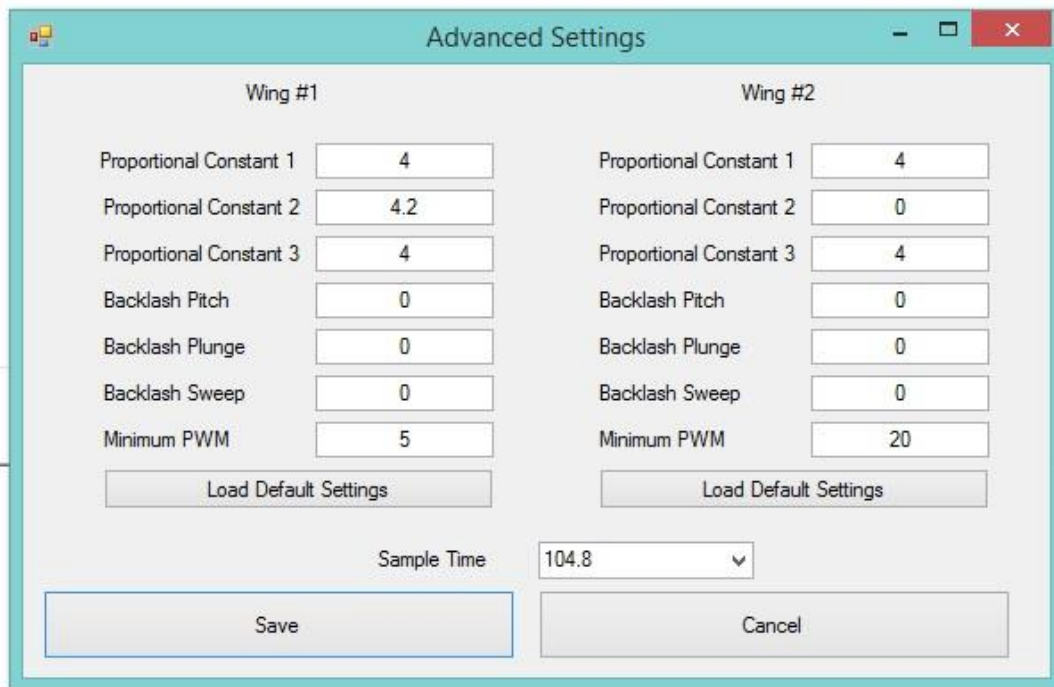


Figure 3. 14 Advanced settings menu

## CHAPTER 4

### EXPERIMENTAL METHOD

Force and moment measurements as part of the experiments are conducted in water tank which is in the Aerodynamic Laboratory at the Department of Aerospace Engineering of METU. There is a special experiment room, which has a purified water source to fill the water tank and drainage to empty them in the laboratory [3]. 0.8mx0.8mx2m water tank is used in the experiments. Three types of wing geometry, which are called as Flat plate, Zimmermann and Hummingbird, are investigated in zero free-stream velocity. ATI Nano 17 IP65/IP68 transducer is used to perform the force and moment measurements. Data obtained from transducer is converted from wing fixed frame to inertial frame in MATLAB. Weight is extracted from the total force via using a MATLAB code.

#### 4.1 Experimental Setup

A brief explanation about the experimental setup is given in this part of the study. Initially, the wing models, water tank, and flapping mechanism and the data collection unit used as part of these experiments will be explained. Secondly important features of the experiments such as flow characteristics, how force and moment measurements are done, converting the wing fixed frame into the inertial frame, the path which wings follow, experimental procedure and conditions will be given.

##### 4.1.1 Wing Models

Three types of wings, which are called as Flat Plate, Hummingbird and Zimmermann, are used as part of this study. The wings, which have same wing span (260 mm) and root chord (79 mm), are made of 3 mm thick carbon plates. They have holes at the intersection of their root chords and leading edges to locate the sensor on. These holes are drilled very carefully to be sure that the axes of the wings and axes of the sensor

are matched perfectly. Since we have mechanical wrist at the back of the wing, the flapping axis is approximately 77 mm away from the wings root chord.



Figure 4. 1 Flat plate wing geometry

The Flat plate wing is a rectangular plate which is used to see how the aerodynamic shape of the wing will affect the results of the cases. It has a bigger area and mass than the other wings (Figure 4.1).



Figure 4. 2 Hummingbird wing geometry

The Hummingbird wing is a carbon fiber replica of a real bird wing (Figure 4.2). It is used to see the aerodynamic effect of a real bird wing in unsteady flow. It is scaled to have same wingspan with the Zimmermann wing since it gives a chance to compare our results with the Mutlu's (Ref. [3]) study.



Figure 4. 3 Zimmermann wing geometry

Zimmermann wing was manufactured as part of Mutlu's (Ref. [3]) study previously. The wing is made by using two quarter ellipse sharing a major axis passing through

wing quarter chord. It was fabricated from multi axial carbon fiber fabric [3] (Figure 4.3).

#### 4.1.2 Water Tank

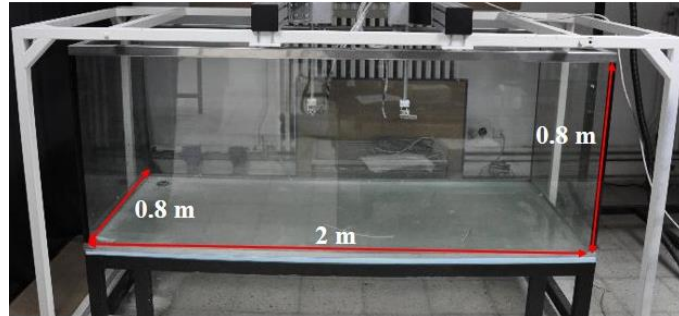


Figure 4. 4 Water tank with its dimensions (Adopted from Ref. [3])

The water tank, which is made of 1.5 cm thick glass, has 0.8 m height, 0.8 m depth and 2 m length. The wing must be placed very carefully to avoid boundary effects of the walls. 12 chord length distances from wings to wall in both forward and backward directions and 7 chord length distances in span wise direction is provided by 2 meter length and 0.8 m depth of the water tank according to Mutlu's study [3]. A shock absorber is put under the water tank to avoid mechanical vibrations [3]. Water tank is filled with water until 0.7 m height.

#### 4.1.3 Positioning System

Robotic mechanism, which is designed to mimic the flapping wing motion, is used as positioning system. It is placed on the Support Bench of the water tank to separate them from the water tank. Robotic mechanism uses PIC based custom made micro-controller boards for data acquisition [3]. They are connected to host computer via using RS-232 cables. As it is seen in Figure 4.5 the wings are submerged in water to perform the flapping motion. They are adjusted to their initial position by using Wing-Sim program. Also by using same program the trajectory of the positioning system is determined. This mechanism needs 220 V AC separate power supply to work.

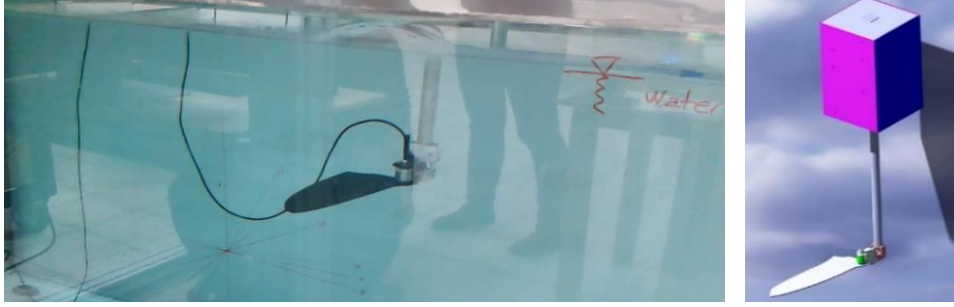


Figure 4. 5 Wings position in water and CAD drawing of the positioning system

#### 4.1.4 Force and Moment Measurement

The transducer has been favored due to its small dimensions and water-proof feature. Sampling frequency of the all experiments was 1000 Hz. NI Labview which is a program to record the data measured by the transducer is used in force and moment measurement. Before the experiment is started, water rested for 10-15 minutes to avoid the noises of the previous case. At the beginning of the experiment, data has been recorded without giving act to the wings for approximately 20 seconds to see the impulsive motion of the wings. This data is erased by using the MATLAB code. 50 flap cycles are performed to obtain phase-averaged flow quantities. The statistical mean values are obtained for a single phase by averaging the data per flap phase. The standard deviation of the mean data is calculated to determine the uncertainty of the mean value. The standard deviation is determined by using following equation:

$$\sigma = \sqrt{\frac{1}{n-1} \sum_{i=1}^n (x_i - \bar{x})^2} \quad (12)$$

Where ‘n’ is the number of flapping frequency  $\bar{x}$  is the mean value of the force or moment for 50 cycles.

#### 4.2 Flow Characteristic

The water is rested before starting the experiment to carry out the experiments in zero free-stream velocity [3]. Kurtuluş [2] expresses that water needs to be rested at least 15 minutes to have a steadiness of the flow in the water tank. The steadiness is also crosschecked by looking the measurements of the transducer since the transducer can show if there is any wave in water or not. The density of the water is  $998.2 \text{ kg/m}^3$ ,

dynamic viscosity is  $1.003 \times 10^{-3}$  and kinematic viscosity is  $1.004 \times 10^{-6}$  at  $20^\circ\text{C}$ . Carbon filters are used to obtain purified water from tap water [3].

### 4.3 Transducer

A transducer, which is capable of 6-axis force and moment measurement and named as ATI Nano17, is used in this study. It is protected against water spray and can be submerged in water until 4 m. It is made of stainless steel and has cylindrical shape with 20 mm diameter and 22 mm heights [3]. Its capabilities are given in Table 4.1. The transducer has three additional parts which are Signal amplifier, DAQ and power supply with it. The transducer is placed to be perpendicular to wing models at the intersection of the leading edge and root chord of the wing. The data obtained from the transducer can be recorded by using NI Labview Software. Detailed information about Labview will be given in next section.

Table 4. 1 Transducer Sensing ranges and resolution (Adopted from Ref. 3)

Calibration	Sensing Ranges				Resolution			
	$F_x, F_y$	$F_z$	$T_x, T_y$	$T_z$	$F_x, F_y$	$F_z$	$T_x, T_y$	$T_z$
SI-12-0.12	12 N	17 N	120 Nmm	120 Nmm	1/320 N	1/320 N	1/64 Nmm	1/64 Nmm
SI-25-0.25	25 N	35 N	250 Nmm	250 Nmm	1/160 N	1/160 N	1/32 Nmm	1/32 Nmm
SI-50-0.50	50 N	70 N	500 Nmm	500 Nmm	1/80 N	1/80 N	1/16 Nmm	1/16 Nmm

### 4.4 Labview Measurement Block

Reading and recording of the data, which is coming from ATI Nano F/T transducer and NI DAQ Board during the experiments, are done by using a Labview program block.

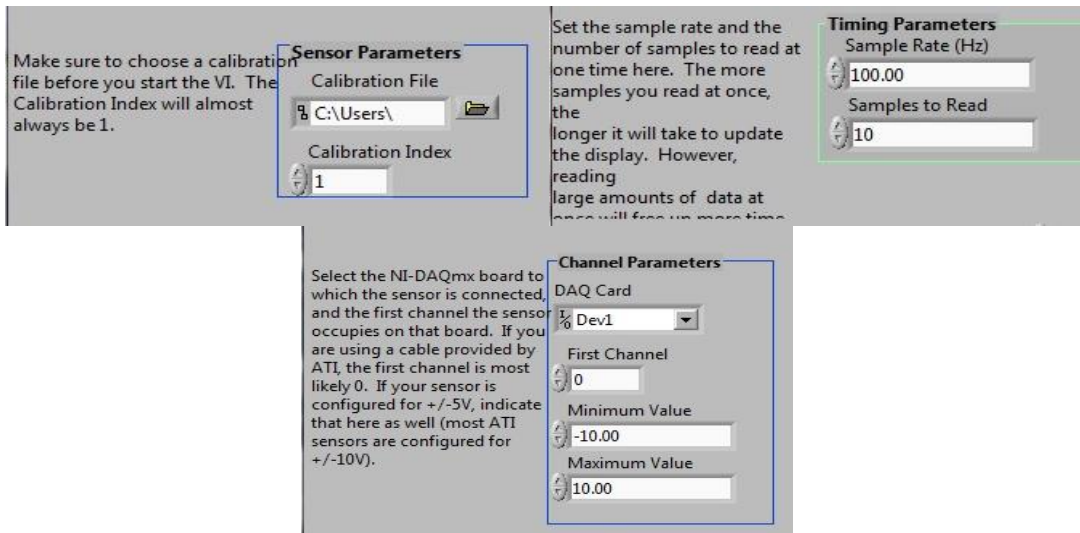


Figure 4. 6 Labview program block-1

Figure 4.6 shows the part that we introduce the sensor parameters, Channel parameters and timing parameters to the program in Labview program block. In sensor parameter section, we choose the calibration file given by the manufacturer of the sensor. In channel parameters section, we choose the DAQ card, minimum and maximum value of the F/T to read. In timing parameter section, sample rate which means how many measurements in a second will be done by transducer, and samples to read which means how many data will be shown on the Labview program are chosen.

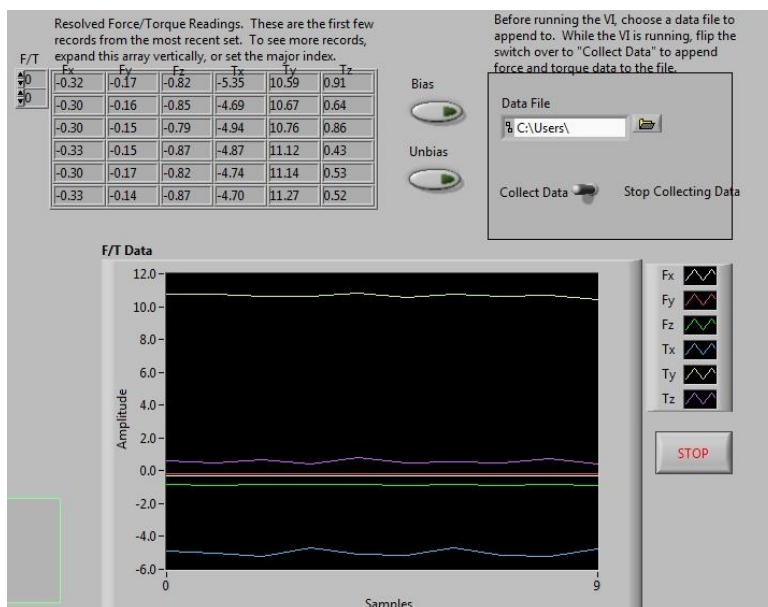


Figure 4. 7 Labview program block-2

All six measurements can be plotted simultaneously as it is seen in Figure 4.7. Real time force and moment readings are shown upside of the Figure 4.7. It can be chosen where to save the output data by this program. Bias of the readings can be eliminated by using Bias section. Figure 4.8 shows the calibration matrix and the voltages measured by the transducer.

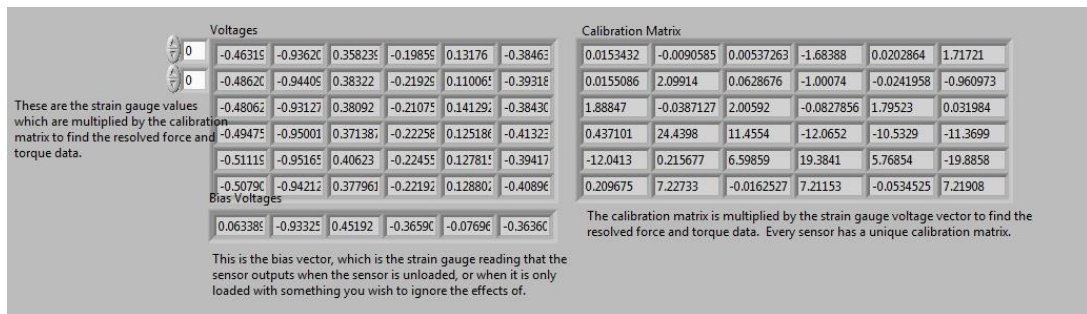


Figure 4. 8 Labview program block-3

## 4.5 Coordinate Transformation

The main objective of the coordinate transformation is to measure the flapping angles, the lift force and the drag force accurately as the mechanism executes specified flapping trajectories [18]. Since we placed the transducer on the wings, the measured quantities are expressed in the wing-fixed coordinate frame. To obtain lift and drag forces we must convert the data into the earth-fixed frame. Figure 4.9 shows the difference between earth-fixed and wing-fixed frames. Euler angle transformation must be done to obtain the data w.r.t earth-fixed frame. In these equations;  $\theta_1$  is the angle around the x axis,  $\theta_2$  is the angle around y axis and  $\theta_3$  is the angle around z axis.

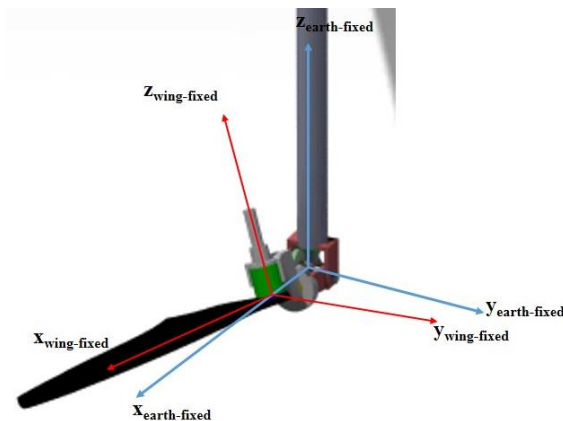


Figure 4. 9 Earth-fixed and wing-fixed coordinate systems

$$R(\theta_3\theta_2\theta_1) = \begin{bmatrix} 1 & 0 & 0 \\ 0 & \cos\theta_3 & -\sin\theta_3 \\ 0 & \sin\theta_3 & \cos\theta_3 \end{bmatrix} \begin{bmatrix} \cos\theta_2 & 0 & \sin\theta_2 \\ 0 & 1 & 0 \\ -\sin\theta_2 & 0 & \cos\theta_2 \end{bmatrix} \begin{bmatrix} \cos\theta_1 & \sin\theta_1 & 0 \\ -\sin\theta_1 & \cos\theta_1 & 0 \\ 0 & 0 & 1 \end{bmatrix} \quad (13)$$

If matrix multiplication is done;

$$R(\theta_3\theta_2\theta_1) = \begin{bmatrix} \cos\theta_2\cos\theta_1 & \cos\theta_2\sin\theta_1 & -\sin\theta_2 \\ \sin\theta_3\sin\theta_2\cos\theta_1 - \cos\theta_3\sin\theta_1 & \sin\theta_3\sin\theta_2\sin\theta_1 + \cos\theta_3\cos\theta_1 & \sin\theta_3\cos\theta_2 \\ \cos\theta_3\sin\theta_2\cos\theta_1 + \sin\theta_3\sin\theta_1 & \cos\theta_3\sin\theta_2\sin\theta_1 - \sin\theta_3\cos\theta_1 & \cos\theta_3\cos\theta_2 \end{bmatrix} \quad (14)$$

The force expressed in the earth-fixed frame can be then found from single component of force measured in the wing-fixed frame using;

$$F_{earth} = R(\theta_3\theta_2\theta_1)^T F_{wing} \quad (15)$$

Then we can write the transpose of the rotational matrix to the equation;

$$F_{earth} = \begin{bmatrix} \cos\theta_3\cos\theta_2 & \cos\theta_3\sin\theta_2\sin\theta_1 - \sin\theta_3\cos\theta_1 & \cos\theta_3\sin\theta_2\cos\theta_1 + \sin\theta_3\sin\theta_1 \\ \sin\theta_3\cos\theta_2 & \sin\theta_3\sin\theta_2\sin\theta_1 + \cos\theta_3\cos\theta_1 & \sin\theta_3\sin\theta_2\cos\theta_1 - \cos\theta_3\sin\theta_1 \\ -\sin\theta_2 & \cos\theta_2\sin\theta_1 & \cos\theta_2\cos\theta_1 \end{bmatrix} F_{wing} \quad (16)$$

Since the plunge angle is zero for this study;

$$F_{earth} = \begin{bmatrix} \cos\theta_3 & -\sin\theta_3\cos\theta_1 & +\sin\theta_3\sin\theta_1 \\ \sin\theta_3 & +\cos\theta_3\cos\theta_1 & -\cos\theta_3\sin\theta_1 \\ 0 & \sin\theta_1 & \cos\theta_1 \end{bmatrix} F_{wing} \quad (17)$$

#### 4.6 Motion Kinematics and Wing Trajectory

Two types of wing trajectories which are 60° and 120° are used in the experiments. Only angular velocities are changed in these trajectories. Figure 4.10, where 'θ' is the sweep angle and α is the pitch angle, shows the path which the wings followed schematically. Before the experiment is started, the pitch angle is set and it is constant during the experiment. As a result, the equation of motion is time (t), sweep angle (θ) and frequency (f) dependent only.

$$\theta(t) = A_0 * \sin(2\pi ft) \quad (18)$$

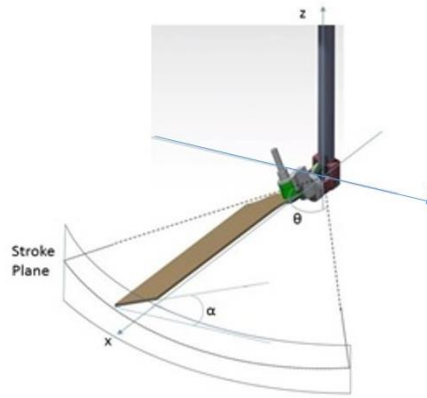


Figure 4. 10 Wing trajectory and stroke plane illustration

#### 4.7 Results of Previous Experimental Setup and Verification Study

Results of previous experimental setup were verified by Mutlu’s study [3] by comparing it with Morrison’s results. Figure 4.11 shows that order of magnitude of the Mutlu’s study is close to Morrison’s results. This verification proved that results of our experimental setup is valid under these circumstances.

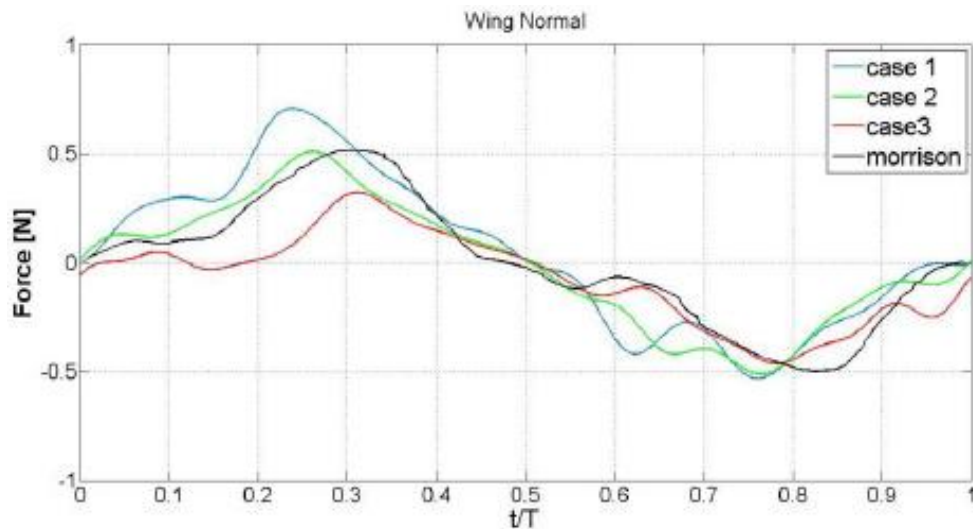


Figure 4. 11 Comparison of the phase averaged normal force time histories of previous experimental setup ( $A_{pitch}=30^\circ, 45^\circ, 57^\circ$ ) and Morrison’s experiment ( $A_{pitch}=57^\circ$ ) for one period of flapping motion

Figure 4.12 shows the time history of the normal forces for both Mutlu’s study [3] and present study. The figure on the left shows the forces for the pure plunge motion of

58 °/s with 30° constant pitch angle. The figure on the right shows the forces for the pure plunge motion of maximum angular velocity of 36 °/s with 30° constant pitch angle. Since two cases use same wing (Zimmermann), we can use the results of the Ref. [3] as the verification results. It is clearly seen that, when the case of present study reaches its maximum angular velocity, the order of magnitude for both case are the same. However, the magnitude of the peak normal force of the present study (Figure 4.12) is smaller than previous study since the angular velocity of the present study (Figure 4.13) is smaller than previous one. Therefore, we could assume that our cases results are valid under these circumstances. Furthermore these results will be compared with the CFD results in future works.

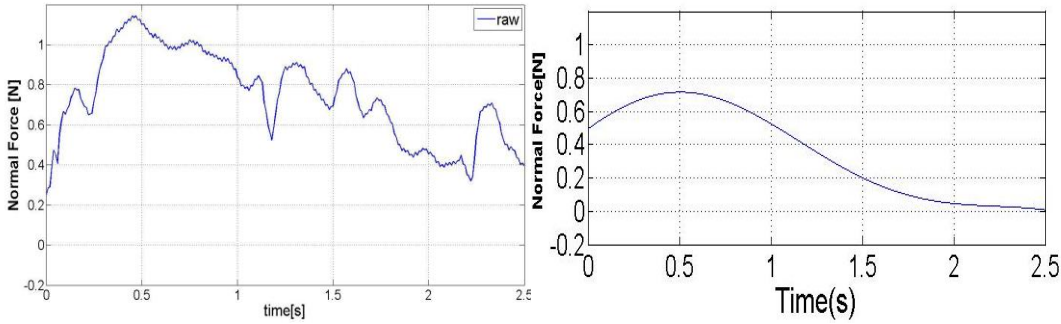


Figure 4. 12 Time history of normal forces of Mutlu’s study (Left) (From Ref. [3]) and present study (Right)

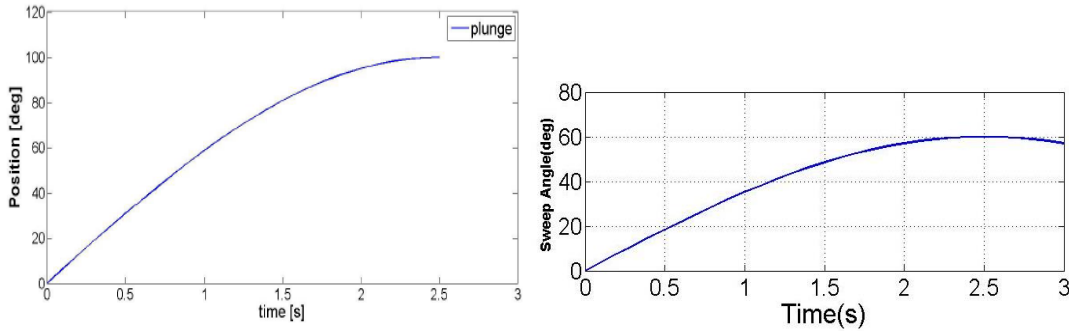


Figure 4. 13 Time history of plunge angle for pure plunge motion of 58 °/s for Mutlu’s study (left), sweep angle variation for pure sweep motion which has a maximum angular velocity of 36 °/s for present study (right)

## 4.8 Experimental Procedure

This part is mainly focuses on preparation before the experiments, performing the experiments and post processing. In preparation section, we fill the tank with purified water till the 70 cm level is reached. The flapping axis is placed 20 cm beneath the water surface, 88 cm away from the side wall and 27 cm away from the rear wall of the tank [3]. The voltage of the power supply is measured constantly during the experiments since a high voltage could damage the transducer. NI Labview program is used to read and record the data. In performing section, wing initial position has been set, bias due to gravitation is set to zero, 50 cycles has been performed and 15 minutes pauses given between the cases. In post processing section, raw data is processed to have filtered data. A low Butterworth filter is used with 0.5 Hz Cut-off frequency to erase the noises (Figure 4.14). However we should be very careful while we are deciding the Cut-off frequency since the Cut-off frequency must include the frequency of the harmonic contents of the normal forces. Then, total lift and drag forces have been calculated. Finally  $C_L$  values have been plotted and compared for each wing.

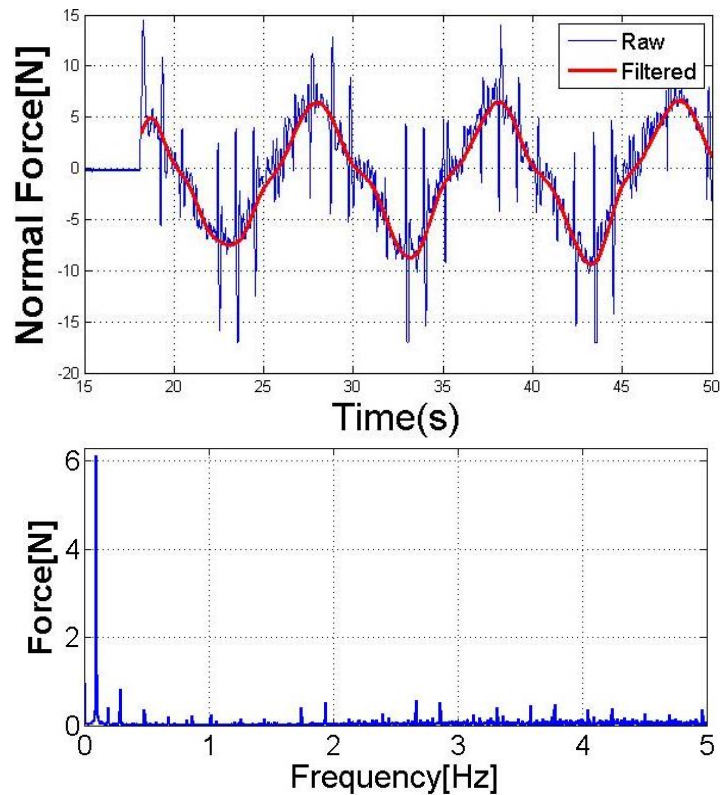


Figure 4. 14 Raw and filtered normal forces in periodic region (above) and normal force harmonic contents of the raw data (below)



## CHAPTER 5

### RESULTS AND DISCUSSION

In this chapter, all results which are obtained from measurements and interpreted from 21 cases (7 cases for each wing geometry) by using a special MATLAB code will be presented. Firstly, 3 wing geometries are compared with each other and each cases are handled separately. Data is filtered by using a Butterworth filter with a 0.5 Hz cut-off frequency. Time history of the normal force components in both impulsive and periodic region are given. Phase averaged normal and total forces for periodic region, the variation of the lift and drag forces for whole case, and  $C_L$  values are calculated by using raw data for each case. Last 40 periods are used to obtain phase averaged data of the aerodynamic forces. 40 data is totalled and averaged for each instant of the strokes by the MATLAB code. Also, FFT analysis is done to see the harmonic contents. In second part of the Chapter 5, variation of the lift forces and  $C_L$  values with respect to angle and time is shown.  $C_L$  values are calculated as follows;

$$C_L = \frac{L}{\frac{1}{2}\rho\bar{U}^2 A_{ref}} \quad (19)$$

where  $\bar{U}$  is given in Eq.(1) and  $A_{ref}$  is the reference areas of the wings given in Table 5.1. In the last part of the Chapter 5, uncertainties of the experiments and added mass effect are investigated. Since, the experiments are performed in water, virtual mass effect of the water must be considered to see the order of magnitude of the added mass with respect to measured normal forces.

Table 5.1 gives detailed information about the operation condition and the wings used as part of the study. Two types of Reynolds number, which are Mean Aerodynamic Chord based and Root Chord based, are calculated for each case. Sampling frequency of the sensor, frequency and period of the system and stroke cycles number are given in Table 5.1.

Table 5. 1 Experimental conditions for all cases

Flat Plate (MAC:75.6 mm) (Root Chord:74.25 mm) (A <sub>ref</sub> :0.019 m <sup>2</sup> )			Hummingbird (MAC:62.46 mm) (Root Chord:73.248 mm) (A <sub>ref</sub> :0.016 m <sup>2</sup> )			Zimmermann (MAC:68.04 mm) (Root Chord:75.11 mm) (A <sub>ref</sub> :0.015 m <sup>2</sup> )			
Case	Sweep	Pitch	Re <sub>1</sub> /Re <sub>2</sub>	Sweep	Pitch	Re <sub>1</sub> /Re <sub>2</sub>	Sweep	Pitch	Re <sub>1</sub> /Re <sub>2</sub>
1	60	5	8980/15160	60	5	6376/14956	60	5	7050/15336
2	60	30	8980/15160	60	30	6376/14956	60	30	7050/15336
3	60	45	8980/15160	60	45	6376/14956	60	45	7050/15336
4	120	5	17960/31120	120	5	12753/29912	120	5	14100/30672
5	120	30	17960/31120	120	30	12753/29912	120	30	14100/30672
6	120	45	17960/31120	120	45	12753/29912	120	45	14100/30672
7	120	90	17960/31120	120	90	12753/29912	120	90	14100/30672
Sampling Frequency			Frequency	Period		Number of Cycle			
1000			0.1	10		50			

## 5.1 Cases

### 5.1.1 Case 1

Pure sweep motion with time dependent angular velocity at constant 5° pitch angle is investigated in Case 1. Wings are sweeping 60° in one half stroke. They are starting the motion at 0° and sweeping between 30° and -30° (Figure 5.1). They reach their maximum angular velocity at 0°.

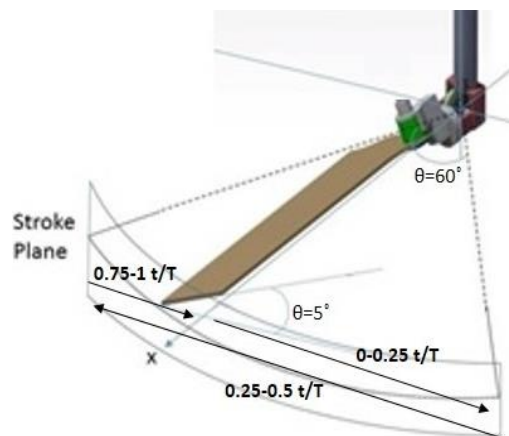


Figure 5. 1 Wing trajectory in one stroke for Case 1

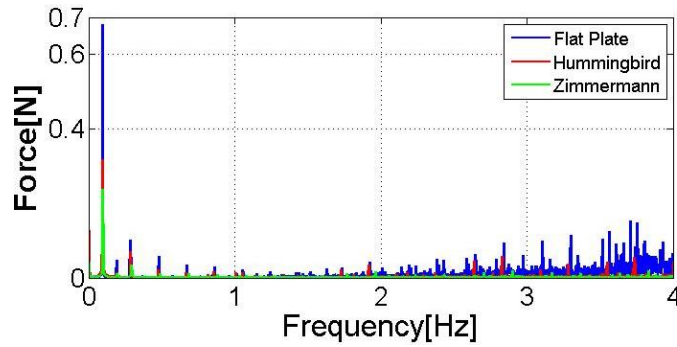


Figure 5. 2 Normal force harmonic contents of the Case 1

In FFT analysis (Figure 5.2), it is clearly seen that maximum force amplitude is at 0.1 Hz which is the flapping frequency of the system. Cut-off frequency can be decided for filtering by looking the FFT analysis.

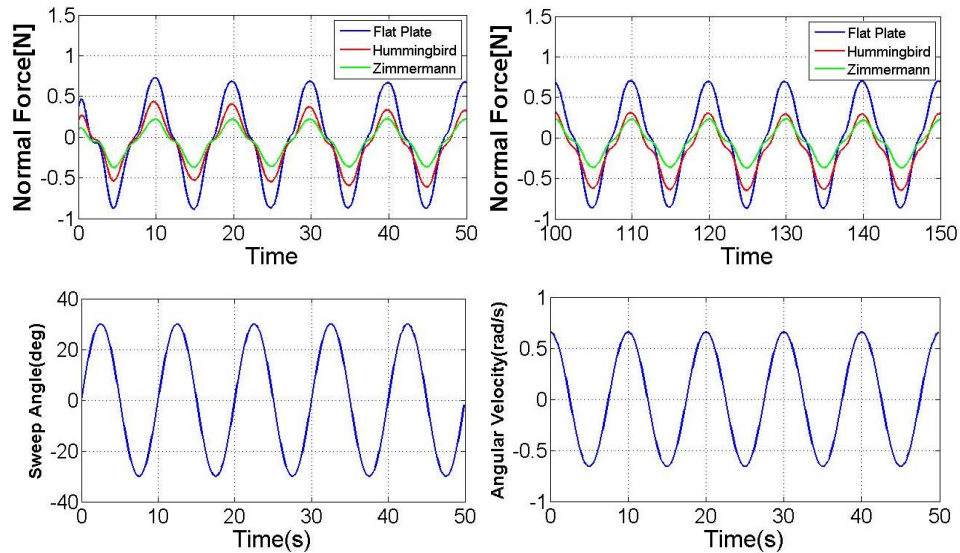


Figure 5. 3 Time history of normal force component in both impulsive and periodic region for 5 stroke cycles with sweep angle and angular velocity variations for Case 1

Approximately, 20 seconds steady state values were recorded before the wings were started to move. This data extracted from raw data and the rest divided into two parts. First 10 cycles are assumed as impulsive region and last 40 cycles are assumed as periodic regions (Figure 5.3). As angular velocity increases, an increase in normal force is clearly seen. Angular velocity has its maximum value at  $0^\circ$ . In both regions normal forces of the flat plate is bigger than the others since it has a bigger reference area.

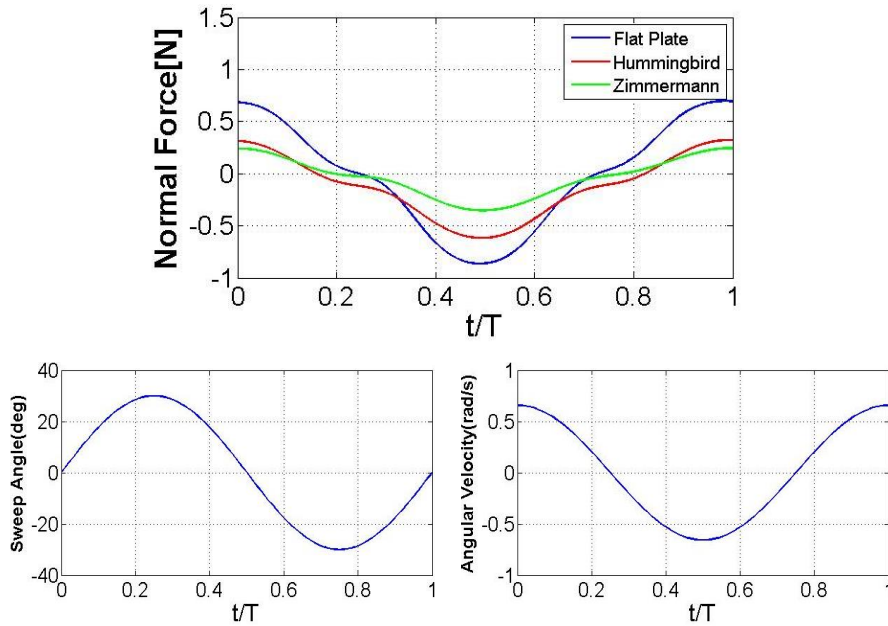


Figure 5. 4 Phase averaged and filtered normal force components in periodic region with sweep angle and angular velocity variations for Case 1

The normal forces for each wing are averaged per flap phase to see their tendency in one cycle. At the half of the stroke the wings reaches their maximum force value since they reach the maximum angular velocity. Zimmermann has less normal forces tendency than others due to its shape and reference area. As it is seen in Figure 5.4, all three wings have almost the same tendencies in both periodic region.

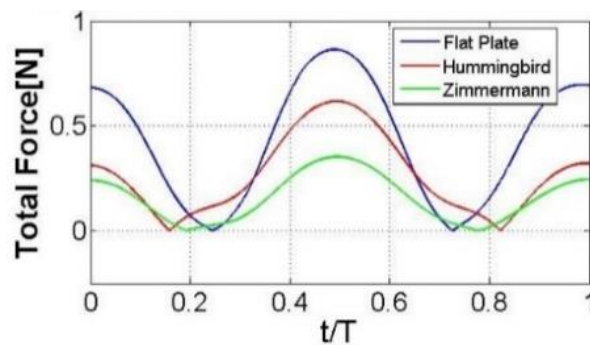


Figure 5. 5 Phase averaged total forces of three wings for Case 1

Figure 5.5 shows the total force calculated from vectorial summation of the normal and tangential forces. It is almost the same as normal force values since the tangential forces are so small for this pitch angle.

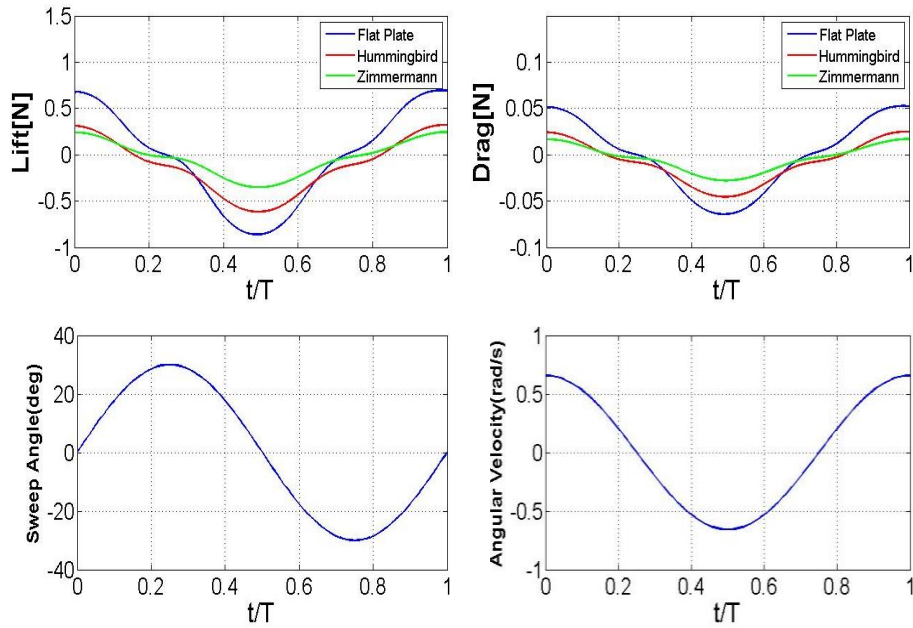


Figure 5. 6 Phase averaged lift and drag forces of three wings with sweep angle and angular velocity variations for Case 1

Lift force is the vertical component of the total force and drag force is the horizontal component of the total force. Note that lift forces are approximately ten times bigger than drag forces. Maximum lift is generated on the flat plate however  $C_L$  values must be checked for the efficiencies of the wings (Figure 5.6). Maximum lift is obtained when the angular velocity is 0.63 rad/s.

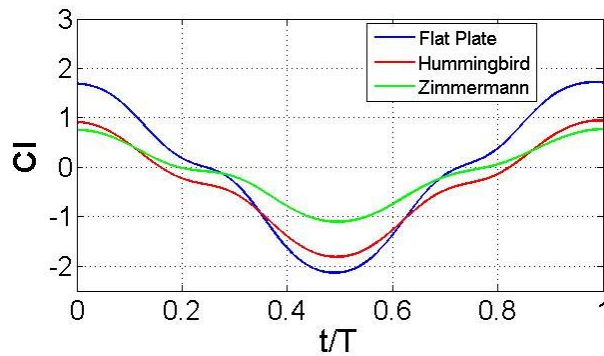


Figure 5. 7  $C_L$  coefficient variations for each three wings for Case 1

Figure 5.7 shows the  $C_L$  values for each wing geometry. In this case Flat plate has maximum  $C_L$  values, hummingbird also efficient in downstroke. Zimmermann has same tendency in both up and down stroke.

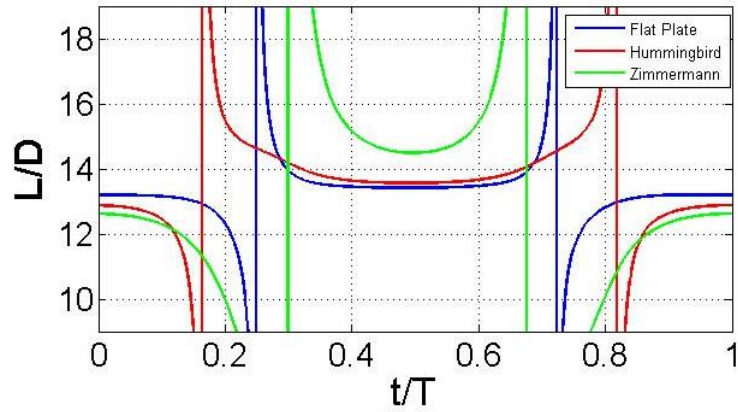


Figure 5. 8 L/D ratios of 3 wings during one cycle for Case 1

L/D ratios for Case 1 is given in Figure 5.8. It is going infinity as lift and drag tends to zero. Since lift and drag goes zero at  $-30^\circ$  and  $30^\circ$ , the curve goes infinity and comes back. In Case 1, constant L/D ratios are 14.5 for Zimmermann, 13.6 for Hummingbird and 13.4 for Flat plate.

### 5.1.2 Case 2

Pure sweep motion with time dependent angular velocity at constant  $30^\circ$  pitch angle is investigated in Case 2. Wings are sweeping  $60^\circ$  in one half stroke. They are starting the motion at  $0^\circ$  and sweeping between  $30^\circ$  and  $-30^\circ$  (Figure 5.9). They reach their maximum angular velocity at  $0^\circ$ .

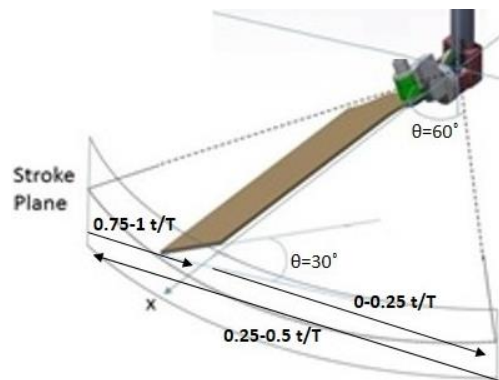


Figure 5. 9 Wing trajectory in one cycle for Case 2

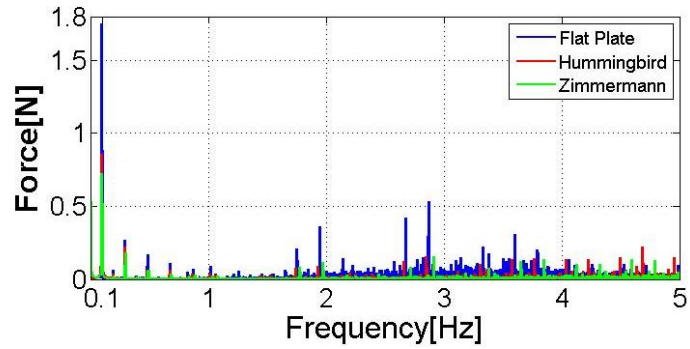


Figure 5. 10 Normal force harmonic contents of each three wings for Case 2

In FFT analysis (Figure 5.10), it is clearly seen that maximum force amplitude is at 0.1 Hz which is the flapping frequency of the system. Cut-off frequency can be decided for filtering by looking the FFT analysis.

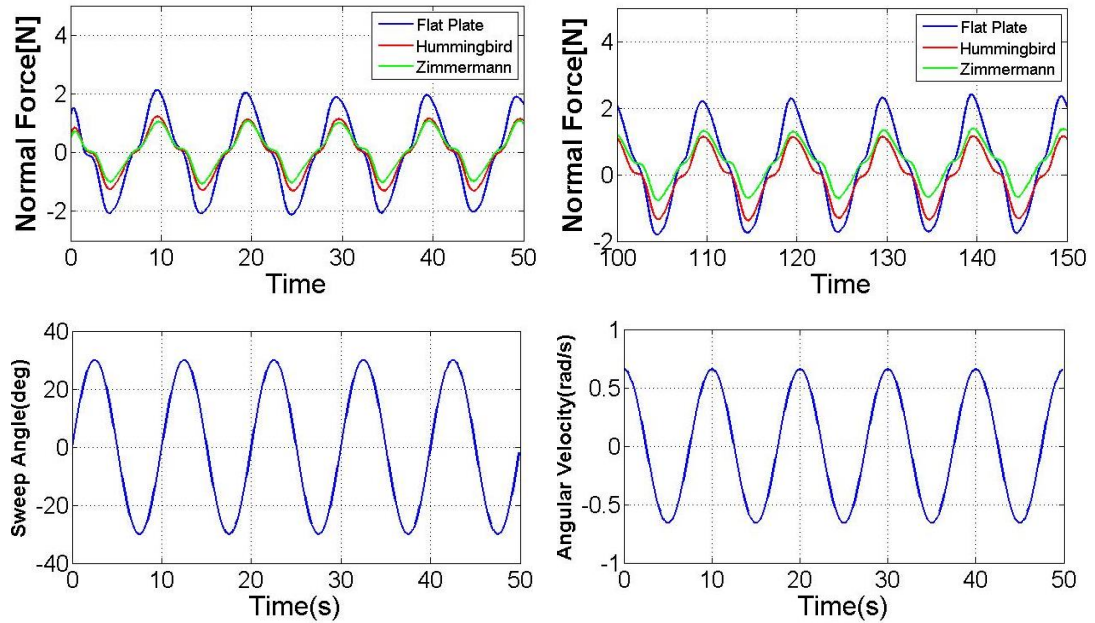


Figure 5. 11 Time history of normal force component in both impulsive and periodic regions for 5 stroke cycle with sweep angle and angular velocity variations for Case 2

In Figure 5.11, it is seen that the tendency of the force variation is the same as Case 1, however their magnitudes are approximately two times bigger than Case 1.

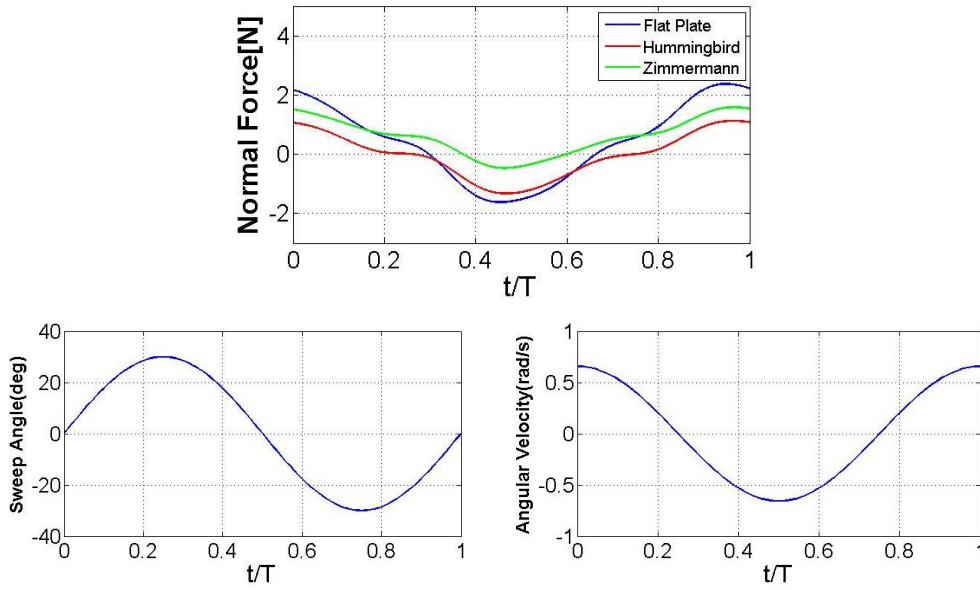


Figure 5. 12 Phase averaged and filtered normal force components in periodic region with sweep angle and angular velocity variations for Case 2

Phase averaged and filtered normal forces in impulsive and periodic regions for Case 2 is seen in the Figure 5.12. Zimmermann and Flat plate wings have little amplitude shifts between periodic and impulsive region.

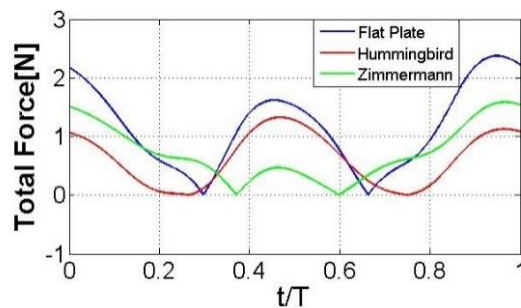


Figure 5. 13 Phase averaged total forces of three wings for Case 2

Figure 5.13 shows the total forces calculated from summation of the normal and tangential forces. Since both tangential and normal forces are big enough, total forces are bigger than normal forces although they are almost the same in previous case.

Lift forces are almost two times bigger than drag forces for Case 2. Maximum lift is generated on the flat plate since it has the biggest reference area however hummingbird

wing approximately have same maximum values with flat plate in the downstroke region (Figure 5.14).

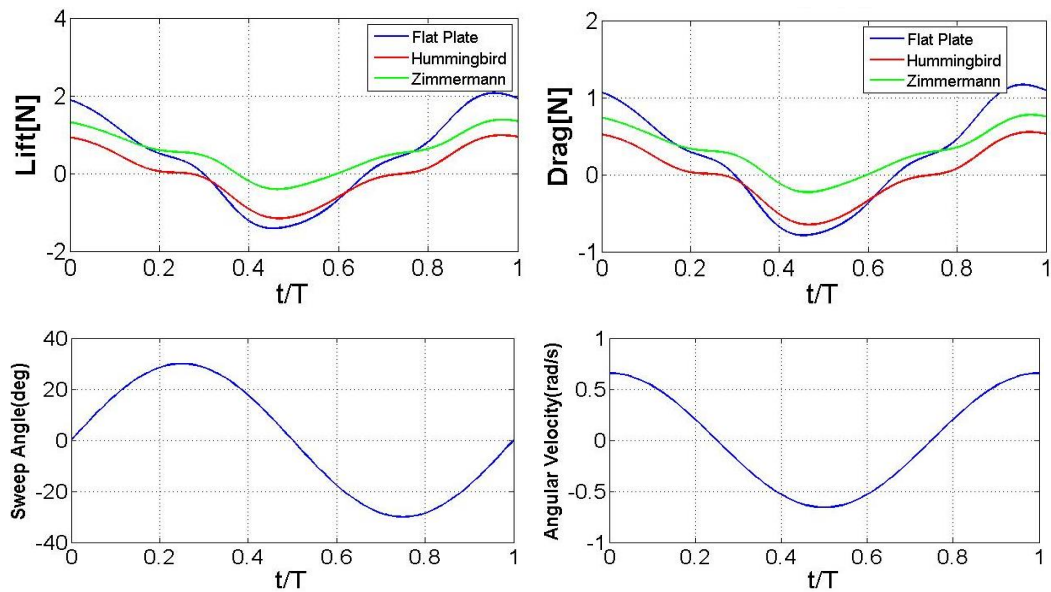


Figure 5. 14 Phase averaged lift and drag forces of three wings with sweep angle and angular velocity variations for Case 2

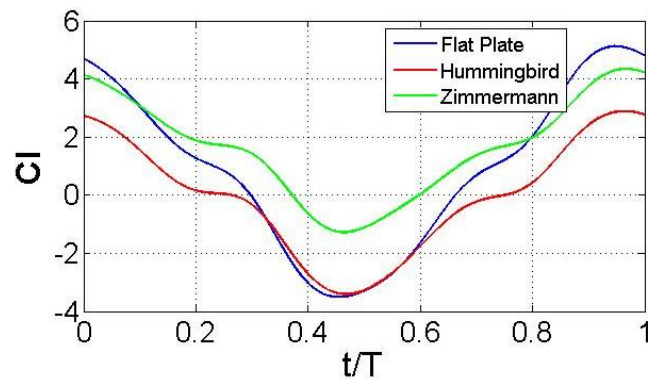


Figure 5. 15  $C_L$  coefficient variations for each three wings for Case 2

Figure 5.15 shows the  $C_L$  values for each wing geometry. In this case, Flat plate and Zimmermann have maximum  $C_L$  values in the upstroke, hummingbird wing has the maximum value in the downstroke due to their geometrical shapes.

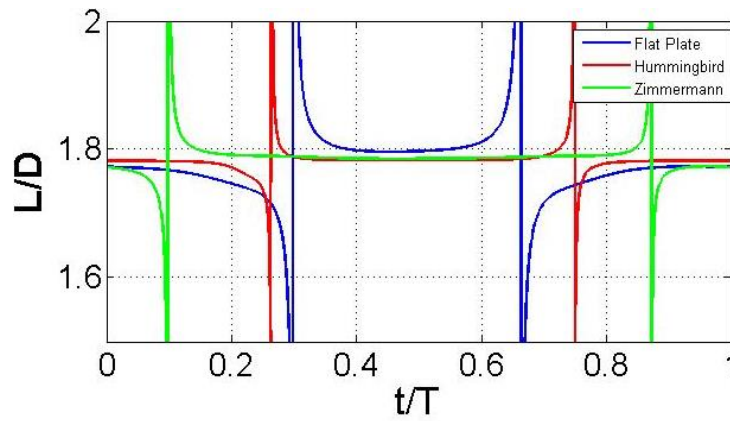


Figure 5.16 Figure 5.8 L/D ratios of 3 wings during one cycle for Case 2

L/D ratios for Case 2 are given in Figure 5.16. It is going infinity as lift and drag tends to zero. Since lift and drag goes zero at  $-30^\circ$  and  $30^\circ$ , the curve goes infinity and comes back to its mean value. When Case 1 and Case 2 are compared, it is clearly seen that mean values of the L/D ratios are decreased as pitch angle increases. In Case 2, constant L/D ratios are 1.78 for Hummingbird, 1.79 for Zimmermann and 1.8 for Flat plate.

### 5.1.3 Case 3

Pure sweep motion with time dependent angular velocity at constant  $45^\circ$  pitch angle is investigated in Case 3. Wings are sweeping  $60^\circ$  in one half stroke. They are starting the motion at  $0^\circ$  and sweeping between  $30^\circ$  and  $-30^\circ$  (Figure 5.17). They reach their maximum angular velocity at  $0^\circ$ .

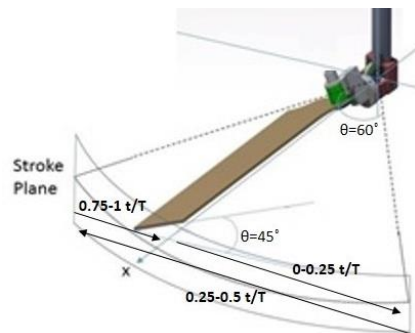


Figure 5.17 Wing trajectory in one cycle for Case 3

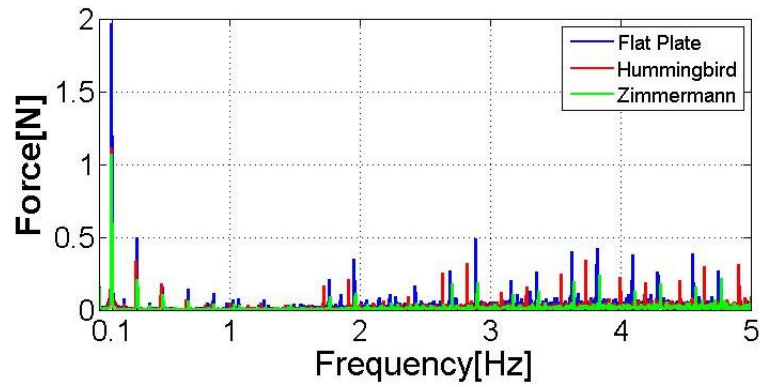


Figure 5.18 Normal force harmonic contents of each three wings for Case 3

In Figure 5.19, it is clearly seen that both the tendency of the force variation and the magnitudes of the forces are almost the same as Case 2, however there is so small difference between magnitudes of the Case 2 and Case 3. Although there is huge pitch angle difference between  $30^\circ$  and  $45^\circ$ , force increases in both regions are so small. However the biggest value of the normal force has obtained at angular velocity of  $0.63 \text{ rad/s}$ .

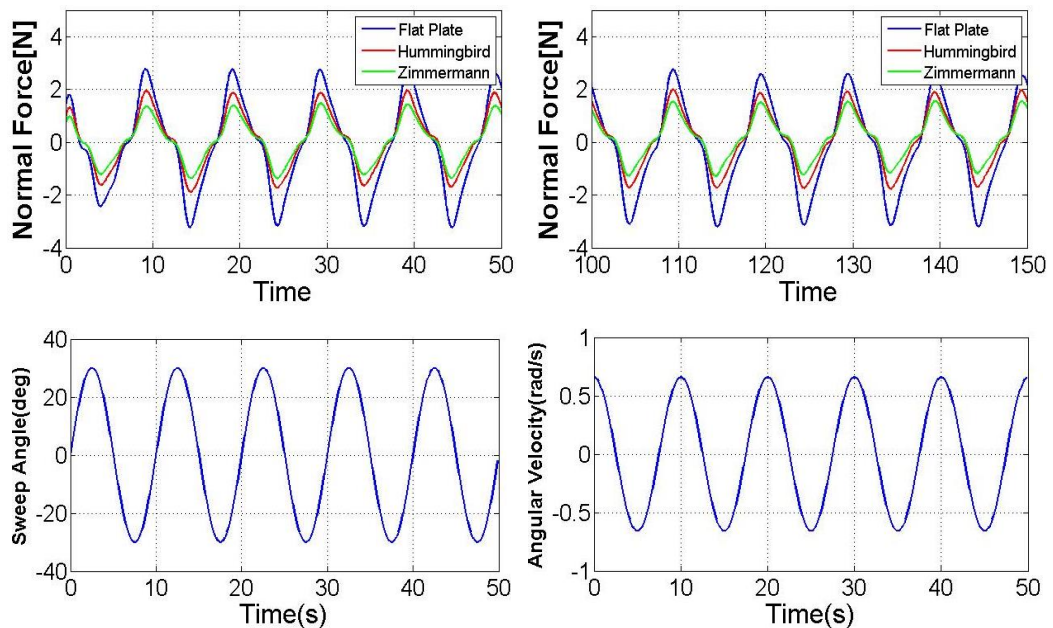


Figure 5.19 Time history of normal force component in both impulsive and periodic regions for 5 stroke cycle with sweep angle and angular velocity variations for Case 3

Phase averaged and filtered normal forces in periodic region for case 3 is seen in the Figure 5.20. All three wings have same tendency in force variation in both periodic and impulsive region.

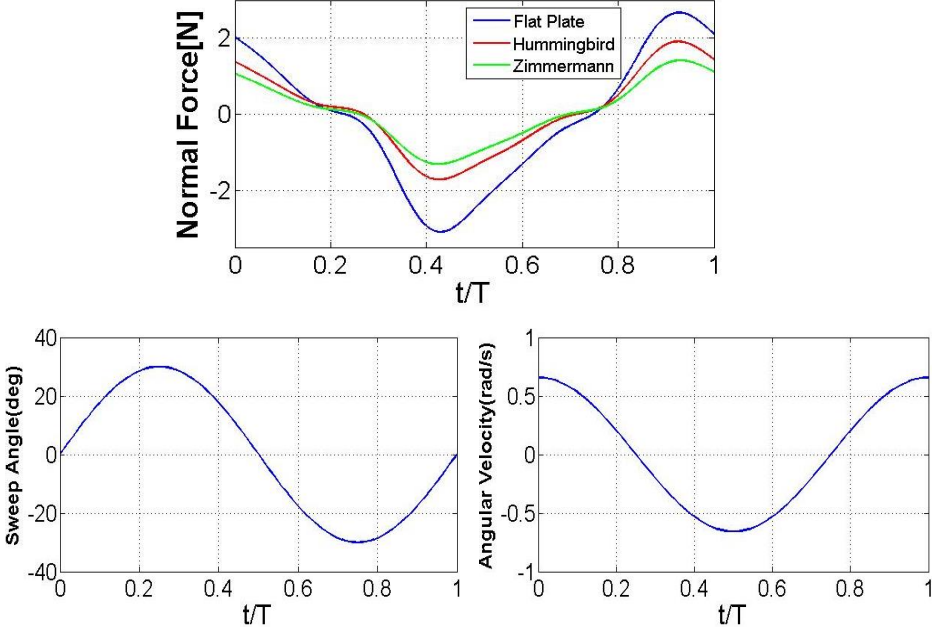


Figure 5. 20 Phase averaged and filtered normal force components in periodic region with sweep angle and angular velocity variations for Case 3

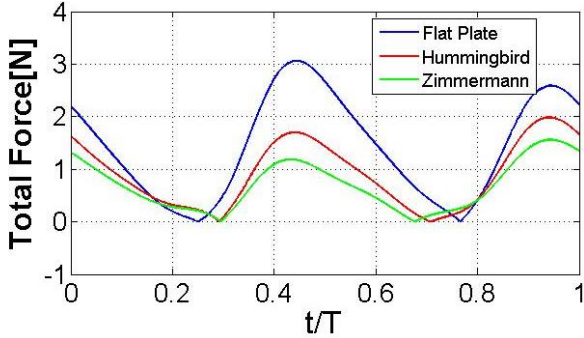


Figure 5. 21 Phase averaged total forces of three wings for Case 3

Lift forces and drag forces have almost same variations in both upstroke and down stroke. Since this case is constant  $45^\circ$  pitch angle case, we expect to get same values for lift and drag forces. Maximum lift is generated on the flat plate since it has the biggest reference area. However, Hummingbird wing approximately has same values with Flat plate in the upstroke which means if we have changed the pitch angle of the

Hummingbird at the end of the stroke, we would get the same values with the Flat plate for both Hummingbird in the downstroke too. (Figure 5.22).

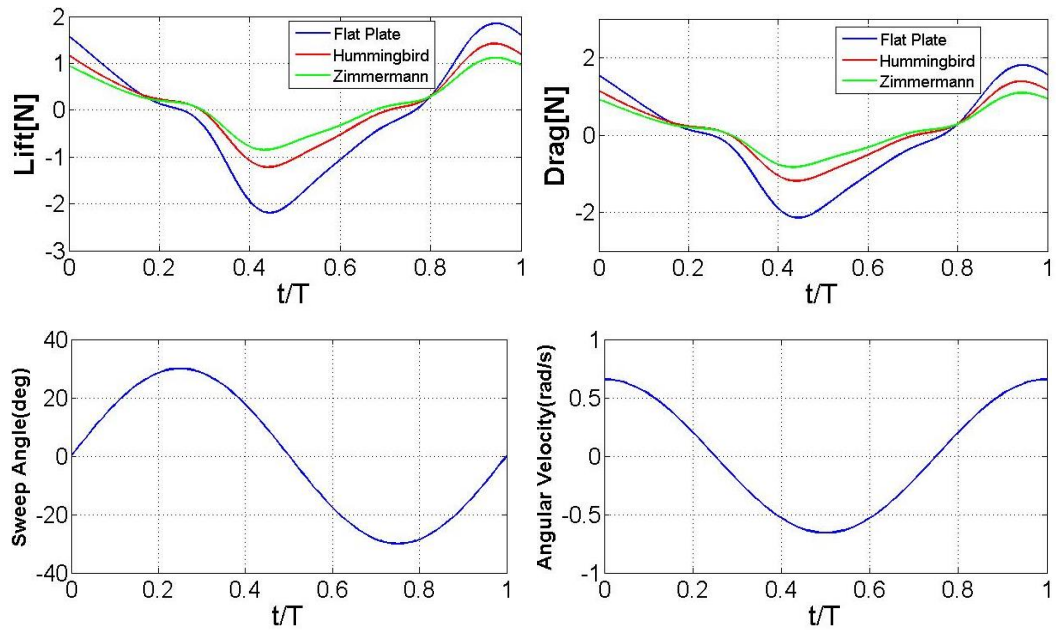


Figure 5. 22 Phase averaged lift and drag forces of three wings with sweep angle and angular velocity variations for Case 3

Figure 5.23 shows the  $C_L$  values for each wing geometry. In this case, all three wings have almost same  $C_L$  variation in the upstroke, flat plate wing has the maximum value in the downstroke.

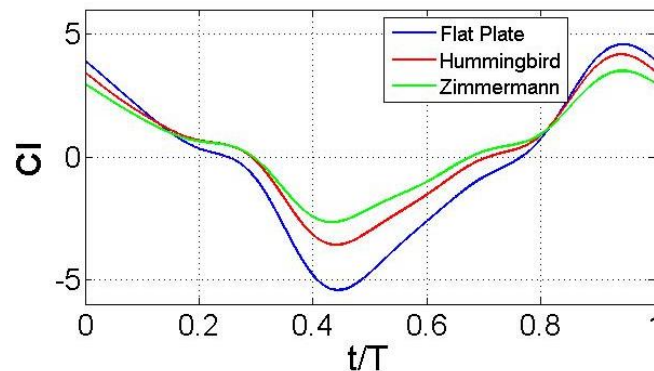


Figure 5. 23  $C_L$  coefficient variations for each three wings for Case 3

Figure 5.24 shows L/D ratios, which are so close to 1 since lift and drag values almost the same, for one cycle. They are going to infinity at  $-30^\circ$  and  $30^\circ$  sweep angles. In

Case 3, constant L/D ratios are 1.027 for Hummingbird, 1.026 for Zimmermann and 1.025 for flat plate.

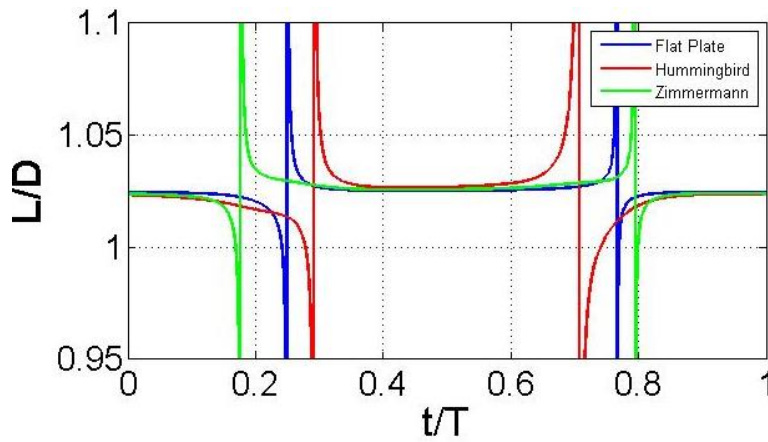


Figure 5. 24 L/D ratios of 3 wings during one cycle for Case 3

#### 5.1.4 Case 4

Pure sweep motion with time dependent angular velocity at constant  $5^\circ$  pitch angle is investigated in Case 4. Wings are sweeping  $120^\circ$  in one half stroke. They are starting the motion at  $0^\circ$  and sweeping between  $60^\circ$  and  $-60^\circ$  (Figure 5.25). They reach their maximum angular velocity at  $0^\circ$ .

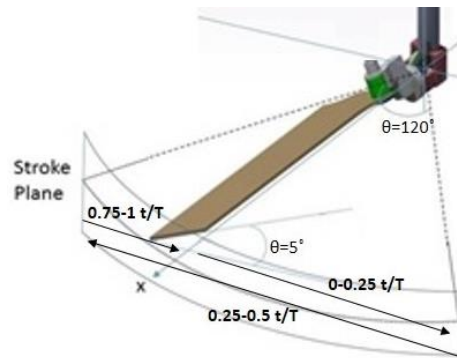


Figure 5. 25 Wing trajectory in one cycle for Case 4

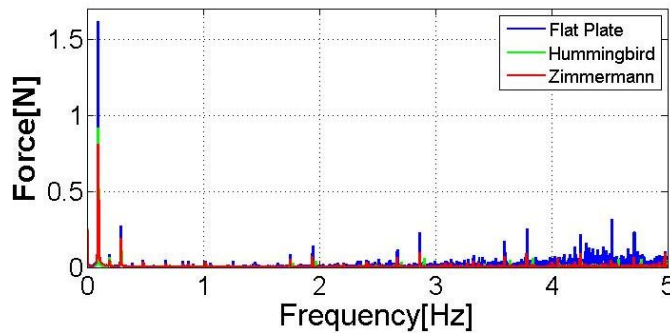


Figure 5. 26 Normal force harmonic contents of each three wings for Case 4

In FFT analysis (Figure 5.26), it is seen that maximum force amplitude is at 0.1 Hz which is the flapping frequency of the system. Cut-off frequency is decided for filtering by looking the FFT analysis. The amplitude of the forces for Hummingbird and Zimmermann are almost equal. However, Flat plate has much more force amplitude than others.

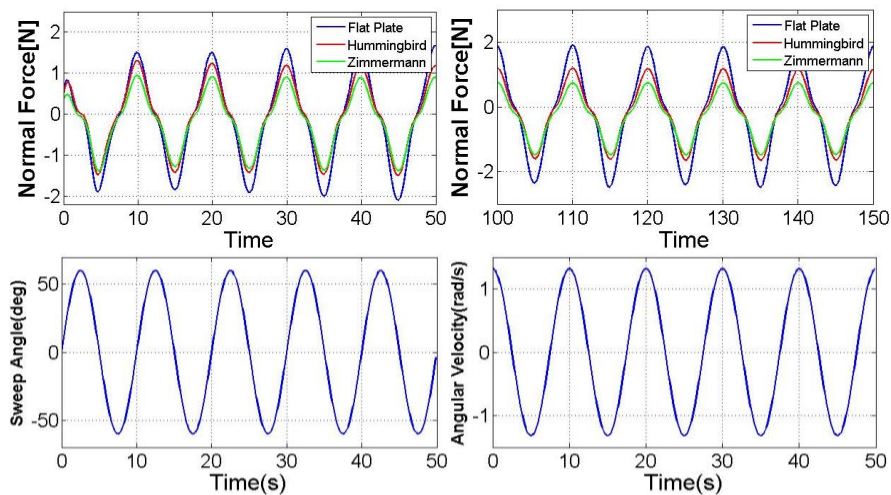


Figure 5. 27 Time history of normal force component in both impulsive and periodic region for 5 stroke cycle with angle and angular velocity variations for Case 4

The difference between normal forces for each wing is getting smaller in  $120^\circ$  sweeping motions. Since the wings have two times bigger velocity whose maximum value is 1.27 rad/s than previous cases, generated forces are much bigger as it is seen in Figure 5.27.

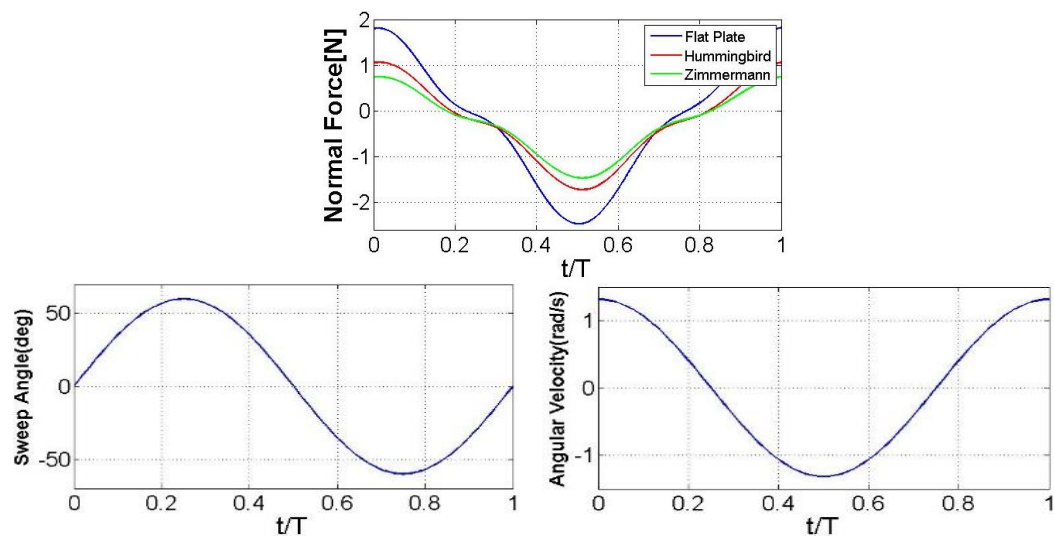


Figure 5. 28 Phase averaged and filtered normal force components in periodic region with sweep angle and angular velocity variations for Case 4

Figure 5.28 shows the variations of the normal forces in averaged one cycle. At the half of the stroke the wings reaches their maximum force value since they reach the maximum angular velocity. Flat plate has more normal force variation than others due to its shape and reference area.

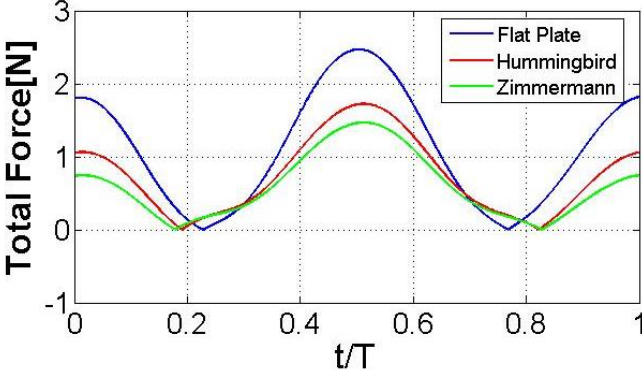


Figure 5. 29 Phase averaged total forces of three wings for Case 4

Figure 5.29 shows the total force calculated from summation of the normal and tangential forces. It is almost the same as normal force values since the tangential forces are so small for this pitch angle.

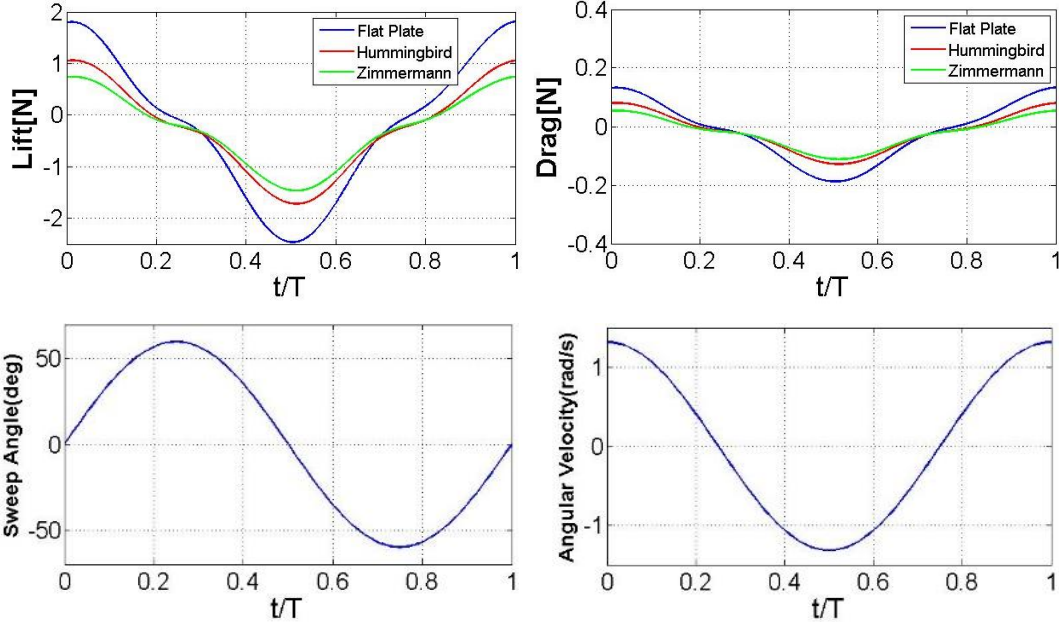


Figure 5. 30 Phase averaged lift and drag forces of three wings with sweep angle and angular velocity variations for Case 4

Lift forces are almost ten times bigger than drag forces for Case 4. Maximum lift which is approximately two times bigger than the others is generated on the flat plate since it has the biggest reference area (Figure 5.30).

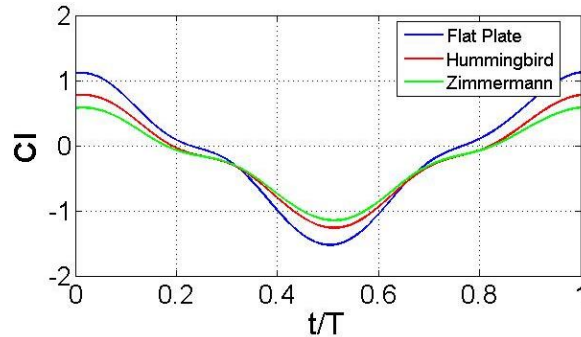


Figure 5. 31  $C_L$  coefficient variations for each three wings for Case 4

Figure 5.31 shows the  $C_L$  values for each wing geometry.  $C_L$  coefficients of three wings are so close each other. In this case Flat plate has maximum  $C_L$  values, hummingbird also efficient in upstroke and downstroke.

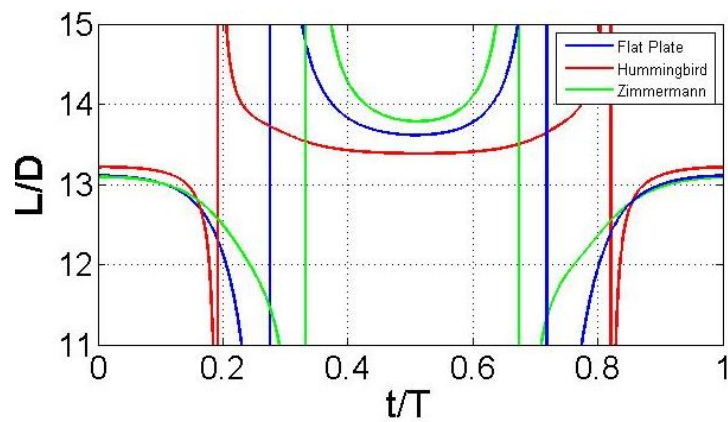


Figure 5. 32 L/D ratios of 3 wings during one cycle for Case 4

In Figure 5.32, L/d ratio variations in one stroke cycle for Case 4 is given. The mean of the L/D ratios are so close to each other. However they are decreased in the next cases as pitch angle increases. In Case 4, constant L/D ratios are 13.8 for Zimmermann, 13.6 for Hummingbird and 13.4 for Flat plate.

### 5.1.5 Case 5

Pure sweep motion with time dependent angular velocity at constant  $30^\circ$  pitch angle is investigated in Case 5. Wings are sweeping  $120^\circ$  in one half stroke. They are starting the motion at  $0^\circ$  and sweeping between  $60^\circ$  and  $-60^\circ$  (Figure 5.33). They reach their maximum angular velocity at  $0^\circ$ .

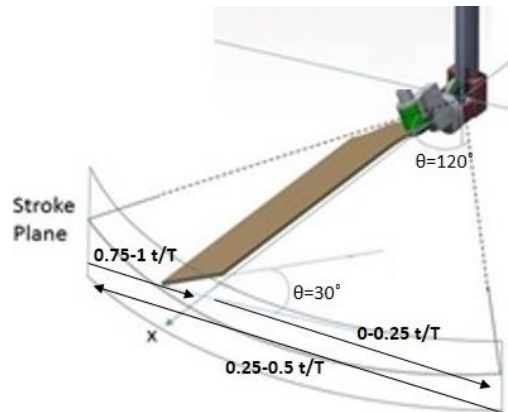


Figure 5. 33 Wing trajectory in one cycle for Case 5

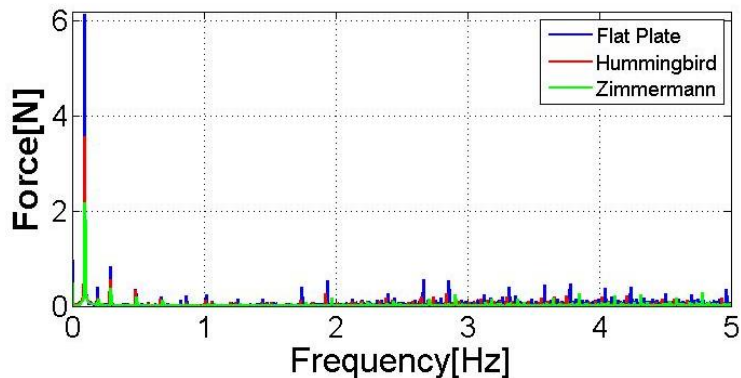


Figure 5. 34 Normal force harmonic contents of each three wings for Case 5

In FFT analysis (Figure 5.7) it is seen that maximum force amplitude is at 0.1 Hz which is the flapping frequency of the system. Maximum amplitude is now much bigger than case 2 since our velocity is two times bigger than velocity of the case 2. Cut-off frequency can be decided for filtering by looking the FFT analysis. So, we decide to cut-off the frequencies bigger than 0.5 Hz.

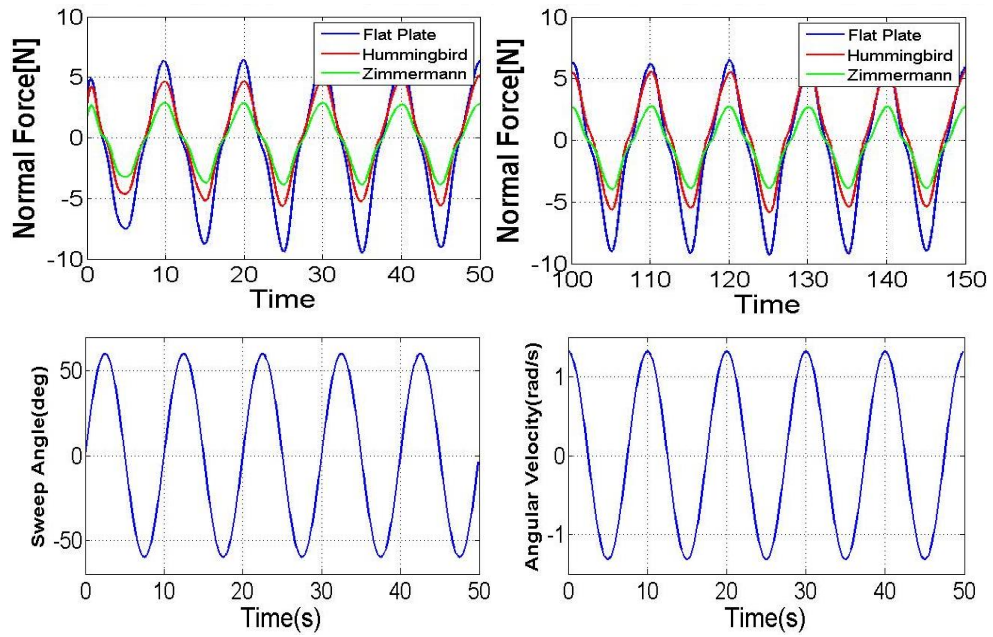


Figure 5. 35 Time history of normal force component in both impulsive and periodic regions for 5 stroke cycles with angle and angular velocity variations for Case 5

Especially in the periodic region, hummingbird has a high efficiency as well as flat plate in the upstroke. But in the downstroke flat plate's normal force is much bigger than the others (Figure 5.35). This condition is also clearly seen in Figure 5.36.

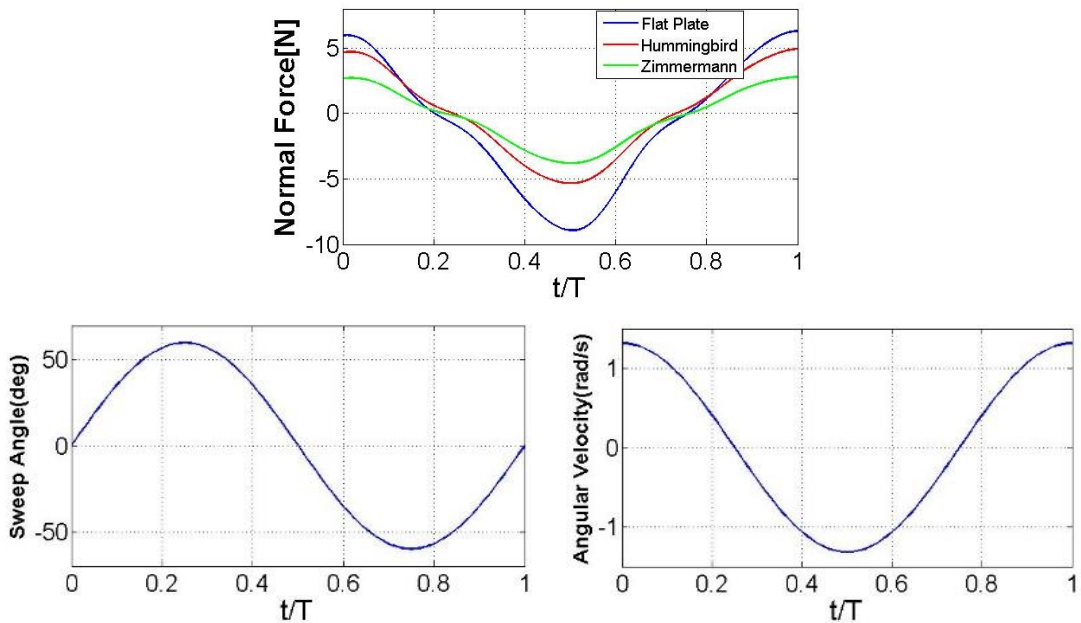


Figure 5. 36 Phase averaged and filtered normal force components in periodic region with sweep angle and angular velocity variations for Case 5

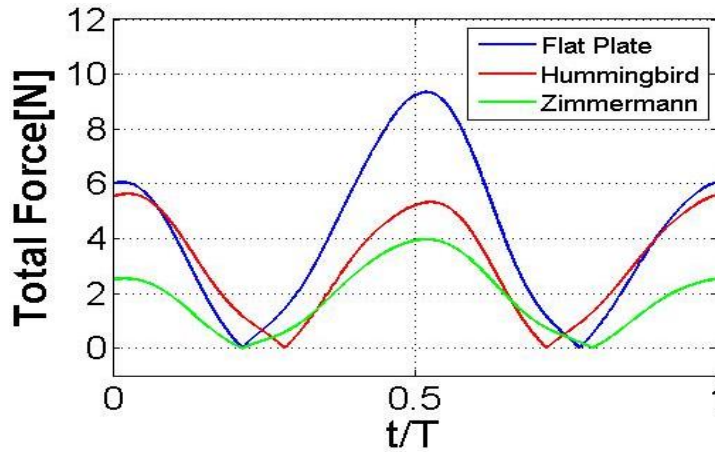


Figure 5.37 Phase averaged total forces of three wings for Case 5

Due to our pitch angle both normal and tangential forces get much bigger than previous cases. Figure 5.37 shows the variation of the total force in one cycle. In the upstroke cycle hummingbird and flat plate having the same values.

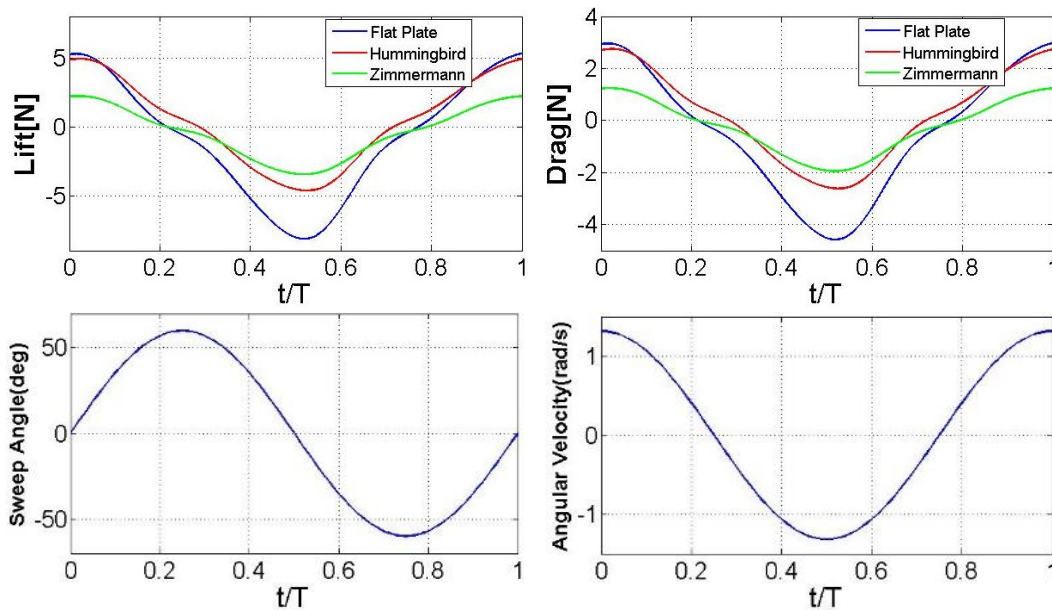


Figure 5.38 Phase averaged lift and drag forces of three wings with sweep angle and angular velocity variations for Case 5

Lift and drag values are so close to each other due to high angle of attack (Figure 5.38). They have their maximum values at  $0^\circ$  sweep angle. Hummingbird shows a pleasurable aerodynamic performance in this case. Upstroke values shows a better picture to see the efficiencies of the wings since in the downstroke region, the leading edge is becoming the trailing edge and vice versa.

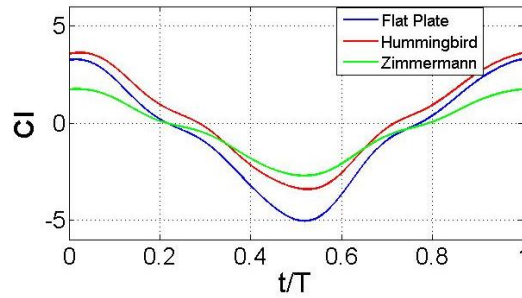


Figure 5. 39  $C_L$  coefficient variations for each three wings for Case 5

It is clearly seen in Figure 5.39 that Hummingbird wing has the maximum  $C_L$  values in this case.  $C_L$  values are approximately the same with Case 2 as expected since the pitch angles in both case are the same.

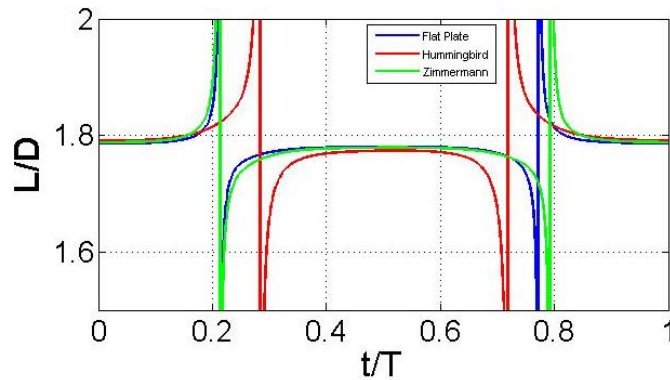


Figure 5. 40 L/D ratios of 3 wings during one cycle for Case 5

In Figure 5.40, L/D ratio variations in one stroke cycle for Case 5 is given. Flat plate and Zimmermann goes infinity before Hummingbird. The mean of the L/D ratios are so close to each other. Since lift and drag forces are so close to each other L/D ratios are small for all wings. Constant L/D ratios are 1.791 for Hummingbird, 1.788 for Zimmermann and 1.785 for Flat plate.

### 5.1.6 Case 6

Pure sweep motion with time dependent angular velocity at constant  $45^\circ$  pitch angle is investigated in Case 6. Wings are sweeping  $120^\circ$  in one half stroke. They are starting the motion at  $0^\circ$  and sweeping between  $60^\circ$  and  $-60^\circ$  (Figure 5.41). They reach their maximum angular velocity at  $0^\circ$ .

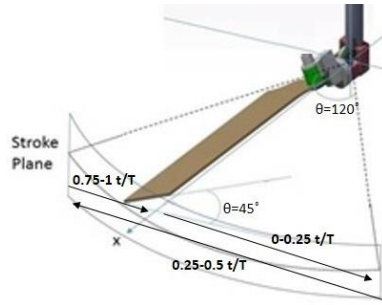


Figure 5. 41 Wing trajectory in one cycle for Case 6

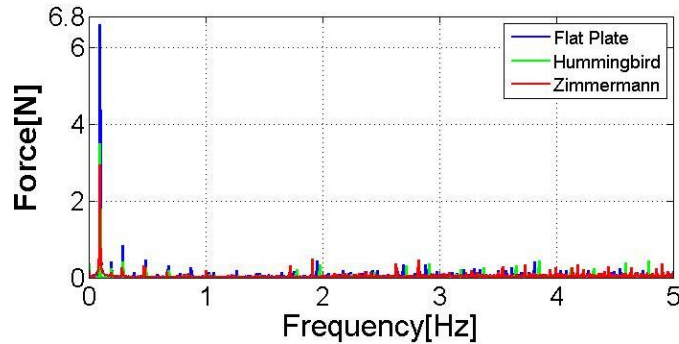


Figure 5. 42 Normal force harmonic contents of each three wings for Case 6

In Figure 5.43, it is clearly seen that the normal force values are now four times bigger than its values in Case 3 due to 2 times increased velocity. Hummingbird and Zimmermann variation is almost the same. However there is so small difference between magnitudes of the Case 5 and Case 6. Although there is huge pitch angle difference between  $30^\circ$  and  $45^\circ$ , force increases in both regions are so small.

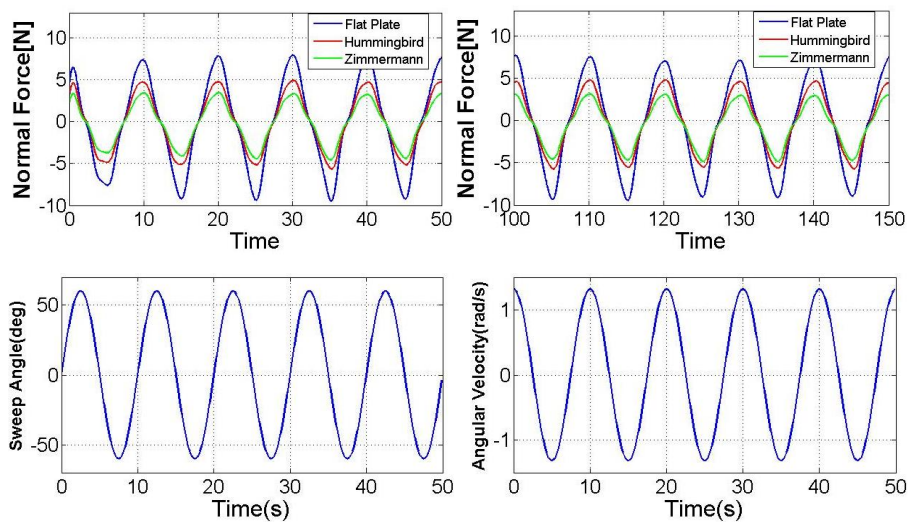


Figure 5. 43 Time history of normal force component in both impulsive and periodic regions for 5 stroke cycles with angle and angular velocity variations for Case 6

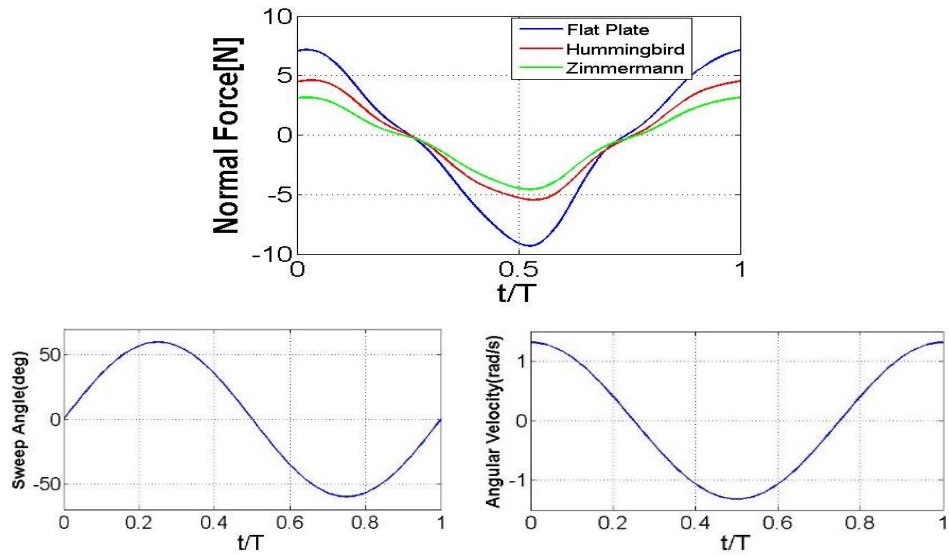


Figure 5. 44 Phase averaged and filtered normal force components in periodic region with sweep angle and angular velocity variations for Case 6

Figure 5.44 shows the phase averaged variation of the normal force in two regions. Normal force values are the same for both impulsive and periodic region. Flat plate mean values seems the biggest one for this case.

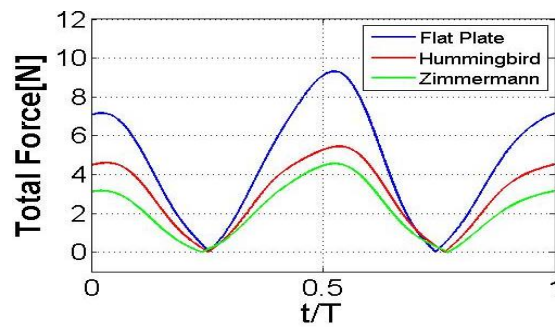


Figure 5. 45 Phase averaged total forces of three wings for Case 6

$30^\circ$  and  $45^\circ$  pitch angles gives same values for both normal and tangential forces. Figure 5.45 shows the variation of the total force in one cycle. Hummingbird and Zimmermann have same trends in upstroke and downstroke.

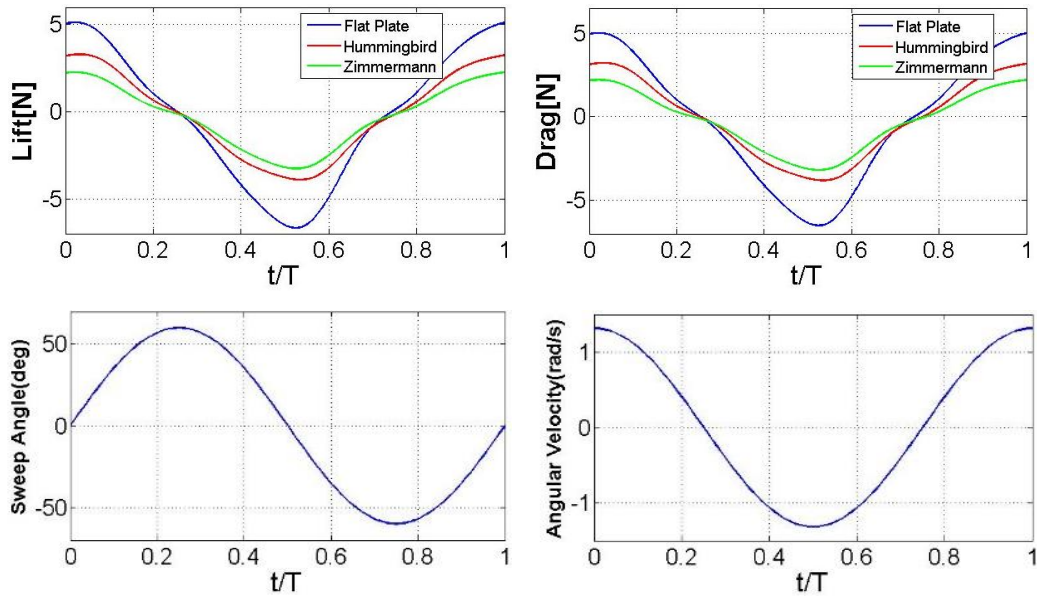


Figure 5. 46 Phase averaged lift and drag forces of three wings with sweep angle and angular velocity variations for Case 6

Lift and drag forces of this case is the same with each other, since  $45^\circ$  has same vertical and horizontal components. Hummingbird and Zimmermann have approximately same trends in both upstroke and downstroke motions (Figure 5.46).

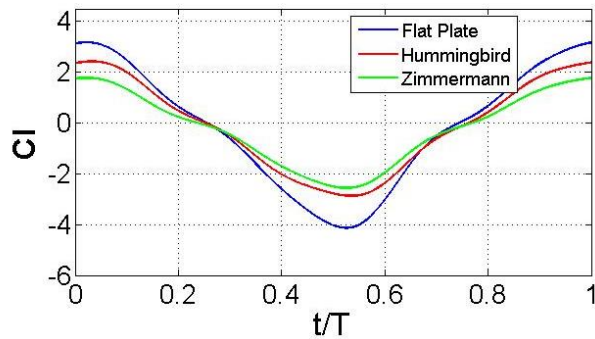


Figure 5. 47 CL coefficient variations for each three wings for Case 6

It is seen in Figure 5.47 that although Case 5 and Case 6 generate same normal forces,  $C_L$  values are decreased. Due to increased pitch angle, vertical component is decreased and horizontal component is increased.

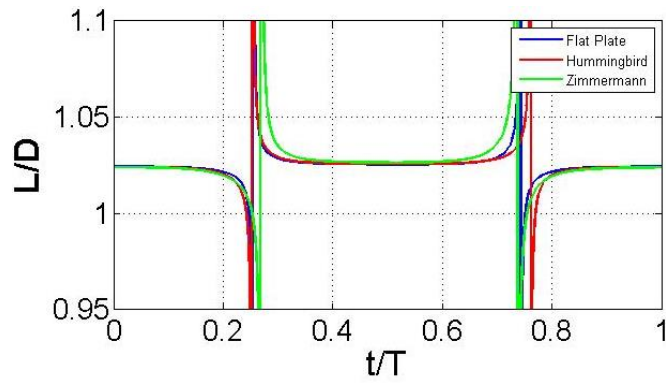


Figure 5. 48 L/D ratios of 3 wings during one cycle for Case 6

In Case 6, constant L/D ratios are 1.027 for Zimmermann, 1.026 for Hummingbird and 1.025 for Flat plate.

### 5.1.7 Case 7

Pure sweep motion with time dependent angular velocity at constant  $90^\circ$  pitch angle is investigated in Case 7. Wings are sweeping  $120^\circ$  in one half stroke. They are starting the motion at  $0^\circ$  and sweeping between  $60^\circ$  and  $-60^\circ$  (Figure 5.49). They reach their maximum angular velocity at  $0^\circ$ .

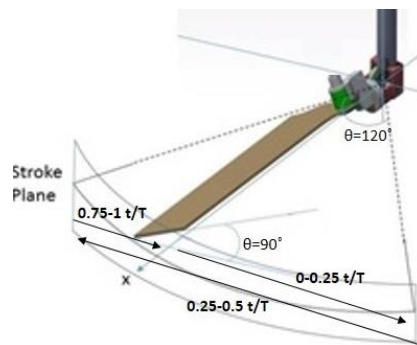


Figure 5. 49 Wing trajectory in one cycle for Case 7

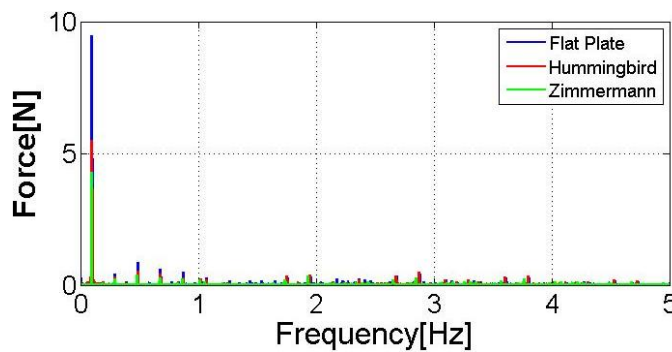


Figure 5. 50 Normal force harmonic contents of each three wings for Case 7

All of the normal forces belong to horizontal component since our pitch angle is  $90^\circ$ . We see from the Figure 5.50 that normal force has the biggest value between all 7 cases. We decide our cut-off frequency for filtering by looking the FFT analysis. Frequencies bigger than 0.5 Hz. are cut-off to get sensible results.

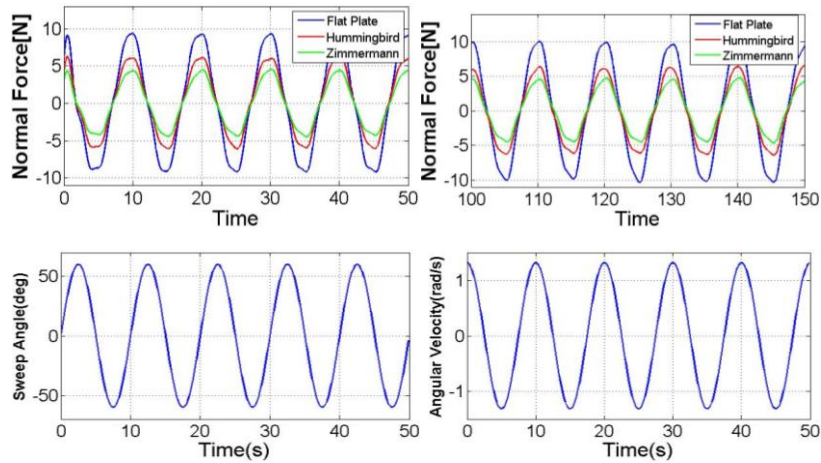


Figure 5. 51 Time history of normal force component in both impulsive and periodic regions for 5 stroke cycle with sweep angle and angular velocity variations for Case 7

Variation of the normal force is seen in Figure 5.51, the magnitudes of the forces are remarkably bigger than the other cases. Forces seen in the Figure 5.51 are not related with aero/hydro dynamics, however they are all about the momentum of the fluid.

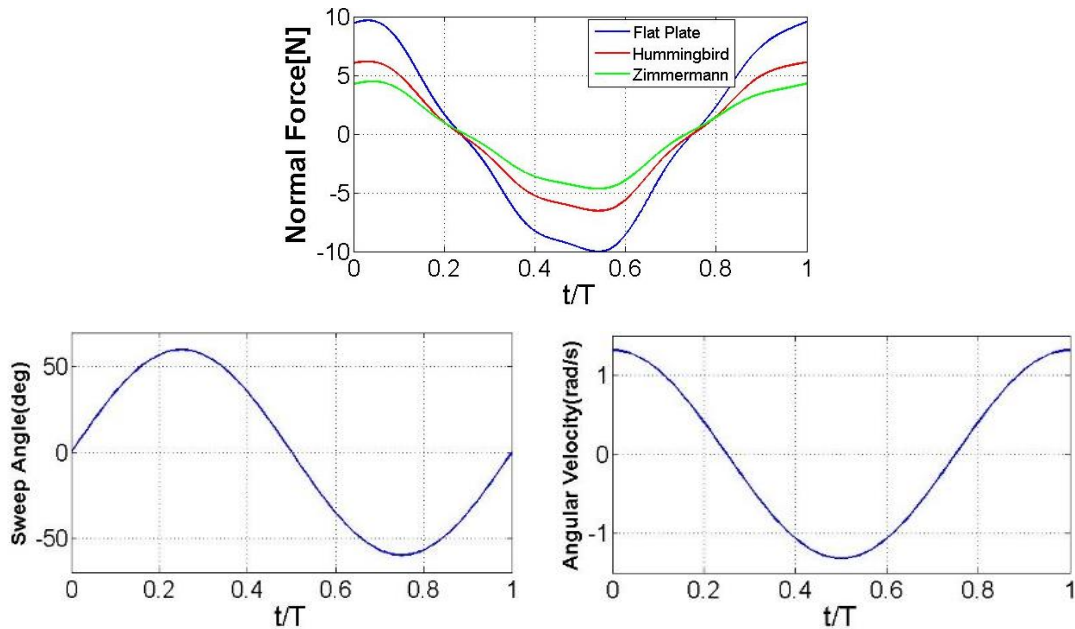


Figure 5. 52 Phase averaged and filtered normal force components in periodic region with sweep angle and angular velocity variations for Case 7

Phase averages and each cycle histories of the normal force are following same trends for this case. All we see as the normal force is equal to drag force (Figure 5.52).

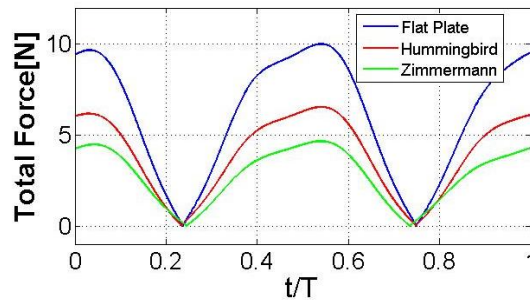


Figure 5. 53 Phase averaged total forces of three wings for Case 7

Figure 5.53 shows the variation of the total forces for three wings at  $90^\circ$  pitch angle. Total force is equal to drag force for both upstroke and downstroke and total forces are only dependent on wing reference area.

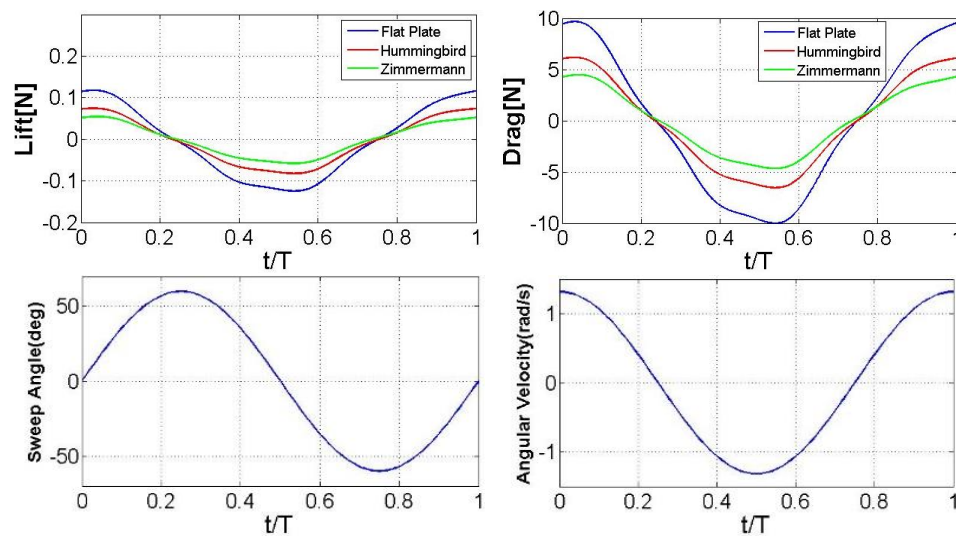


Figure 5. 54 Phase averaged lift and drag forces of three wings for Case 7

It is seen in Figure 5.54 that the only force generated in this case is drag force. The drag force variation only depends on the reference area of the wings. Because the reference area of the flat plate is the biggest one, maximum force is obtained when flat plate is used.

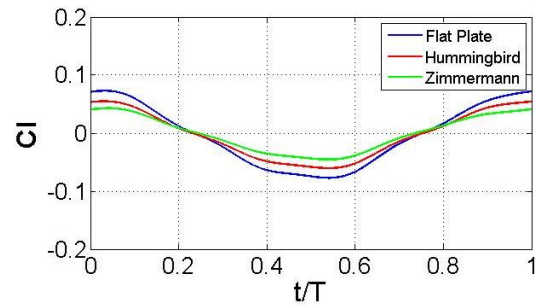


Figure 5. 55  $C_L$  coefficient variations for each three wings for Case 7

$C_L$  variation of phase averaged data is shown in the Figure 5.55. They tend to zero since our lift force is almost zero. All three wings have same values during a stroke.

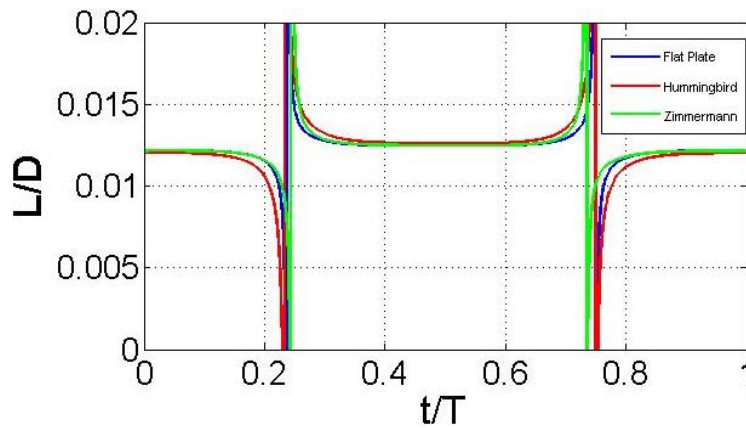


Figure 5. 56 L/D ratios of 3 wings during one cycle for Case 7

In Case 7, constant L/D ratios are 0.0125 for Hummingbird, 0.0125 for Flat plate and Zimmermann.

## 5.2 Mean and Peak Values of the Lift Forces Drag Forces and $C_L$ Values

In this part of the study, mean and peak values of the lift forces and drag forces and  $C_L$  coefficients for all cases are calculated. We can compare each cases for different geometries by looking these graphics and tables.

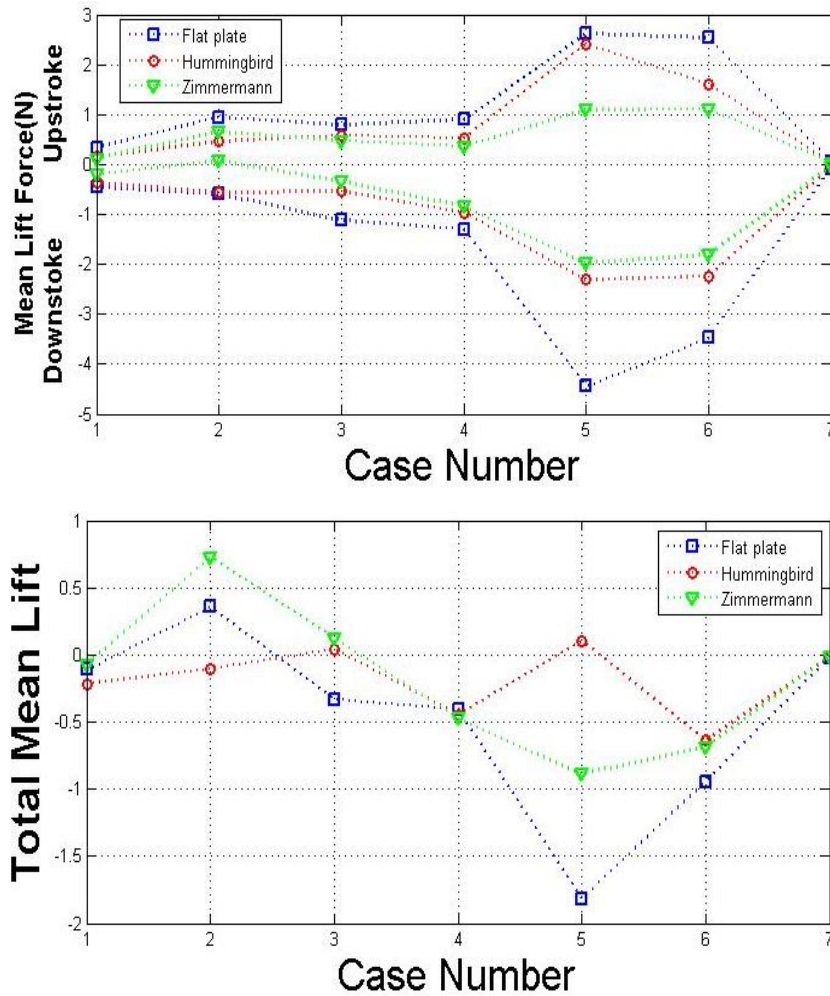


Figure 5.57 Mean lift values of 3 geometries for all cases

The trajectories of the curves are similar to each other for all 3 geometries. The lines, which are above zero, are upstroke mean values and the rest are downstroke values for all cases (Figure 5.57).

Table 5.2 Mean and peak values of lift forces for all cases

Case	Flat Plate				Hummingbird				Zimmermann			
	Upstroke		Downstroke		Upstroke		Downstroke		Upstroke		Downstroke	
	Mean	Peak	Mean	Peak	Mean	Peak	Mean	Peak	Mean	Peak	Mean	Peak
1	0.3410	0.6946	-0.4509	-0.8616	0.1561	0.3204	-0.3711	-0.6163	0.1200	0.2448	-0.1918	-0.3517
2	0.9465	2.0674	-0.5886	-1.4146	0.4637	0.9813	-0.5642	-1.1566	0.6594	1.3842	0.0693	-0.4067
3	0.7864	1.8514	-1.1162	-2.1921	0.5821	1.4201	-0.5409	-1.2181	0.4704	1.1167	-0.3450	-0.8496
4	0.8971	1.8155	-1.3013	-2.4626	0.5248	1.0593	-0.9717	-1.7181	0.3678	0.7441	-0.8404	-1.4637
5	2.6180	5.3030	-4.4369	-8.1468	2.4181	4.9182	-2.3129	-4.6433	1.0969	2.2177	-1.9817	-3.4612
6	2.5317	5.1309	-3.4737	-6.6706	1.6043	3.2942	-2.2416	-3.9041	1.1170	2.2657	-1.8056	-3.2631
7	0.0573	0.1177	-0.0792	0.1247	0.0364	0.0743	-0.0519	-0.0824	0.0258	0.0545	-0.0351	-0.0581

Mean and peak values of the lift forces for both upstroke and downstroke regions of 3 wings are given in Table 5.2. These values, which are calculated in MATLAB, are employed to get Figure 5.57.

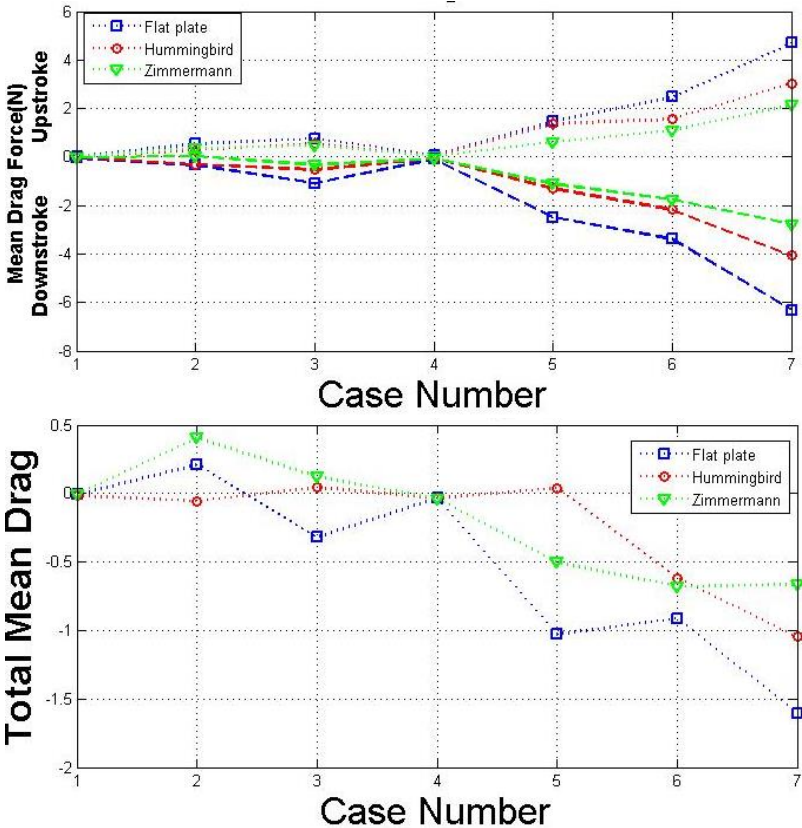


Figure 5. 58 Mean drag values of 3 geometries for all cases

As it is seen in the Figure 5.58, downstroke region affects total drag very much. Since the leading edge and trailing edges are changing in the downstroke this drastic increase in the drag forces could be normal.

Table 5. 3 Mean and peak values of drag forces for all cases

Case	Flat Plate				Hummingbird				Zimmermann			
	Upstroke		Downstroke		Upstroke		Downstroke		Upstroke		Downstroke	
	Mean	Peak	Mean	Peak	Mean	Peak	Mean	Peak	Mean	Peak	Mean	Peak
1	0.0258	0.0526	-0.0334	-0.0643	0.0121	0.0249	-0.0270	-0.0454	0.0083	0.0169	-0.0159	-0.0279
2	0.5340	1.1660	-0.3243	-0.7877	0.2603	0.5507	-0.3164	-0.6487	0.3693	0.7754	0.0377	-0.2294
3	0.7676	1.8070	-1.0884	-2.1382	0.5688	1.3873	-0.5259	-1.1867	0.4586	1.0888	-0.3373	-0.8296
4	0.0659	0.1333	-0.1007	-0.1879	0.0397	0.0802	-0.0723	-0.1284	0.0267	0.0540	-0.0650	-0.1118
5	1.4659	2.9693	-2.4952	-4.5766	1.3503	2.7466	-1.3105	-2.6179	0.6135	1.2404	-1.1157	-1.9457
6	2.4718	5.0094	-3.3858	-6.5049	1.5666	3.2168	-2.1842	-3.8063	1.0882	2.2074	-1.7648	-3.1869
7	4.7137	9.6728	-6.3162	-10.0125	3.0244	6.1716	-4.0720	-6.5460	2.1265	4.4797	-2.7928	-4.6616

Mean and peak values of drag forces for both upstroke and downstroke regions of 3 wings are given in Table 5.3. These values which are calculated in MATLAB are employed to get Figure 5.58.

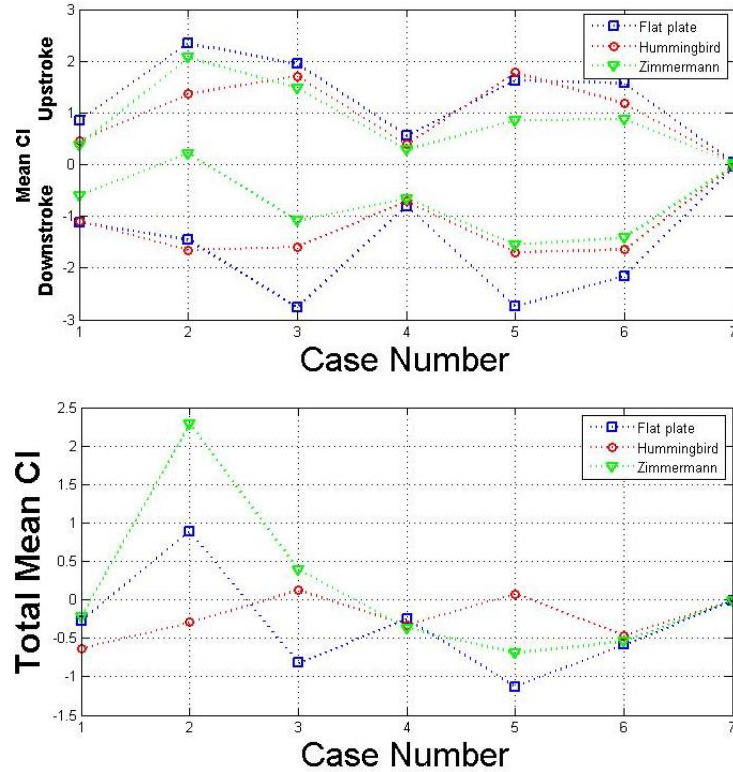


Figure 5. 59 Mean  $C_L$  values of 3 geometries for all cases

$C_L$  values increase with the increase of the pitch angle. They are affected with the velocity changes however the difference is so small. The trends of the  $C_L$  lines are almost the same for each wings (Figure 5.59).

Table 5. 4 Mean and peak values of  $C_L$  coefficients for all cases

Case	Flat Plate				Hummingbird				Zimmermann			
	Upstroke		Downstroke		Upstroke		Downstroke		Upstroke		Downstroke	
	Mean	Peak	Mean	Peak	Mean	Peak	Mean	Peak	Mean	Peak	Mean	Peak
1	0.8448	1.7204	-1.1167	-2.1342	0.4592	0.9423	-1.0917	-1.8127	0.3765	0.7680	-0.6019	-1.1034
2	2.3444	5.1210	-1.4580	-3.5039	1.3640	2.8862	-1.6597	-3.4021	2.0687	4.3429	0.2174	-1.2761
3	1.9480	4.5859	-2.7648	-5.4298	1.7121	4.1771	-1.5909	-3.5829	1.4757	3.5035	-1.0824	-2.6655
4	0.5555	1.1242	-0.8058	-1.5249	0.3859	0.7789	-0.7145	-1.2635	0.2885	0.5836	-0.6592	-1.1481
5	1.6212	3.2838	-2.7475	-5.0448	1.7781	3.6166	-1.7008	-3.4144	0.8604	1.7395	-1.5544	-2.7148
6	1.5677	3.1773	-2.1511	-4.1307	1.1797	2.4223	-1.6483	-2.8709	0.8761	1.7771	-1.4162	-2.5595
7	0.0355	0.0729	-0.0490	-0.0772	0.0268	0.0546	-0.0381	-0.0606	0.0203	0.0427	-0.0275	-0.0456

Mean and peak values for both upstroke and downstroke regions of 3 wings are given in Table 5.4. These values which are calculated in MATLAB are employed to get Figure 5.59.

### 5.3 Lift Forces, Drag Forces and $C_L$ Values for All Cases of Flat Plate

In this part of the Chapter V, aerodynamic features of each wing are handled in terms of their lift, drag and  $C_L$  capabilities. Since there are 7 cases at all, every figure will presents 7 phase averaged sinusoidal curves at different pitch angles.

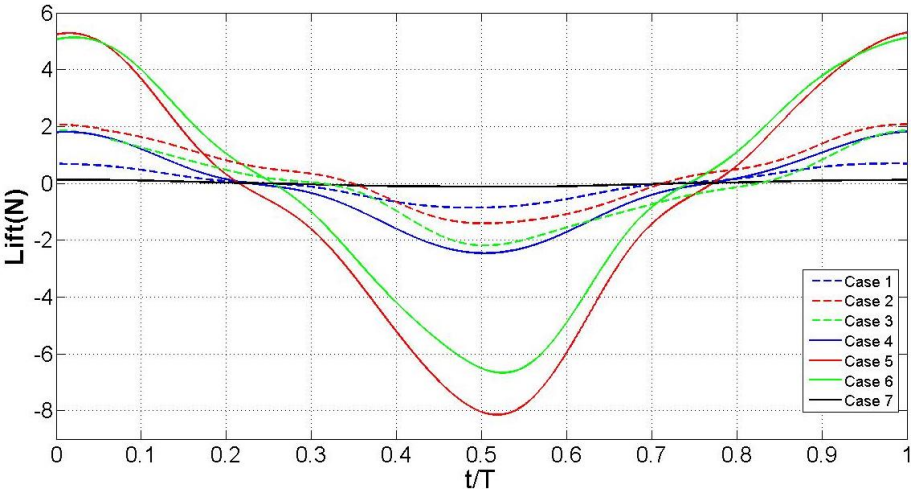


Figure 5. 60 Lift force curves of Flat plate for 7 cases

Figure 5.60 gives lift force variations of the flat plate wing in different cases. Maximum lift is obtained in Case 5 in both upstroke and downstroke. Although the lift is increasing with the increasing pitch angle, after a certain value of pitch angle it is starting to decrease.

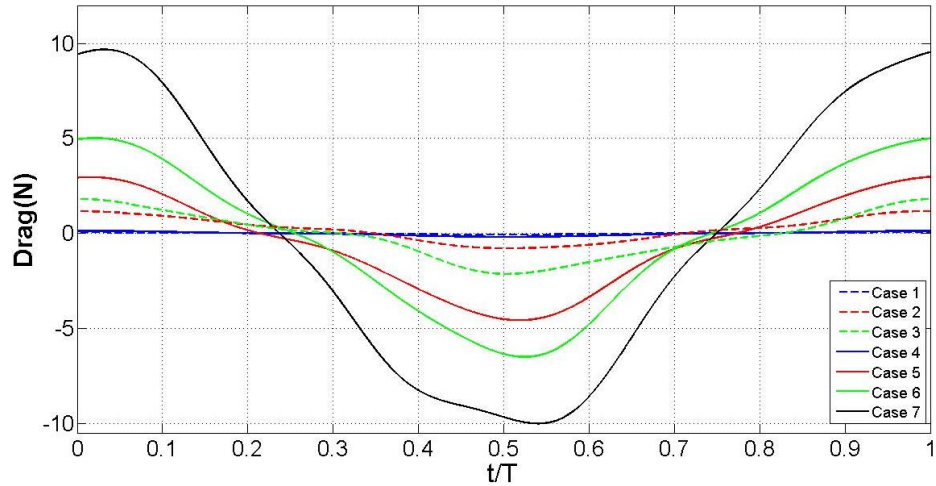


Figure 5. 61 Drag force curves of Flat plate for 7 cases

Drag forces of the Flat plate for each case is given in Figure 5.61. Drag forces are getting increased as pitch angles are increasing.  $90^\circ$  pitch angle which is the case with the biggest pitch angle has the maximum drag force.

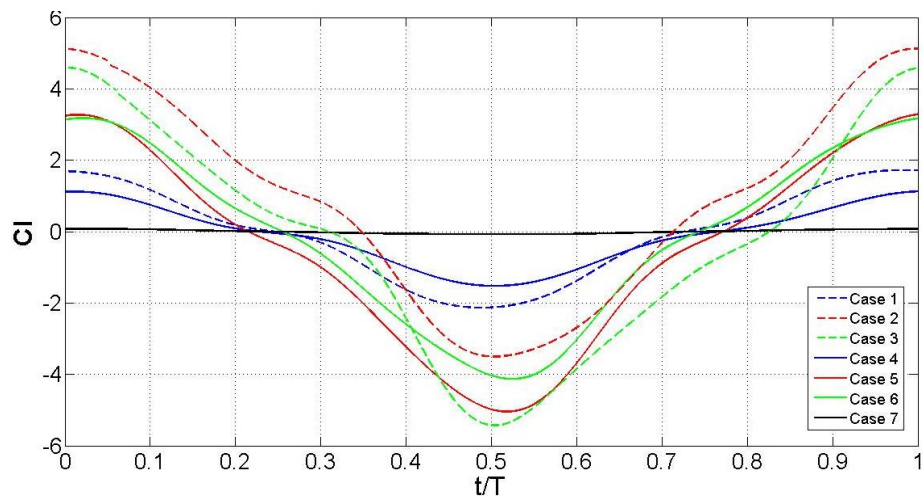


Figure 5. 62  $C_L$  curves of Flat plate for 7 cases

Figure 5.62 shows the  $C_L$  value variations of the flat plate in different cases. It is clearly seen that biggest  $C_L$  value is obtained at  $30^\circ$  pitch angle in the upstroke. However in the downstroke motion,  $45^\circ$  pitch angle has the biggest value. The cases with slower velocities have bigger values which shows that we have experimental uncertainties. Although  $C_L$  value does not change with the velocity, it is changing in these cases. Experimental uncertainties will be handled next pages.

**5.4 Lift Forces, Drag Forces and  $C_L$  Values for All Cases of Hummingbird**

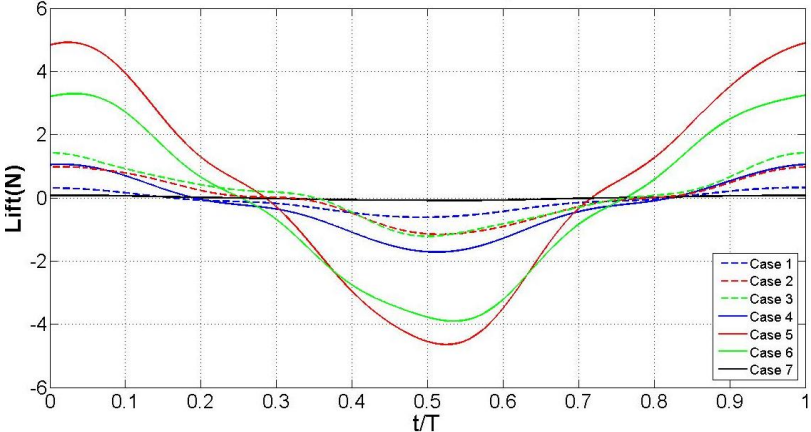


Figure 5. 63 Lift force curves of Hummingbird for 7 cases

Phase averaged lift forces of Hummingbird for 7 cases are presented in Figure 5.63. Maximum lift is obtained at  $30^\circ$  pitch angle. Small velocities are not sufficient for this geometry. Note that  $120^\circ$  sweep angle at constant  $5^\circ$  pitch angle produces more lift than  $60^\circ$  sweep angle at constant  $30^\circ$  pitch angle.

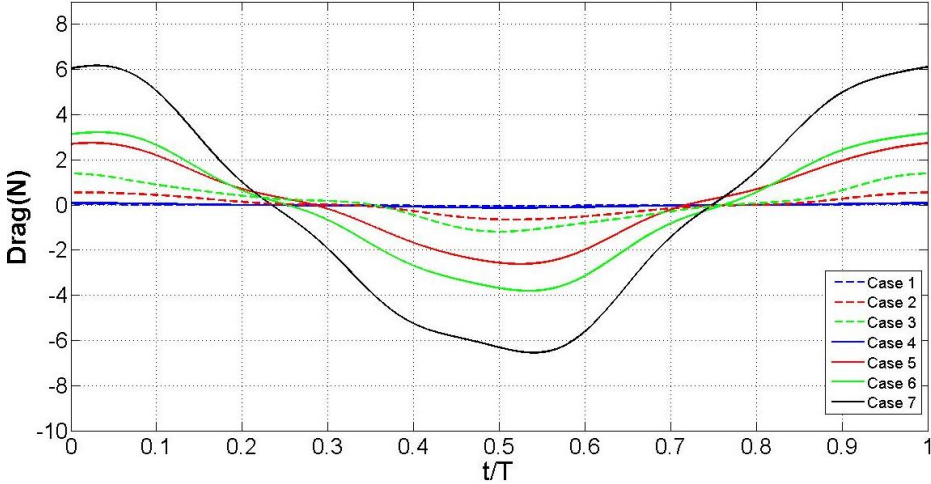


Figure 5. 64 Drag force curves of Hummingbird for 7 cases

In Figure 5.64 drag forces of the Hummingbird for all cases are plotted. Their tendencies are almost same with drag forces of the Flat plate except for a decrease in magnitude.

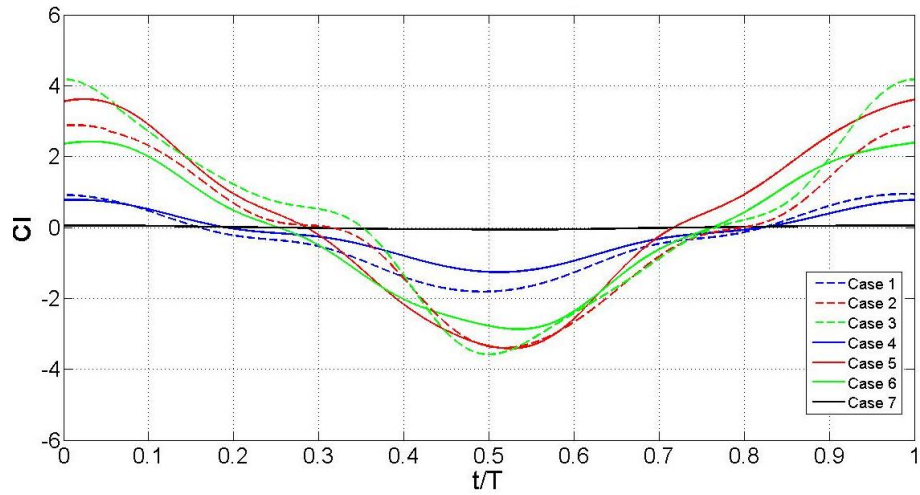


Figure 5. 65  $C_L$  curves of Hummingbird for 7 cases

Hummingbird  $C_L$  value variations are given in Figure 5.65.  $C_L$  values are not dependent to velocity as expected. Therefore it is seen in the figure that same pitch angles have almost same  $C_L$  values.

### 5.5 Lift Forces, Drag Forces and $C_L$ Values for All Cases of Zimmermann

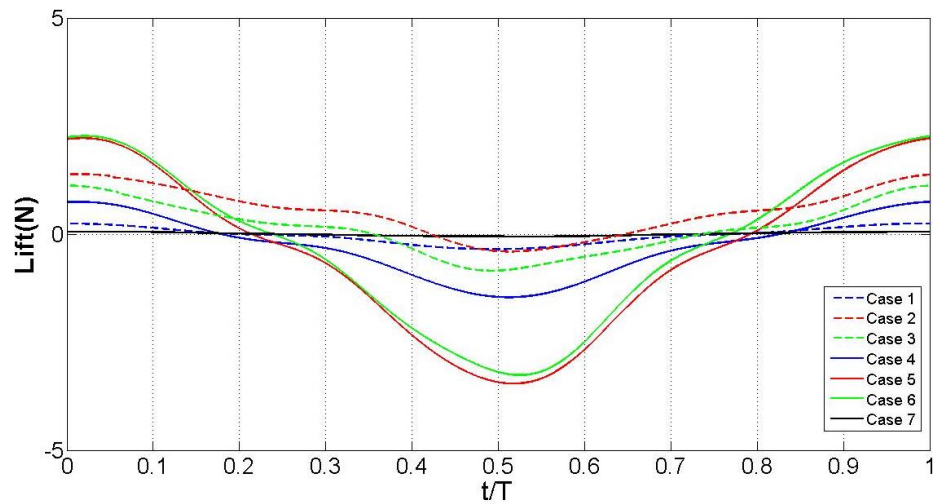


Figure 5. 66 Lift force curves of Zimmermann for 7 cases

Figure 5.66 shows the lift forces of the Zimmermann wing for 7 cases. It is clearly seen that constant  $30^\circ$  and  $45^\circ$  pitch angles have same lift force variation. So  $45^\circ$  pitch angles is efficient because of their increased drag forces.

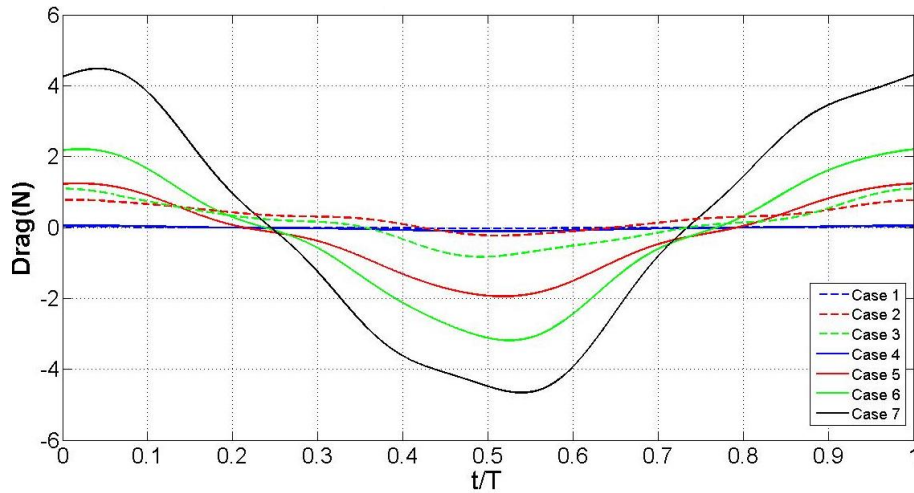


Figure 5. 67 Drag force curves of Zimmermann for 7 cases

Drag force variations of Zimmermann wing in 7 cases are given in Figure 5.67. Drag forces of the constant  $5^\circ$  pitch angle cases tend to zero due to small pitch angle. Moreover, drag force of the Case 7 is not big when it is compared to Flat plate. Note that although Case 5 and Case 6 have same lift values, Case 6 has much bigger drag force than Case 5.

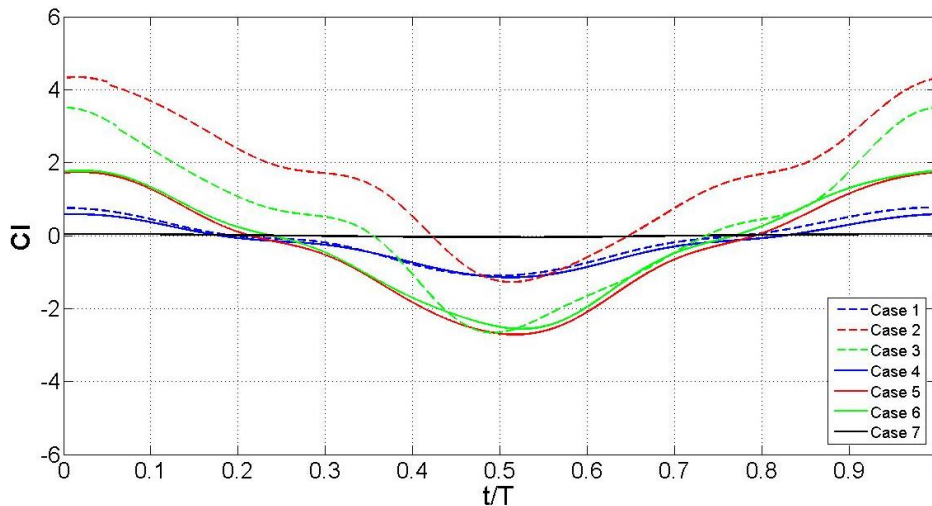


Figure 5. 68  $C_L$  curves of Zimmermann for 7 cases

Phase averaged  $C_L$  value variations are shown in the Figure 5.68.  $C_L$  values are the same at constant  $5^\circ$  pitch angles as expected.  $30^\circ$  and  $45^\circ$  pitch angles have same values for  $120^\circ$  sweep angle which means after  $30^\circ$  pitch angles are not very effective on lift

generation. Although there is a shift in magnitude at 30° and 45° pitch angles for 60° sweep angle motion, total variations of the  $C_L$  are so close with 120° sweep motion.

## **5.6 Experimental Uncertainties and Added Mass Effect**

Low force measurements like the one performed in this study have some challenges due to high effect of noises on the measurement and cyclic wing motion. Cycling wing motion introduces systematic errors that must be account for [19]. Also transducer must be chosen with ensuring a good signal-to-noise ratio. The transducer must be placed on the wing providing that the transducer and the wing have same axis [19]. Since the transducer used in the experiments is very sensitive, any mechanical vibration must be absorbed during the experiments. Also electronic noises must be considered. These all noises is canceled from data by using a low-pass Butterworth filter in MATLAB.

The tank must be large enough to avoid the wall effects which are a potential source of error. Additionally water surface must be sufficiently away from the wing to avoid wave formations [19].

There are additional errors caused by bearings and gears. The commands given by the computer and wings motion trajectories have little differences due to spaces between bearings and gears. A position sensor must be located on the system and the Wing-Sim program should use these position data as feedback to have a precise trajectory.

This study consists of the experiments which are conducted in water. However the aerodynamic performance of the wing is seen in air in real life. Although we know that Reynolds and Strouhal numbers are the same for both our experiments and a real bird flight conditions, additional force errors which can be occurred when we conduct the experiments in water should be considered. There are three components of the measured force at the wing base. These components are gravitational, inertial and aerodynamic based. Aerodynamic forces are occurs due to both the pressure distribution around the wing and viscous forces in the fluid [21]. The gravitational

contribution of the sensor and wing mass to the measured force is gravitational forces and can be easily subtracted from total force measured since when system is at rest, all measured forces are gravitational forces [30]. The aerodynamic forces which we want to obtain can be easily found if the inertial forces could be addressed. The inertial components mostly represent forces which we called as the “added mass” of the fluid around the wing.

Added mass, virtual mass or apparent mass is the added inertia to the system which is caused by the increase or decrease in the body acceleration and this acceleration makes the fluid move around the body to let the body can move through it since body and the fluid cannot occupy same physical space simultaneously. This can be modeled as the volume of the fluid moves along the object [31]. The non-circulatory forces due to added mass are more difficult to measure when it is compared with gravity and wing inertia, since the fluid acceleration induced by a moving wing changes dynamically as the wing rotates or accelerates [30]. However the potential contribution of added mass can be calculated by using an analytical model for an infinitesimally thin 2D plate moving in an inviscid fluid modified towards 2D conditions using a blade element approach [21]. This approximation is valid only when wing rotates around an axis located at one quarter chord length from the leading edge. Since the wings used in this study are located at one quarter chord length from the leading edge, this approximation can be used to calculate the added mass. The force contribution normal to the wing surface due to added mass inertia is given by [21] [30]:

$$F_{added}(t) = \frac{1}{4} \left[ \pi \rho R^2 \bar{c}^2 (\ddot{\phi} \sin \alpha + \dot{\phi} \dot{\alpha} \cos \alpha) \int_0^1 \hat{r} \hat{c}^2(\hat{r}) d\hat{r} \right] + \frac{1}{16} \left[ \pi \rho R \bar{c}^3 \ddot{\alpha} \int_0^1 \hat{c}^3(\hat{r}) d\hat{r} \right] \quad (20)$$

Where  $\rho$  is the fluid density,  $R$  is the wing length,  $\bar{c}$  is the mean chord length,  $\hat{r}$  is the non-dimensional radial position along the wing,  $\hat{c}(\hat{r})$  is the non-dimensional wing chord,  $\phi$  is the angular position of the wing and  $\alpha$  is the angle of attack. In this study all cases are constant pitch angle cases therefore  $\dot{\alpha}$  and  $\ddot{\alpha}$  goes to zero and the equation becomes:

$$F_{added}(t) = \frac{1}{4} \left[ \pi \rho R^2 \bar{c}^2 \ddot{\phi} \sin \alpha \int_0^1 \hat{r} \hat{c}^2(\hat{r}) d\hat{r} \right] \quad (21)$$

Since the angular acceleration is changing sinusoidal during the motion for this study added mass force will be changed sinusoidal too. Integral part of the equation is calculated numerically. Each case has different values of added mass force due to variation of pitch angle. Density of the water is assumed as  $998 \text{ kg/m}^3$  and total radius of the motion which is constant for all cases is  $0.31 \text{ m}$ .  $\bar{c}$  is the mean aerodynamic chord of each wing which is given in Table 5.1. Therefore Equation 19 becomes;

$$F_{added\ Flat}(t) = 0.0153\ddot{\phi} \sin \alpha \quad (22)$$

$$F_{added\ Hum}(t) = 0.00675\ddot{\phi} \sin \alpha \quad (23)$$

$$F_{added\ Zimm}(t) = 0.00705\ddot{\phi} \sin \alpha \quad (24)$$

Since angular acceleration is known, all added mass forces can be calculated now. The added mass for the Flat plate, Hummingbird and Zimmermann are varying between  $0.000533\text{-}0.0122 \text{ N}$ ,  $0.000235\text{-}0.0054 \text{ N}$  and  $0.000245\text{-}0.00564 \text{ N}$  respectively. As it is seen from the added mass values, they have quite small effect on normal forces. Thus for similar kinematics and geometry, provided that Reynolds and Strouhal number is the same, experiments can be performed both in air or water tank.



## CHAPTER 6

### CONCLUSION

In first part of this study, modifications on the mechanism which is capable of mimicking the insect flight have been performed at different experimental conditions and presented. Various problems about the experimental setup have been solved via appropriate modifications. Flapping wing mechanisms working in water or oil in the literature are studied to see their capabilities. Dynamic scaling is mentioned to find the system working frequency. A brief explanation about test procedure and experimental setup is given.

Several flapping trajectories have been investigated thanks to adjustable kinematic of the mechanism. Experiments performed with this mechanism are given in the second part of the study. During performing the cases followings are done. Pitch angle of the each wing is adjusted before the experiment is started. Wings make pure sweep motion in all cases. Experimental analysis have been done between Reynolds number 6000 and 32000 for 7 cases. In these cases the effect of increase in pitch and stroke angles are investigated. Three types of wings (Flat plate, Hummingbird, Zimmermann) are used to see the effect of wing geometry on the aerodynamic efficiency. 50 flapping cycle has been performed to reduce the effect of the noises. Force and moment measurement are done by using ATI Nano 17 transducer. A MATLAB code is used to interpret the data obtained during the experiments. This code erases the steady state data and divides the rest into two pieces which are impulsive and periodic regions. After that the code filters the data by using a Butterworth filter with a 0.5 Hz. cut-off frequency. Furthermore it obtains the phase averaged forces and calculates the total forces. Finally it plots the graphics needed.

Forces and  $C_L$  values are compared and discussed for each case and each wing separately. An increase is observed on the Lift forces until 30° pitch angle is reached.

After 30° lift force is not increased however a drastic increase is seen on the drag forces. Flat plate has the biggest values for all cases for the Lift force due to its large reference area. On the other hand Hummingbird has a sufficient efficiency in the upstrokes of the cases.  $C_L$  values are increased with the increasing pitch angle. However, it is shown by this study that Zimmermann is the most efficient wing with its high L/D ratios. Furthermore, 30 degree pitch angle cases are the most efficient cases of all cases.

The data obtained from our cases can be used to design a flapping Micro Air Vehicle. It could be said to robotic people to guide them that the added mass effect should be considered for varying pitch angles since it is getting increased with varying pitch angles. Its order of magnitude could become considerable while pitch angle is varying. Moreover, since L/D ratios are getting so small after 30° pitch angle, the micro air vehicle can be design to flap between 0 and 30° degree pitch angles. Finally, by looking the order of magnitude of the lift forces, robotic people can decide which frequency and stroke angle are needed for their weight of the system.

## **6.1 Recommendations for the Further Studies**

Although there had been some modifications on the mechanical part new modifications can be done as part of further studies. Bearings of the gears and rods must be strengthened since there are spaces between bearings and gears and this condition cause an uncertainty. A sensor which is measuring wings position must be located to the system to obtain accurate results. The mechanism should be used wings position data as feedback to correct the wing trajectory. PIV measurement is suggested to have a better understanding of the vortex topology. Another recommendation as part of this study is making the experiment in air to see the effect of virtual mass. The experiment must be done by only changing the frequency of the system. New frequency for the air experiment can be found by using Equation 8. If lift forces generated in air is known the difference between two experiments can be defined as virtual mass effect.

## REFERENCES

- [1] Moskowitz, C. “Many Mysteries of Flight Remain”  
[Online]. Available: <http://www.livescience.com/2344-mysteries-flight-remain.html>  
[Accessed 7 February 2015].
- [2] Kurtuluş, D. F., Numerical and Experimental Analysis of Flapping Motion in Hover. Application to Micro Air Vehicle, Joint Ph.D. Thesis, Poitiers University/ENSMA (Poitiers-France) and METU (Ankara-Turkey), June 2005.
- [3] Mutlu, T., Development and Testing of a 3 DoF Tandem Flapping Wing Mechanism, M.S. Thesis, Middle East Technical University METU (Ankara-Turkey), February 2014.
- [4] Sane, S., “The Aerodynamics of the Insect Flight” *Department of Biology, University of Washington, Seattle, WA 98195, USA*, 2003
- [5] Birch, J., Dickinson M., “Spanwise flow and the attachment of the leading-edge vortex on insect wings” *Department of Integrative Biology, University of California, Berkeley, California 94720, USA*, 2001.
- [6] Ansari, S., Zbikowski, R., Knowles, K., “Aerodynamic modelling of insect-like flapping flight for micro air vehicles” *Department of Aerospace, Power and Sensors, Cranfield University, Defence Academy of the United Kingdom, Shrivenham, England*, 2006
- [7] Scientific American, “Catching the Wake”  
[Online]. Available: <http://www.scientificamerican.com/article/catching-the-wake/>  
[Accessed 22 June 2015].

[8] Dickinson, M., “The Effects of Wing Rotation on Unsteady Aerodynamic Performance at Low Reynolds Numbers” *Department of Organismal Biology and Anatomy, The University of Chicago, USA, 1994*

[9] Isaac, K., Rolwes, J., “Unsteady Flow Features of a Flapping and Pitching Wing at Low Reynolds Number” *25th AIAA Aerodynamic Measurement Technology and Ground Testing Conference, California, 2006*

[10] Günaydinoğlu, E., Low Reynolds Number Aerodynamics of Flapping Airfoils in Hover and Forward Flight, M.S. Thesis, Middle East Technical University METU (Ankara-Turkey), September 2010.

[11] Viieru, D., Tang, J., Lian, Y., Liu, H., Shyy, W., “Flapping and Flexible Wing Aerodynamics of Low Reynolds Number Flight Vehicles” *44th AIAA Aerospace Sciences Meeting and Exhibit, Nevada, 2006*

[12] Cheng, B., Fry, S., Huang, Q., Deng, X., “Aerodynamic damping during rapid flight maneuvers in the fruit fly *Drosophila*” *The Journal of Experimental Biology, Newark, USA, 2010*

[13] Dickinson, M., Götz, K., “The Wake Dynamics and Flight Forces of the Fruit fly *Drosophila Melanogaster*” *The Journal of Experimental Biology, Berkeley, USA, Tübingen, Germany, 1996*

[14] Wikimedia “Insect Flight Upstroke and Downstroke”

[Online]. Available: [https://upload.wikimedia.org/wikipedia/commons/thumb/3/34/Insect\\_flight\\_downstroke.svg/564px-Insect\\_flight\\_downstroke.svg.png](https://upload.wikimedia.org/wikipedia/commons/thumb/3/34/Insect_flight_downstroke.svg/564px-Insect_flight_downstroke.svg.png)

[Accessed 1 June 2015]

[15] Deppe, A., “Hummingbirds”

[Online]. Available: <http://smileimfine.com/2014/09/26/hummingbirds/>

[Accessed 10 June 2015]

- [16] Artis, S. "A Plethora of Black-Chinned Hummingbirds"  
[Online]. Available: <http://journalowl.com/a-plethora-of-black-chinned-hummingbirds/>  
[Accessed 10 June 2015].
- [17] Han, J., Chang, J., Kang, I., Kim, S., "Flow Visualization and Force Measurement of an Insect-based Flapping Wing" *48th AIAA Aerospace Sciences Meeting Including the New Horizons Forum and Aerospace Exposition*, 4 - 7 January 2010, Orlando, Florida
- [18] George, R., Colton, M., Mattson, C., Thomson, S., "A Differentially Driven Flapping Wing Mechanism for Force Analysis and Trajectory Optimization", *Brigham Young University, Ira A. Fulton College of Engineering and Technology, Department of Mechanical Engineering, USA*, 2012
- [19] Isaac, K., Colozza, A., Rolwes, J., "Force Measurements on a Flapping and Pitching Wing at Low Reynolds Numbers" *44<sup>th</sup> AIAA Aerospace Sciences Meeting and Exhibit*, 9-12 Jan. 2006
- [20] Hu, Z., Deng, X., "Aerodynamic Effect of Forewing-Hindwing Interactions in Hovering and Forward Flight of Dragonfly" *Department of Mechanical Engineering, University of Delaware*, 2009
- [21] Maybury, W., Lehmann, F., "The fluid dynamics of flight control by kinematic phase lag variation between two robotic insect wings" *The Journal of Experimental Biology* 207, 4707-4726 Published by The Company of Biologists, 2004
- [22] Zhang, X., Lua, K., Chang, R., Lim, T., Yeo, K., "Experimental Study of Ground Effect on Three-Dimensional Insect-Like Flapping Motion", *5th International Symposium on Physics of Fluids (ISPF5) International Journal of Modern Physics, Singapore*, 2014

- [23] Morrison, C., Vandenheede, R., Kumar, D., Bernal, L., Cesnik, C., “Force Measurements of a Flapping Wing with Two Angular Degrees of Freedom and Bio-Inspired Kinematics”, *50th AIAA Aerospace Sciences Meeting including the New Horizons Forum and Aerospace Exposition, Tennessee*, 2012
- [24] Nagai, H., Isogai, K., Hayase, T., “Measurement of Unsteady Aerodynamic Forces of 3D Flapping Wing in Hovering to Forward Flight” *26<sup>th</sup> International Congress of the Aeronautical Sciences*, 2008
- [25] Wang, Z., Birch, J., Dickinson, M., “Unsteady forces and flows in low Reynolds number hovering flight: two-dimensional computations vs. robotic wing experiments” *California Institute of Technology*, 2003
- [26] Banerjee, A., Ghosh, S., Das, D., “Aerodynamics of Flapping Wing at Low Reynolds Numbers: Force Measurement and Flow Visualization” *International Scholarly Research Network ISRN Mechanical Engineering Volume 2011*, 2011
- [27] Milano, M., Gharib, M., “Uncovering the physics of flapping flat plates with artificial evolution” *Graduate Aeronautics Laboratories, Option of Bioengineering, California Institute of Technology, USA*, 2005
- [28] Dickinson, M., “Unsteady Mechanisms of Force Generation in Aquatic and Aerial Locomotion” *Department of Integrative Biology, University of California, Berkeley, California*, 1996
- [29] Sohn, M., Chang, J., “Flow visualization and aerodynamic load calculation of three types of clap-fling motions in a Weis-Fogh mechanism” *Aerospace Science and Technology, Korea*, 2006
- [30] Sane, S., Dickinson, M., “The Control of Flight Force by a Flapping Wing: Lift and Drag Production” *Department of Integrative Biology, University of California, Berkeley, USA*, 2001

- [31] Ghassemi, H., Yari, E., “The Added Mass Coefficient computation of sphere, ellipsoid and marine propellers using Boundary Element Method” *Polish Maritime Research*, 2011
- [32] Wu, D., Yeo, K., Lim, T., “A numerical study on the free hovering flight of a model insect at low Reynolds number” *Department of Mechanical Engineering, National University of Singapore*, 2014
- [33] Aono, H., Liu H., “Flapping wing aerodynamics of a numerical biological flyer model in hovering flight” *Institute of Space and Astronautical Science/Japan Aerospace, Exploration Agency, Japan*, 2012
- [34] Shyy, W., Aono, H., Chimakurthi S.K., Trizila, P., Kang, C.-K., Cesnik, C.E.S., Liu, H., “Recent progress in flapping wing aerodynamics and aeroelasticity” *Department of Aerospace Engineering, University of Michigan, USA*, 2010
- [35] Sane, S., “Steady or Unsteady? Uncovering the aerodynamic mechanisms of insect flight” *The Journal of Experimental Biology*, 2011
- [36] Maxworthy, T., “Experiments on the Weis-Fogh mechanism of lift generation by insects in hovering flight. Part 1. Dynamics of the ‘fling’” *Departments of Mechanical and Aerospace Engineering, University of Southern California*, 1978
- [37] Berg, V., Ellington, C., “The three-dimensional leading-edge vortex of a ‘hovering’ model hawkmoth” *Department of Zoology, University of Cambridge, UK*, 1997
- [38] Salles, R., Schiele, A., “Analysis of Flapping Wing Robots for Planetary Exploration, an Evolutionary Approach” *Departments of Mechanical and Aerospace Engineering, University of Southern California*, 2004

- [39] Campos, D., Ukeiley, L., Bernal, L., “Flow Around Flapping Flexible Flat Plate Wings” *50th AIAA Aerospace Sciences Meeting including the New Horizons Forum and Aerospace Exposition, Nashville, Tennessee, 2012*
- [40] Naegle, N.S., Force Optimization and Flow Field Characterization from a Flapping Wing Mechanism, M.S. Thesis, Brigham Young University, October 2012.
- [41] Ho, S., Nassef, H., Pornsinsirak, N., Tai, Y., Ho, C., “Unsteady aerodynamics and flow control for flapping wing flyers” *Department of Mechanical Engineering, University of California, Los Angeles, USA, 2003*
- [42] Rosis, A., “Ground-induced lift enhancement in a tandem of symmetric flapping wings: Lattice Boltzman-immersed boundry simulations” *Laboratoire de Mécanique des Fluides et d’Acoustique (LMFA), France, 2014*
- [43] Soltani, M., Marzabadi, F., “Effect of Reduced Frequency on the Aerodynamic Behavior of an Airfoil Oscillating in a Plunging Motion” *Transaction B: Mechanical Engineering, Sharif University of Technology, Persia, 2009*
- [44] DeLaurier, J.D., “An aerodynamic model for flapping-wing flight” *Institute of Aerospace Studies, University of Toronto, Canada, 1993*
- [45] Mueller, T., “Aerodynamic Measurements at Low Reynolds Numbers for Fixed Wing Micro-Air Vehicles” *Hessert Center for Aerospace Research University of Notre Dame, 1999*
- [46] Brunton, S., Rowley, C., “Modeling the unsteady aerodynamic forces on small-scale wings” *47<sup>th</sup> AIAA Aerospace Sciences Meeting, 2009*
- [47] Zhang, G., Peyada, N. Go, T., Yu, S., “Design and investigation of a bio-inspired ventilated flapping wing” *Journal of Aerospace Engineering, 2014*

- [48] Hubel, T., Tropea, C., “Experimental investigation of a flapping wing model” *Experiments in Fluids*, 2008
- [49] Omoware, W., Maheri, A., Azimov, U., “Aerodynamic Analysis of Flapping-Pitching Flat Plates” *Faculty of Engineering and Environment Northumbria University at Newcastle Newcastle upon Tyne, United Kingdom*, 2014
- [50] Razak, N., Dimitriadis, G., “Experimental study of wings undergoing active root flapping and pitching” *School of Aerospace Engineering, Universiti Sains Malaysia, Malaysia*, 2013
- [51] Ghommem, M., Collier, N., Niemi, A., Calo, V., “Shape Optimisation and Performance Analysis of Flapping Wings” *Proceedings of the Eighth International Conference on Engineering Computational Technology, Scotland*, 2012
- [52] Lu, H., Lua, K., Lim, T., Yeo, K., “Aerodynamics of a two-dimensional hovering wing in ground effect” *Department of Mechanical Engineering, National University of Singapore, Singapore*, 2014
- [53] Percin, M., Ziegler, L., Oudheusden, B., “Flow around a Suddenly Accelerated Rotating Plate at Low Reynolds Number” *Faculty of Aerospace Engineering, Delft University of Technology, Delft, The Netherlands*, 2014
- [54] Lock, R., Vaidyanathan, R., Burgess, S., “Impact of Marine Locomotion Constraints on a Bio-inspired Aerial-Aquatic Wing: Experimental Performance Verification” *Journal of Mechanisms and Robotics*, 2014
- [55] Legowo, A., Mohamad, Z., “Investigation on Flow Visualization of Beetle Mimicking Ornithopter” *Asian Journal of Applied Sciences*, 2014
- [56] Baik, Y., Bernal, L., “Experimental study of pitching and plunging airfoils at low Reynolds numbers” *Experiments in Fluids*, 2012

[57] Wu, J., Sun, M., “Unsteady aerodynamic forces of a flapping wing” Institute of Fluid Mechanics, Beijing *University of Aeronautics & Astronautics, People’s Republic of China*, 2004

[58] Mueller, T., J., Fixed and Flapping Wing Aerodynamics for Micro Air Vehicle Applications, Reston, Virginia: AIAA, 2001

[59] Ennos, A., R., “The Kinematics and Aerodynamics of the Free Flight of Some Diptera” *Department of Biological Sciences, Hatherly Laboratories, University of Exeter*, Great Britain, 1988

[60] Thompson, M., Burnett, J., Batra, A., Ixtabalan, D., Tran, D., “Experimental Design of a Flapping Wing Micro Air Vehicle through Biomimicry of Bumblebees” *Arizona State University, Arizona, United States*, 2015

[61] Altshuler, D., L., Dudley, R., Ellington, C., “Aerodynamic forces of revolving hummingbird wings and wing models” *The Zoological Society of London, United Kingdom*, 2004

## APPENDIX A

### DATA ANALYSIS

```
%*****
%*
%*   ATI NANO 17 Data Analyzer Version 1.6
%*
%*   Modified By Hasan ÇAKIR - 08.03.2015
%*
%*   Department of Aerospace Engineering
%*   Middle East Technical University
%*
%*   Date: 08.03.2015
%*
%*****
%*
%*   Clear the Workspace before starting the analysis
%*
clc
clear all
close all
%*
%% Load input file
%* Data Format: t,t/T,F_n,F_t
%* t:time[s]
%* Initially we enter the beginning time for each case since there
is a rest time at first.
a=input('Please enter the beginning time for Flat plate=');
b=input('Please enter the beginning time for Hummingbird=');
c=input('Please enter the beginning time for Zimmermann=');
d_derece=input('Please enter the pitch angle for the airfoils in
degree=');
d=d_derece*pi/180;% we convert the pitch angle to the radians
e_derece=input('Please enter the sweep angle for the airfoils in
degree=');
e=e_derece*pi/180;% we convert the sweep angle to the radians
%% Now the raw data of Flat Plate will be read.
fid1 = fopen('1plunge30_pitch30.txt','r+');
data_flat=textscan(fid1, '%f %f %f %f %f %f','delimiter',
',','EmptyValue', -Inf);
data1=[data_flat{2} data_flat{3}];
data1_flat=zeros(length(data1)-a*1000,3);
data1_flat_imp=zeros(100000,3);
data1_flat_norm=zeros(length(data1_flat)-100000,3);
for i=2:3
L1_flat = length(data_flat{i});
data_flat{i}=data_flat{i}-data_flat{i}(1,1)*ones(L1_flat,1);
data_flat{i}(1:a*1000)=[];
[t1] = 0.001:0.001:(length(data_flat{i}))/1000;
data1_flat(:,i)=data_flat{i};
```

```

for j=1:length(data1_flat(:,i))
if j<=100000
data1_flat_imp(j,i)=data1_flat(j,i);
end
if (100000<j)&&(j<=length(data1_flat(:,i)))
data1_flat_norm(j-100000,i)=data1_flat(j,i);
end
end
end
end
%% Now the raw data of Hummingbird will be read.
fid2 = fopen('2plunge30_pitch30.txt','r+');
data_hum=textscan(fid2, '%f %f %f %f %f %f','delimiter',
',','EmptyValue', -Inf);
data2=[data_hum{2} data_hum{3}];
data2_hum=zeros(length(data2)-b*1000,3);
data2_hum_imp=zeros(100000,3);
data2_hum_norm=zeros(length(data2_hum)-100000,3);
for i=2:3
L1_hum = length(data_hum{i});
data_hum{i}=data_hum{i}-data_hum{i}(1,1)*ones(L1_hum,1);
data_hum{i}(1:b*1000)=[];
[t2] = 0.001:0.001:(length(data_hum{i}))/1000);
data2_hum(:,i)=data_hum{i};
for j=1:length(data2_hum(:,i))
if j<=100000
data2_hum_imp(j,i)=data2_hum(j,i);
end
if (100000<j)&&(j<=length(data2_hum(:,i)))
data2_hum_norm(j-100000,i)=data2_hum(j,i);
end
end
end
end
%% Now the raw data of Zimmermann will be read.
fid3 = fopen('3plunge30_pitch30.txt','r+');
data_tlh=textscan(fid3, '%f %f %f %f %f %f','delimiter', ',',
'EmptyValue', -Inf);
data3=[data_tlh{2} data_tlh{3}];
data3_tlh=zeros(length(data3)-c*1000,3);
data3_tlh_imp=zeros(100000,3);
data3_tlh_norm=zeros(length(data3_tlh)-100000,3);
for i=2:3
L1_tlh = length(data_tlh{i});
data_tlh{i}=data_tlh{i}-data_tlh{i}(1,1)*ones(L1_tlh,1);
data_tlh{i}(1:c*1000)=[];
[t3] = 0.001:0.001:(length(data_tlh{i}))/1000);
data3_tlh(:,i)=data_tlh{i};
for j=1:length(data3_tlh(:,i))
if j<=100000
data3_tlh_imp(j,i)=data3_tlh(j,i);
end
if (100000<j)&&(j<=length(data3_tlh(:,i)))
data3_tlh_norm(j-100000,i)=data3_tlh(j,i);
end
end
end
end
t_imp=0.001:0.001:100;
%% FFT Analysis(for Flat plate)
T=0.001; % Sample time
Fs=1/T; % Sampling frequency
t_flat= (0:L1_flat-1)*T;% Time vector

```

```

Y1_flat = fft(data_flat{2})/L1_flat;
f1_flat = Fs/2*linspace(0,1,L1_flat/2+1);

Y2_flat = fft(data_flat{3})/L1_flat;
f2_flat = Fs/2*linspace(0,1,L1_flat/2+1);
%% FFT Analysis(for Hummingbird)
T=0.001; % Sample time
Fs=1/T; % Sampling frequency
t_hum= (0:L1_hum-1)*T;% Time vector

Y1_hum = fft(data_hum{2})/L1_hum;
f1_hum = Fs/2*linspace(0,1,L1_hum/2+1);

Y2_hum = fft(data_hum{3})/L1_hum;
f2_hum = Fs/2*linspace(0,1,L1_hum/2+1);
%% FFT Analysis(for Zimmermann)
T=0.001; % Sample time
Fs=1/T; % Sampling frequency
t_tlh= (0:L1_tlh-1)*T;% Time vector

Y1_tlh = fft(data_tlh{2})/L1_tlh;
f1_tlh = Fs/2*linspace(0,1,L1_tlh/2+1);

Y2_tlh = fft(data_tlh{3})/L1_tlh;
f2_tlh = Fs/2*linspace(0,1,L1_tlh/2+1);
%% Filter force measurement by using Butterworth filter(for flat-
plate)
cut_off_freq = 0.5;
samp_freq=1000;
[b,a] = butter(5,2*cut_off_freq/samp_freq,'low');

fdata_flat_imp(:,2:3) = filter(b,a,data1_flat_imp(:,2:3));

fdata_flat_norm(:,2:3) = filter(b,a,data1_flat_norm(:,2:3));

l_imp=length(fdata_flat_imp);
fdata1_flat_imp=zeros(length(fdata_flat_imp),3);
l_norm=length(fdata_flat_norm);
fdata1_flat_norm=zeros(length(fdata_flat_norm),3);
%reverse the data string
for j=1:l_imp
fdata1_flat_imp(j,2:3)=fdata_flat_imp(l_imp+1-j,2:3);

end
for j=1:l_norm
fdata1_flat_norm(j,2:3)=fdata_flat_norm(l_norm+1-j,2:3);

end

%filter again to cancel out the phase shift
fdata2_flat_imp(:,2:3) = filter(b,a,fdata1_flat_imp(:,2:3));

fdata2_flat_norm(:,2:3) = filter(b,a,fdata1_flat_norm(:,2:3));

```

```

%reverse the data string to original order
for j=1:l_imp
    fdata_flat_imp(j,2:3)=fdata2_flat_imp(l_imp+1-j,2:3);

end
for j=1:l_norm
fdata_flat_norm(j,2:3)=fdata2_flat_norm(l_norm+1-j,2:3);

end

%% Filter force measurement by using Butterworth filter(for
hummingbird)
cut_off_freq = 0.5;
samp_freq=1000;
[b,a] = butter(5,2*cut_off_freq/samp_freq,'low');
fdata_hum_imp(:,2:3) = filter(b,a,data2_hum_imp(:,2:3));

fdata_hum_norm(:,2:3) = filter(b,a,data2_hum_norm(:,2:3));

l_imp=length(fdata_hum_imp);
fdata1_hum_imp=zeros(length(fdata_hum_imp),3);
l_norm=length(fdata_hum_norm);
fdata1_hum_norm=zeros(length(fdata_hum_norm),3);
%reverse the data string

for j=1:l_imp
    fdata1_hum_imp(j,2:3)=fdata_hum_imp(l_imp+1-j,2:3);

end
for j=1:l_norm
    fdata1_hum_norm(j,2:3)=fdata_hum_norm(l_norm+1-j,2:3);

end
%filter again to cancel out the phase shift
fdata2_hum_imp(:,2:3) = filter(b,a,fdata1_hum_imp(:,2:3));

fdata2_hum_norm(:,2:3) = filter(b,a,fdata1_hum_norm(:,2:3));

%reverse the data string to original order
for j=1:l_imp
    fdata_hum_imp(j,2:3)=fdata2_hum_imp(l_imp+1-j,2:3);

end
for j=1:l_norm
    fdata_hum_norm(j,2:3)=fdata2_hum_norm(l_norm+1-j,2:3);

end

%% Filter force measurement by using Butterworth filter(for
Zimmermann)
cut_off_freq = 0.5;
samp_freq=1000;
[b,a] = butter(5,2*cut_off_freq/samp_freq,'low');
fdata_tlh_imp(:,2:3) = filter(b,a,data3_tlh_imp(:,2:3));

```

```

fdata_tlh_norm(:,2:3) = filter(b,a,data3_tlh_norm(:,2:3));

l_imp=length(fdata_tlh_imp);
fdata1_tlh_imp=zeros(length(fdata_tlh_imp),3);
l_norm=length(fdata_tlh_norm);
fdata1_tlh_norm=zeros(length(fdata_tlh_norm),3);
%reverse the data string

for j=1:l_imp
    fdata1_tlh_imp(j,2:3)=fdata_tlh_imp(l_imp+1-j,2:3);

end
for j=1:l_norm
    fdata1_tlh_norm(j,2:3)=fdata_tlh_norm(l_norm+1-j,2:3);

end
%filter again to cancel out the phase shift
fdata2_tlh_imp(:,2:3) = filter(b,a,fdata1_tlh_imp(:,2:3));

fdata2_tlh_norm(:,2:3) = filter(b,a,fdata1_tlh_norm(:,2:3));

%reverse the data string to original order
for j=1:l_imp
    fdata_tlh_imp(j,2:3)=fdata2_tlh_imp(l_imp+1-j,2:3);

end
for j=1:l_norm
    fdata_tlh_norm(j,2:3)=fdata2_tlh_norm(l_norm+1-j,2:3);

end

%% Phase average filtered data force(for flat plate)
% * Normal force
N_phase_flat = floor(length(fdata_flat_norm)/10000)-1;
phase_avg1_flat=zeros(10000,1);
phase_avg2_flat=zeros(10000,1);
phase_avg1_avg_flat=zeros(10000,1);
phase_avg2_avg_flat=zeros(10000,1);
Fz_Normal_flat=zeros(10000,1);
Fy_Normal_flat=zeros(10000,1);
for j=1:10000
    sum = 0;
    for i=1:N_phase_flat
        temp = fdata_flat_norm(j+10000*(i-1),3);
        sum = sum + temp;
    end
    phase_avg1_flat(j) = sum / N_phase_flat;
    Fz_Normal_flat(j)=phase_avg1_flat(j)*cos(d);
    Fy_Normal_flat(j)=phase_avg1_flat(j)*sin(d);
end
%% Average of the Phase average for normal force
for j=1:10000
    sum = 0;
for i=1:10000
        temp = phase_avg1_flat(i);
        sum = sum + temp;
end
phase_avg1_avg_flat(j)=sum/10000;

```

```

end

%% Tangential force
Fz_Tangential_flat=zeros(10000,1);
Fy_Tangential_flat=zeros(10000,1);
for j=1:10000
    sum = 0;
    for i=1:N_phase_flat
        temp = fdata_flat_norm(j+10000*(i-1),2);
        sum = sum + temp;
    end
    phase_avg2_flat(j) = sum / N_phase_flat;
    Fz_Tangential_flat(j)=phase_avg2_flat(j)*sin(d);
    Fy_Tangential_flat(j)=phase_avg2_flat(j)*cos(d);
end
Fz_flat=zeros(10000,1);
Fy_flat=zeros(10000,1);
for j=1:10000
    Fz_flat(j)=Fz_Normal_flat(j)-Fz_Tangential_flat(j);
    Fy_flat(j)=Fy_Normal_flat(j)+Fy_Tangential_flat(j);
end
%% Average of the Phase average
for j=1:10000
    sum = 0;
    for i=1:10000
        temp = phase_avg2_flat(i);
        sum = sum + temp;
    end
    phase_avg2_avg_flat(j)=sum/10000;
end

%% Phase average filtered data force(for hummingbird)
% * Normal force
N_phase_hum = floor(length(fdata_hum_norm)/10000)-1;
phase_avg1_hum=zeros(10000,1);
phase_avg2_hum=zeros(10000,1);
phase_avg1_avg_hum=zeros(10000,1);
phase_avg2_avg_hum=zeros(10000,1);
Fz_Normal_hum=zeros(10000,1);
Fy_Normal_hum=zeros(10000,1);
for j=1:10000
    sum = 0;
    for i=1:N_phase_hum
        temp = fdata_hum_norm(j+10000*(i-1),3);
        sum = sum + temp;
    end
    phase_avg1_hum(j) = sum / N_phase_hum;
    Fz_Normal_hum(j)=phase_avg1_hum(j)*cos(d);
    Fy_Normal_hum(j)=phase_avg1_hum(j)*sin(d);
end
%% Average of the Phase average for normal force
for j=1:10000
    sum = 0;
    for i=1:10000
        temp = phase_avg1_hum(i);
        sum = sum + temp;
    end
    phase_avg1_avg_hum(j)=sum/10000;
end

```

```

%% Tangential force
Fz_Tangential_hum=zeros(10000,1);
Fy_Tangential_hum=zeros(10000,1);
for j=1:10000
    sum = 0;
    for i=1:N_phase_hum
        temp = fdata_hum_norm(j+10000*(i-1),2);
        sum = sum + temp;
    end
    phase_avg2_hum(j) = sum / N_phase_hum;
    Fz_Tangential_hum(j)=phase_avg2_hum(j)*sin(d);
    Fy_Tangential_hum(j)=phase_avg2_hum(j)*cos(d);
end
Fz_hum=zeros(10000,1);
Fy_hum=zeros(10000,1);
for j=1:10000
    Fz_hum(j)=Fz_Normal_hum(j)-Fz_Tangential_hum(j);
    Fy_hum(j)=Fy_Normal_hum(j)+Fy_Tangential_hum(j);
end
%% Average of the Phase average for tangential force
for j=1:10000
    sum = 0;
    for i=1:10000
        temp = phase_avg2_hum(i);
        sum = sum + temp;
    end
    phase_avg2_avg_hum(j)=sum/10000;
end

%% Phase average filtered data force(for Zimmermann)
% * Normal force
N_phase_tlh = floor(length(fdata_tlh_norm)/10000)-1;
phase_avg1_tlh=zeros(10000,1);
phase_avg2_tlh=zeros(10000,1);
phase_avg1_avg_tlh=zeros(10000,1);
phase_avg2_avg_tlh=zeros(10000,1);
Fz_Normal_tlh=zeros(10000,1);
Fy_Normal_tlh=zeros(10000,1);
for j=1:10000
    sum = 0;
    for i=1:N_phase_tlh
        temp = fdata_tlh_norm(j+10000*(i-1),3);
        sum = sum + temp;
    end
    phase_avg1_tlh(j) = sum / N_phase_tlh;
    Fz_Normal_tlh(j)=phase_avg1_tlh(j)*cos(d);
    Fy_Normal_tlh(j)=phase_avg1_tlh(j)*sin(d);
end
%% Average of the Phase average for normal force
for j=1:10000
    sum = 0;
    for i=1:10000
        temp = phase_avg1_tlh(i);
        sum = sum + temp;
    end
    phase_avg1_avg_tlh(j)=sum/10000;
end
%% Tangential force
Fz_Tangential_tlh=zeros(10000,1);

```

```

Fy_Tangential_tlh=zeros(10000,1);
for j=1:10000
    sum = 0;
    for i=1:N_phase_tlh
        temp = fdata_tlh_norm(j+10000*(i-1),2);
        sum = sum + temp;
    end
    phase_avg2_tlh(j) = sum / N_phase_tlh;
    Fz_Tangential_tlh(j)=phase_avg2_tlh(j)*sin(d);
    Fy_Tangential_tlh(j)=phase_avg2_tlh(j)*cos(d);
end
Fz_tlh=zeros(10000,1);
Fy_tlh=zeros(10000,1);
for j=1:10000
    Fz_tlh(j)=Fz_Normal_tlh(j)-Fz_Tangential_tlh(j);
    Fy_tlh(j)=Fy_Normal_tlh(j)+Fy_Tangential_tlh(j);
end

%% Phase average filtered data force for impulsive region(for flat
plate)
%* Normal force
N_phase_flat_imp = floor(length(fdata_flat_imp)/10000)-1;
phase_avg1_flat_imp=zeros(10000,1);
phase_avg2_flat_imp=zeros(10000,1);
phase_avg1_avg_flat_imp=zeros(10000,1);
phase_avg2_avg_flat_imp=zeros(10000,1);
for j=1:10000
    sum = 0;
    for i=1:N_phase_flat_imp
        temp = fdata_flat_imp(j+10000*(i-1),3);
        sum = sum + temp;
    end
    phase_avg1_flat_imp(j) = sum / N_phase_flat_imp;
end
%% Tangential force
for j=1:10000
    sum = 0;
    for i=1:N_phase_flat_imp
        temp = fdata_flat_imp(j+10000*(i-1),2);
        sum = sum + temp;
    end
    phase_avg2_flat_imp(j) = sum / N_phase_flat_imp;
end
%% Phase average filtered data force for impulsive region(for
hummingbird)
%* Normal force
N_phase_hum_imp = floor(length(fdata_hum_imp)/10000)-1;
phase_avg1_hum_imp=zeros(10000,1);
phase_avg2_hum_imp=zeros(10000,1);
phase_avg1_avg_hum_imp=zeros(10000,1);
phase_avg2_avg_hum_imp=zeros(10000,1);
for j=1:10000
    sum = 0;
    for i=1:N_phase_hum_imp
        temp = fdata_hum_imp(j+10000*(i-1),3);
        sum = sum + temp;
    end
    phase_avg1_hum_imp(j) = sum / N_phase_hum_imp;
end

```

```

%% Tangential force
for j=1:10000
    sum = 0;
    for i=1:N_phase_hum_imp
        temp = fdata_hum_imp(j+10000*(i-1),2);
        sum = sum + temp;
    end
    phase_avg2_hum_imp(j) = sum / N_phase_hum_imp;
end

%% Phase average filtered data force for impulsive region(for
Zimmermann)
%* Normal force
N_phase_tlh_imp = floor(length(fdata_tlh_imp)/10000)-1;
phase_avg1_tlh_imp=zeros(10000,1);
phase_avg2_tlh_imp=zeros(10000,1);
phase_avg1_avg_tlh_imp=zeros(10000,1);
phase_avg2_avg_tlh_imp=zeros(10000,1);
for j=1:10000
    sum = 0;
    for i=1:N_phase_tlh_imp
        temp = fdata_tlh_imp(j+10000*(i-1),3);
        sum = sum + temp;
    end
    phase_avg1_tlh_imp(j) = sum / N_phase_tlh_imp;
end

%% Tangential force
for j=1:10000
    sum = 0;
    for i=1:N_phase_tlh_imp
        temp = fdata_tlh_imp(j+10000*(i-1),2);
        sum = sum + temp;
    end
    phase_avg2_tlh_imp(j) = sum / N_phase_tlh_imp;
end

%% Average of the Phase average
for j=1:10000
    sum = 0;
    for i=1:10000
        temp = phase_avg2_tlh(i);
        sum = sum + temp;
    end
    phase_avg2_avg_tlh(j)=sum/10000;
end

%% Phase average raw data force(for Flat Plate)
%* Normal force
N_phase_flat = floor(length(data1_flat_norm)/10000)-1;
phase_avg1r_flat=zeros(10000,1);
phase_avg2r_flat=zeros(10000,1);
phase_avg1r_avg_flat=zeros(10000,1);
phase_avg2r_avg_flat=zeros(10000,1);
for j=1:10000
    sum = 0;
    for i=1:N_phase_flat
        temp = data1_flat_norm(j+10000*(i-1),3);
        sum = sum + temp;
    end
    phase_avg1r_flat(j) = sum / N_phase_flat;

```

```

end
%% Average of the Phase average
for j=1:10000
    sum = 0;
    for i=1:10000
        temp = phase_avg1r_flat(i);
        sum = sum + temp;
    end
    phase_avg1r_avg_flat(j)=sum/10000;
end
%% Tangential force
for j=1:10000
    sum = 0;
    for i=1:N_phase_flat
        temp = data1_flat_norm(j+10000*(i-1),2);
        sum = sum + temp;
    end
    phase_avg2r_flat(j) = sum / N_phase_flat;
end
%% Average of the Phase average
for j=1:10000
    sum = 0;
    for i=1:10000
        temp = phase_avg2r_flat(i);
        sum = sum + temp;
    end
    phase_avg2r_avg_flat(j)=sum/10000;
end
%% Phase average raw data force(for hummingbird)
%* Normal force
N_phase_hum = floor(length(data2_hum_norm)/10000)-1;
phase_avg1r_hum=zeros(10000,1);
phase_avg2r_hum=zeros(10000,1);
phase_avg1r_avg_hum=zeros(10000,1);
phase_avg2r_avg_hum=zeros(10000,1);
for j=1:10000
    sum = 0;
    for i=1:N_phase_hum
        temp = data2_hum_norm(j+10000*(i-1),3);
        sum = sum + temp;
    end
    phase_avg1r_hum(j) = sum / N_phase_hum;
end
%% Average of the Phase average
for j=1:10000
    sum = 0;
    for i=1:10000
        temp = phase_avg1r_hum(i);
        sum = sum + temp;
    end
    phase_avg1r_avg_hum(j)=sum/10000;
end
%% Tangential force
for j=1:10000
    sum = 0;
    for i=1:N_phase_hum
        temp = data2_hum_norm(j+10000*(i-1),2);
        sum = sum + temp;
    end
    phase_avg2r_hum(j) = sum / N_phase_hum;
end

```

```

end
%% Average of the Phase average
for j=1:10000
    sum = 0;
    for i=1:10000
        temp = phase_avg2r_hum(i);
        sum = sum + temp;
    end
    phase_avg2r_avg_hum(j)=sum/10000;
end

%% Phase average raw data force(for Zimmermann)
%* Normal force
N_phase_tlh = floor(length(data3_tlh_norm)/10000)-1;
phase_avg1r_tlh=zeros(10000,1);
phase_avg2r_tlh=zeros(10000,1);
phase_avg1r_avg_tlh=zeros(10000,1);
phase_avg2r_avg_tlh=zeros(10000,1);
for j=1:10000
    sum = 0;
    for i=1:N_phase_tlh
        temp = data3_tlh_norm(j+10000*(i-1),3);
        sum = sum + temp;
    end
    phase_avg1r_tlh(j) = sum / N_phase_tlh;
end
%% Average of the Phase average
for j=1:10000
    sum = 0;
    for i=1:10000
        temp = phase_avg1r_tlh(i);
        sum = sum + temp;
    end
    phase_avg1r_avg_tlh(j)=sum/10000;
end
%% Tangential force
for j=1:10000
    sum = 0;
    for i=1:N_phase_tlh
        temp = data3_tlh_norm(j+10000*(i-1),2);
        sum = sum + temp;
    end
    phase_avg2r_tlh(j) = sum / N_phase_tlh;
end
%% Average of the Phase average
for j=1:10000
    sum = 0;
    for i=1:10000
        temp =phase_avg2r_tlh(i);
        sum = sum + temp;
    end
    phase_avg2r_avg_tlh(j)=sum/10000;
end

%% Calculate Raw Total Force(for flat plate)
total1_flat=zeros(10000,1);
for j=1:10000
    total1_flat(j)=
sqrt(data1_flat_norm(j,2)^2+data1_flat_norm(j,3)^2);
end

```

```

%% Calculate Raw Total Force(for hummingbird)
total1_hum=zeros(10000,1);
for j=1:10000
    total1_hum(j)=
sqrt(data2_hum_norm(j,2)^2+data2_hum_norm(j,3)^2);
end
%% Calculate Raw Total Force(for zimmermann)
total1_tlh=zeros(10000,1);
for j=1:10000
    total1_tlh(j)=
sqrt(data3_tlh_norm(j,2)^2+data3_tlh_norm(j,3)^2);
end
%% Calculate Phase Averaged and Filtered Total Force(for flat plate)
total_flat=zeros(10000,1);
for j=1:10000
    total_flat(j)= sqrt(phase_avg1_flat(j)^2+phase_avg2_flat(j)^2);
end
%% Calculate Phase Averaged and Filtered Total Force(for
hummingbird)
total_hum=zeros(10000,1);
for j=1:10000
    total_hum(j)= sqrt(phase_avg1_hum(j)^2+phase_avg2_hum(j)^2);
end
%% Calculate Phase Averaged and Filtered Total Force(for Zimmermann)
total_tlh=zeros(10000,1);
for j=1:10000
    total_tlh(j)= sqrt(phase_avg1_tlh(j)^2+phase_avg2_tlh(j)^2);
end
%% Calculate Phase Averaged Raw Total Force(for flat plate)
totalr_flat=zeros(10000,1);
for j=1:10000
    totalr_flat(j)=
sqrt(phase_avg1r_flat(j)^2+phase_avg2r_flat(j)^2);
end
%% Calculate Phase Averaged Raw Total Force(for hummingbird)
totalr_hum=zeros(10000,1);
for j=1:10000
    totalr_hum(j)= sqrt(phase_avg1r_hum(j)^2+phase_avg2r_hum(j)^2);
end
%% Calculate Phase Averaged Raw Total Force(for Zimmermann)
totalr_tlh=zeros(10000,1);
for j=1:10000
    totalr_tlh(j)= sqrt(phase_avg1r_tlh(j)^2+phase_avg2r_tlh(j)^2);
end

%% Calculate Phase Averaged Cl Value for all three wings
l=0.31;%Distance from rotation center to the tip chord
f=0.1;%Frequency in Hertz
V=2*1*e*f;% e is the sweep angle for a stroke, V is the mean
velocity
Vmax=3.17829*V;% Vmax is the maximum velocity for a stroke which is
seen at the middle of a stroke
Rho=998; %Density of water
S_flat=0.019;% Reference area for flat plate
S_hum=0.016;% Reference area for hummingbird
S_tlh=0.015;% Reference area for zimmermann
Dyn_Press_flat=0.5*(Rho*S_flat*Vmax*Vmax);
Dyn_Press_hum=0.5*(Rho*S_hum*Vmax*Vmax);
Dyn_Press_tlh=0.5*(Rho*S_tlh*Vmax*Vmax);
Cl_flat=Fz_flat/Dyn_Press_flat;

```

```

Cl_hum=Fz_hum/Dyn_Press_hum;
Cl_tlh=Fz_tlh/Dyn_Press_tlh;

%% Plot Raw and Filtered Data of Normal Force, Tangential Force,
Total Force
figure(1)
plot((0.001:0.001:100),data1_flat_imp(:,3),'b',(0.001:0.001:100),...
data2_hum_imp(:,3),'r',(0.001:0.001:100),data3_tlh_imp(:,3),'g','lin
ewidth',2);
set(gca,'fontsize',20,'Xlim',[0 50],'Ylim',[-15 15])
h(4)=title('Raw Normal Forces in Impulsive Region');
h(3) = legend('Flat Plate','Hummingbird','Zimmermann');
h(1) = xlabel('Time','fontsize',24);
h(2) = ylabel('Normal Force[N]','fontsize',24,'fontweight','bold');
set(h(3),'fontsize',14)
grid on

figure(2)
plot((0.001:0.001:(length(data1_flat_norm(:,3))/1000)),...
data1_flat_norm(:,3),'b',(0.001:0.001:(length(data2_hum_norm(:,3))
/1000))...
,data2_hum_norm(:,3),'r',(0.001:0.001:(length(data3_tlh_norm(:,3))
/1000))...
,data3_tlh_norm(:,3),'g','linewidth',2);
set(gca,'fontsize',20,'Xlim',[50 100],'Ylim',[-15 15])
h(4) = title('Raw Normal Forces in Periodic Region');
h(3) = legend('Flat Plate','Hummingbird','Zimmermann');
h(1) = xlabel('Time','fontsize',24);
h(2) = ylabel('Normal Force[N]','fontsize',24,'fontweight','bold');
set(h(3),'fontsize',14)
grid on

figure(3)
plot(f1_flat,2*abs(Y1_flat(1:L1_flat/2+1)),'b',...
f1_hum,2*abs(Y1_hum(1:L1_hum/2+1)),'r',...
f1_tlh,2*abs(Y1_tlh(1:L1_tlh/2+1)),'g','linewidth',2)
set(gca,'fontsize',20,'Xlim',[0 1],'Ylim',[0 0.5])
hold on
h(4) = title('FFT(Fast Fourier Transform) Analysis for Tangential
Force');
h(3) = legend('Flat Plate','Hummingbird','Zimmermann');
h(1) = xlabel('Frequency[Hz]','fontsize',24);
h(2) = ylabel('Force[N]','fontsize',24,'fontweight','bold');
set(h(3),'fontsize',14)
grid on
[max1_flat,I1]=max(abs(Y1_flat));
f_max1_flat=f1_flat(I1);
[max1_hum,I1]=max(abs(Y1_hum));
f_max1_hum=f1_hum(I1);
[max1_tlh,I1]=max(abs(Y1_tlh));
f_max1_tlh=f1_tlh(I1);

figure(4)
plot(f2_flat,2*abs(Y2_flat(1:L1_flat/2+1)),'b',...
f2_hum,2*abs(Y2_hum(1:L1_hum/2+1)),'r',...
f2_tlh,2*abs(Y2_tlh(1:L1_tlh/2+1)),'g','linewidth',2)
set(gca,'fontsize',20,'Xlim',[0 1],'Ylim',[0 5])
hold on

```

```

h(4) = title('FFT(Fast Fourier Transform) Analysis for Normal
Force');
h(3) = legend('Flat Plate', 'Hummingbird', 'Zimmermann');
h(1) = xlabel('Frequency[Hz]', 'fontsize', 24);
h(2) = ylabel('Force[N]', 'fontsize', 24, 'fontweight', 'bold');
set(h(3), 'fontsize', 14)
grid on
[max2_flat, I2]=max(abs(Y2_flat));
f_max2_flat=f2_flat(I2);
[max2_hum, I2]=max(abs(Y2_hum));
f_max2_hum=f2_hum(I2);
[max2_tlh, I2]=max(abs(Y2_tlh));
f_max2_tlh=f2_tlh(I2);

figure(5)
plot((0.001:0.001:100), fdata_flat_imp(:, 3), 'b', (0.001:0.001:100), ...
fdata_hum_imp(:, 3), 'r', (0.001:0.001:100), fdata_tlh_imp(:, 3), 'g', 'lin
ewidth', 2);
set(gca, 'fontsize', 20, 'Xlim', [0 50], 'Ylim' , [-10 10])
h(4)=title('Filtered Normal Forces in Impulsive Region');
h(3) = legend('Flat Plate', 'Hummingbird', 'Zimmermann');
h(1) = xlabel('Time', 'fontsize', 24);
h(2) = ylabel('Normal Force[N]', 'fontsize', 24, 'fontweight', 'bold');
set(h(3), 'fontsize', 14)
grid on

figure(6)
plot((0.001:0.001:(length(fdata_flat_norm(:, 3)))/1000)), ...
fdata_flat_norm(:, 3), 'b', (0.001:0.001:(length(fdata_hum_norm(:, 3))
/1000)) ...
, fdata_hum_norm(:, 3), 'r', (0.001:0.001:(length(fdata_tlh_norm(:, 3))
/1000)) ...
, fdata_tlh_norm(:, 3), 'g', 'linewidth', 2);
set(gca, 'fontsize', 20, 'Xlim', [100 150], 'Ylim' , [-10 10])
h(4) = title('Filtered Normal Forces in Periodic Region');
h(3) = legend('Flat Plate', 'Hummingbird', 'Zimmermann');
h(1) = xlabel('Time', 'fontsize', 24);
h(2) = ylabel('Normal Force[N]', 'fontsize', 24, 'fontweight', 'bold');
set(h(3), 'fontsize', 14)
grid on

figure(7)
plot((1:10000)/10000, phase_avg1_flat, 'b', ...
(1:10000)/10000, phase_avg1_hum, 'r', ...
(1:10000)/10000, phase_avg1_tlh, 'g', 'linewidth', 2)
set(gca, 'fontsize', 20, 'Xlim', [0 1], 'Ylim' , [-10 10])
h(4) = title(...
'Average of the Filtered Normal Force in Periodic Region');
h(3) = legend('Flat Plate', 'Hummingbird', 'Zimmermann');
h(1) = xlabel('t/T', 'fontsize', 24);
h(2) = ylabel('Normal Force[N]', 'fontsize', 24, 'fontweight', 'bold');
set(h(3), 'fontsize', 14)
grid on

figure(8)
plot((1:10000)/10000, phase_avg1_flat_imp, 'b', ...
(1:10000)/10000, phase_avg1_hum_imp, 'r', ...
(1:10000)/10000, phase_avg1_tlh_imp, 'g', 'linewidth', 2)
set(gca, 'fontsize', 20, 'Xlim', [0 1], 'Ylim' , [-10 10])

```

```

h(4) = title('Average of the Filtered Normal Forces in Impulsive
Region');
h(3) = legend('Flat Plate', 'Hummingbird', 'Zimmermann');
h(1) = xlabel('t/T', 'fontsize', 24);
h(2) = ylabel('Normal Force[N]', 'fontsize', 24, 'fontweight', 'bold');
set(h(3), 'fontsize', 14)
grid on

figure(9)
plot((1:10000)/10000, phase_avg1_avg_flat, 'b', ...
      (1:10000)/10000, phase_avg1_avg_hum, 'r', ...
      (1:10000)/10000, phase_avg1_avg_tlh, 'g', 'linewidth', 2)
set(gca, 'fontsize', 20, 'Xlim', [0 1], 'Ylim' , [-4 4])
h(4) = title('Average of the Averaged and Filtered Normal Forces in
Periodic Region');
h(3) = legend('Flat Plate', 'Hummingbird', 'Zimmermann');
h(1) = xlabel('t/T', 'fontsize', 24);
h(2) = ylabel('Normal Force[N]', 'fontsize', 24, 'fontweight', 'bold');
set(h(3), 'fontsize', 14)
grid on

figure(10)
plot((1:10000)/10000, total_flat, 'b', ...
      (1:10000)/10000, total_hum, 'r', ...
      (1:10000)/10000, total_tlh, 'g', 'linewidth', 2)
set(gca, 'fontsize', 20, 'Xlim', [0 1], 'Ylim' , [-1 12])
h(4) = title(...
'Average of the Filtered Total Force in Periodic Region');
h(3) = legend('Flat Plate', 'Hummingbird', 'Zimmermann');
h(1) = xlabel('t/T', 'fontsize', 24);
h(2) = ylabel('Total Force[N]', 'fontsize', 24, 'fontweight', 'bold');
set(h(3), 'fontsize', 14)
grid on

figure(11)
plot((1:10000)/10000, totalr_flat, 'b', ...
      (1:10000)/10000, totalr_hum, 'r', ...
      (1:10000)/10000, totalr_tlh, 'g', 'linewidth', 2)
set(gca, 'fontsize', 20, 'Xlim', [0 1], 'Ylim' , [-10 10])
h(4) = title(...
'Phase Averaged Raw Total Forces');
h(3) = legend('Flat Plate', 'Hummingbird', 'Zimmermann');
h(1) = xlabel('t/T', 'fontsize', 24);
h(2) = ylabel('Total Force[N]', 'fontsize', 24, 'fontweight', 'bold');
set(h(3), 'fontsize', 14)
grid on

figure(12)

plot((1:10000)/10000, Fy_flat, 'b', ...
      (1:10000)/10000, Fy_hum, 'r', ...
      (1:10000)/10000, Fy_tlh, 'g', 'linewidth', 2)
set(gca, 'fontsize', 20, 'Xlim', [0 1], 'Ylim' , [-10 10]);
h(4) = title('Drag vs. t/T');
h(3) = legend('Flat Plate', 'Hummingbird', 'Zimmermann');
h(1) = xlabel('t/T', 'fontsize', 24);
h(2) = ylabel('Drag[N]', 'fontsize', 24, 'fontweight', 'bold');
set(h(3), 'fontsize', 14);
grid on

```

```

figure(13)
plot((1:10000)/10000,Fz_flat,'b',...
      (1:10000)/10000,Fz_hum,'r',...
      (1:10000)/10000,Fz_tlh,'g','linewidth',2)
set(gca,'fontsize',20,'Xlim',[0 1],'Ylim',[-15 15]);
h(4) = title('Lift vs. t/T');
h(3) = legend('Flat Plate','Hummingbird','Zimmermann');
h(1) = xlabel('t/T','fontsize',24);
h(2) = ylabel('Lift[N]','fontsize',24,'fontweight','bold');
set(h(3),'fontsize',14);
grid on

figure(14)
plot((1:10000)/10000,C1_flat,'b',...
      (1:10000)/10000,C1_hum,'r',...
      (1:10000)/10000,C1_tlh,'g','linewidth',2)
set(gca,'fontsize',20,'Xlim',[0 1],'Ylim',[-6 6])
h(4) = title(...
  'C1 Values for Flat Plate,Hummingbird and Zimmermann');
h(3) = legend('Flat Plate','Hummingbird','Zimmermann');
h(1) = xlabel('t/T','fontsize',24);
h(2) = ylabel('C1','fontsize',24,'fontweight','bold');
set(h(3),'fontsize',14)
grid on

```